# Studying nociceptive processing in the rat brain by PET imaging and digital atlasing

---

A dissertation submitted to
the University of Oslo
for the degree of
**Philosophiae Doctor (Ph.D)**
2009

---

by
**Trine Hjørnevik**
Department of Anatomy and CMBN
Institute of Basic Medical Sciences
University of Oslo


CENTRE FOR
MOLECULAR BIOLOGY
AND NEUROSCIENCE

*Series of dissertations submitted to the*
*Faculty of Medicine, University of Oslo*
*No. 1013*

ISBN 978-82-8072-382-6



Cover: Inger Sandved Anfinsen.
Printed in Norway: AiT e-dit AS.

Produced in co-operation with Unipub.
The thesis is produced by Unipub merely in connection with the
thesis defence. Kindly direct all inquiries regarding the thesis to the copyright
holder or the unit which grants the doctorate.

# Table of Contents

# Publications

**Paper I**

Three-dimensional atlas system for mouse and rat brain imaging data

Hjornevik T, Leergaard TB, Darine D, Moldestad O, Dale AM, Willoch F, and Bjaalie JG

Frontiers in Neuroinformatics 2007:1

---

**Paper II**

Metabolic plasticity in the supraspinal pain modulating circuitry after noxious stimulus-induced spinal cord LTP

Hjornevik T, Jacobsen LM, Qu H, Bjaalie JG, Gjerstad J, and Willoch F

PAIN 2008; 140: 456-464

---

**Paper III**

Synthesis and Evaluation of a Full-Agonist Orvinol for PET-Imaging of Opioid Receptors: [$^{11}$C]PEO

Marton J, Schoultz BW, Hjornevik T, Drzezga A, Yousefi BH, Wester HJ, Willoch F, and Henriksen G

Journal of Medicinal Chemistry, Epub ahead of print

---

**Paper IV**

Spinal long-term potentiation is associated with reduced opioid neurotransmission in the rat brain

Hjornevik T, Schoultz BW, Marton J, Gjerstad J, Drzezga A, Henriksen G, and Willoch F

Submitted

---

**Paper V**

Evaluation of the Kappa-Opioid Receptor Selective Tracer [11C]GR103545 in Awake Rhesus Macaques

Schoultz BW*, Hjornevik T*, Willoch F, Marton J, Noda A, Murakami Y, Miyoshi S, Nishimura S, Årstad E, Drzezga A, Matsunari I, and Henriksen G

Submitted

*Shared first authorship

# ABBREVIATIONS

1TCM: 1-tissue compartment model
2TCM: 2-tissue compartment model
3DRP: 3-D reprojection
3TCM: 3-tissue compartment model
Acb: nucleus accumbens
$B_{max}$: available receptor site concentration
BP: binding potential
CNS: central nervous system
CPu: caudate putamen
CT: computed tomography
DH: dorsal horn
DLPT: dorsolateral pontine tegmentum
FBP: filtered back-projection
HFS: high-frequency stimulation
$K_D$: equilibrium dissociation constant
LOR: line-of-response
LTP: long-term potentiation
MAP: maximum a posteriori
MRI: magnetic resonance imaging
MRTM0: Ichise Multi-linear Reference Tissue Method
OP: opioid peptide
OR: opioid receptor
OSEM: ordered subsets expectation maximization
PAG: periaqueductal grey
PET: positron emission tomography
PNS: peripheral nervous system
ROI: region-of-interest
RT-PCR: real-time polymerase chain reaction
RVM: rostroventromedial medulla
SPM: statistical parametric mapping
TAC: time-activity curve
VOI: volume-of-interest
$V_T$: volume-of-distribution

# Preface

After completing my studies abroad I returned to Norway without any specific intention of pursuing a career in research. However, when offered to join the first PET research group in Norway along with an opportunity to conduct a Ph.D I couldn't resist. In May 2005 I started at the Small Animal Imaging Unit located at the Neural Systems and Graphics Computing Laboratory (NeSys) at the Department of Anatomy, Institute of Basic Medical Sciences, University of Oslo. In April 2006 I was enrolled in the Ph.D program with fundings from the Research Council of Norway. 4 years later I am happy and proud to submit my Ph.D thesis. These years have consisted of challenges; which is a consequence of starting up with a new technology, excitements; by obtaining new knowledge and succeeding by having papers published, and travelling; to places such as London, Heidelberg, Munich, Atlanta, Espoo, Stockholm, Osaka, Tuebingen, Glasgow, Kobe and Chicago. Coming from a background in physics, a whole new world has revealed itself for me during this project. I have been introduced to the world of molecular biology, neuroscience, neuroimaging, neuroinformatics, and radiochemistry.

This work would not have been completed without my three supervisors: Johannes Gjerstad, Jan G. Bjålie, and Frode Willoch. I would like to thank Johannes for his enthusiasm and support, Jan for being solution oriented and his straightforward thinking, and Frode for believing in me and teaching me the world of imaging and pain.

This project has been generously founded by the Research Council of Norway and the University of Oslo.

I want to acknowledge Prof Markus Schwaiger for the use of the small animal imaging facilities at Department of Nuclear Medicine at the University of Munich, together with his excellent technical staff. Gjermund Henriksen and Bent W. Schoultz for involving me in their reseach and miraculously producing the radiochemical substances which are crucial in PET research. I would also like to thank Trygve Leergaard for his supervision in preparing written and oral presentations and for organizing the annual NeSys sailcruises. My "office mates" Hong Qu for the endless hours behind the shower curtains, for her straightforwardness and critical comments, and Dmitri Darine for being my computer wizard,

feeding me dark chocolate, and our discussions about anything non-scientific. Line Jacobsen at STAMI for excellent electrophysiological measurements and collaboration. All my co-authors which have played an important role in the individual studies. Further I would like to thank all former and current colleagues at Nesys for interesting scientific and non-scientific discussions, ski trips, dinners, and chocolate Fridays. Also, I truly appreciate the excellent scientific environment of the Centre of Molecular Biology and Neuroscience (CMBN). Last but not least, I am grateful for the support of friends and family and their persistent attempts to understand my work.

*Oslo, September 2009*
*Trine Hjørnevik*

# SYNOPSIS

# Introduction

Although acute pain is a necessity for survival, long-lasting pain, which persists longer than the natural time for healing, has no adaptive function and causes disease and strain on both the patient and society. Studies show that 20 % of Europe's adult population suffers from hypersensitivity, hyperalgesia, and allodynia. This thesis aims to contribute to a better understanding of the mechanisms underlying the development of long-lasting pain. Positron Emission Tomography (PET) was employed to study supraspinal functional changes in a rat model of persistent pain (papers II and IV), together with a customized digitalized atlas system which provided localization of the PET signals (paper I). In addition, this work also encompasses the development and evaluation of two novel PET tracers aimed for investigations of the endogenous opioid receptor (OR) system (papers III and V), which is a major neurotransmitter system involved in pain processing. Below, some theoretical background is given together with the specific aims of the present work.

## Pain perception and modulation

Pain is a subjective perception of nociceptive signal input mixed with emotions and previous experiences. From the peripheral nervous system (PNS) nociceptive information is transmitted through C- and Aδ-nociceptors to the dorsal horn (DH) of the spinal cord, and from there, through second order neurons, to supraspinal regions where the signal is interpreted. There are several ascending pathways, including the main spinothalamic tract, spinomesencephalic tract, and spinoreticular tract. Brain regions involved in pain processing include the sensory cortex, anterior cingulate cortex, thalamus, and limbic structures. Belonging to the latter category, nucleus accumbens (Acb), amygdala, hippocampus, hypothalamus, and caudate putamen (CPu) are all involved in processing emotions, mood, motivation, and pain sensations. Involvement of these structures reflects an affective-emotional response to a noxious event. Together with the hippocampus, amygdala is also involved in learning and memory of noxious stimuli. In particular, amygdala plays a major role in associating the stimuli with emotions, and might contribute to the formation of "pain memory".

The idea of pain modulation was introduced by Head and Holmes as early

as 1911, but first in 1965 the existence of a specific pain modulatory system was articulated by the famous "Gate Control Theory" by Melzack and Wall [27]. Nociceptive transmission is filtered and modulated by interneurons either locally in the DH or in descending pathways to the spinal cord. These interneurons either suppress (descending inhibition) or potentiate (descending facilitation) nociceptive signaling to the brain. Today, complex networks are known to play a crucial role in pain modulation, and the best described network is the descending nociceptive inhibitory circuitry (DNIC) which includes the amygdala, periaqueductal grey (PAG), rostroventromedial medulla (RVM), and dorsolateral pontine tegmentum (DLPT) (Fig. 1) [8]. These brain and brain stem structures control nociceptive transmission in the spinal cord by inhibiting nociresponsive neurons in the dorsal horn. A dysfunction in this inhibitory system could cause a reduced antinociceptive effect, which might lead to an increased activity in the ascending second order neurons. This hypothesis has been investigated

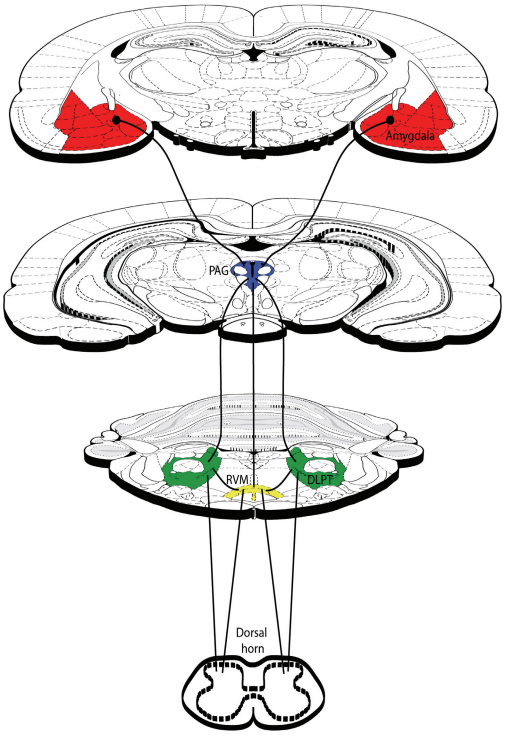


**Figure 1. Descending nociceptive modulation.** Amygdala, PAG, RVM, and DLTP constitute a major descending pain modulatory network. There are reciprocal projections between the midbrain region PAG, and DLTP and RVM in the brain stem. RVM and DLTP exert control over nociceptive transmission in the dorsal horn of the spinal cord. PAG, periaqueductal grey; DLPT, dorsolateral pontine tegmentum; RVM, rostral ventromedial medulla.

in papers II and IV. The complexity of this pain-control network involves several neurotransmitters and their specific receptors (for review see [29]), but this thesis will, in paper IV, focus on the OR system which plays a key role in pain inhibition.

## Neuroimaging of pain

*In vivo* functional neuroimaging by means of PET and functional magnetic resonance imaging (fMRI) have contributed to increased knowledge of the functional anatomy of pain. *In vivo* non-invasive imaging facilitates longitudinal investigations, where the pain matrix can be studied as a whole, revealing interactions between brain regions, and not just the effect on individual regions. PET was chosen as method in the present study based on high sensitivity and its unique ability to localize and quantify specific neuroreceptor systems. Further information about the PET technology and areas of application is given in Methods. Currently, PET is used comprehensively in clinical studies of various pain models (for review see [38]), but few studies based on animal research have been published. The present thesis utilizes PET scanners dedicated for imaging of small animals to study supraspinal functional changes in a rat model of persistent pain.

## Central sensitization and long-term potentiation

Central sensitization is defined by the International Association for the Study of Pain (IASP) as "an enhanced responsiveness of nociceptive neurons in the central nervous system (CNS) to their afferent input" [28]. Some forms of central sensitization may cause enhanced pain experience to a noxious stimulus (hyperalgesia) or a non-noxious stimulus to be experienced as painful (allodynia) or both.

It has been suggested that induction of long-term potentiation (LTP) by noxious stimuli (e.g. electrical stimuli, noxious heat, nerve injury, and tissue damage) [46,49] is one mechanism underlying hypersensitivity, hyperalgesia, and allodynia [48]. LTP is defined as a long-lasting increase in neuronal synaptic strength [1,25], and is considered to contribute to learning and memory formation in the brain [1]. In the present thesis, a rat model was utilized for investigating the correlation between spinal LTP and supraspinal nociceptive processing. Spinal LTP was induced by high-frequency stimulation (HFS) conditioning applied to the rat sciatic nerve, which is an established model for

studying cellular memory of nociceptive information. It is tempting to speculate that the applied conditioning not only induces LTP at the spinal level, but also at supraspinal synapses. Particularly in brain regions included in the pain neuromatrix such as the sensory cortex, thalamus, cingulated cortex, and PAG. Spinal LTP is here defined as C-fibre LTP, which represents an increase in C-fibre response (measured in papers II og IV) together with a reduction in C-fibre threshold (paper IV). A lowering of the C-fibre threshold will result in second order neurons (i.e. neurons which transmit signals from the spinal cord to supraspinal sites) firing at lower input frequencies. Spinal LTP has been shown to last for hours [54] and if such a long-lasting increase in the responsiveness of nociceptive neurons persists it might result in central sensitization. Evidence indicate that induction of spinal LTP is followed by a long-lasting ipsilateral reduction of paw withdrawal latency, i.e. hyperalgesia [62]. Moreover, a perceptual correlate to LTP in nociceptive pathways has also been described in humans [20]. It is therefore likely that the conditioning used in the present thesis to induce spinal LTP contribute to central sensitization, an underlying mechanism of hypersensitivity, hyperalgesia, and allodynia.

## The opioid receptor system

The ORs are widely distributed in the CNS and are divided into three major subtypes (i.e. μ, δ, and κ) in addition to the opioid-receptor-like NOP [15]. Rat brain regions which contain dense distributions of ORs include the neocortex, CPu, thalamus, Acb, hippocampus, amygdala, and inferior/superior colliculi [26]. Activation of ORs, by endogenous or administrated exogenous ligands, contribute to functional changes in areas such as pain and analgesia, tolerance and dependence, learning and memory, and alcohol and drug abuse (for review see [16]).

The present thesis (paper IV) focuses on the role of ORs in nociceptive processing, where the opioid peptides (OPs), such as β-endorphin, enkephalin, and dynorphin, are key neurotransmitters involved in nociceptive signaling mechanisms and in controlling the descending modulatory system to the spinal cord. The ORs play an important role in affective-emotional processing and antinociception, and particularly μ-OR activation seems to be important for the mechanisms underlying opioid analgesia [7,26]. Also δ- and κ-ORs are most likely involved in modulating

supraspinal nociception, where the latter subtype is believed to suppress the antinociceptive action of the μ-OR (for review see [43]). However, the relative low abundance of κ-ORs (9 %) compared to μ-ORs (41 %) [26] in the rat brain limits this pronociceptive effect in rats. Changes in endogenous opioidergic signaling might influence various molecular mechanisms seen in chronic pain states where persistent noxious stimuli have been shown to result in changes in opioid action (for review see [41]).

## Aims of study

The following main questions were addressed in the present thesis:

1) Can small animal PET be used to measure putative supraspinal functional changes associated with spinal LTP induced by noxious conditioning?
2) Can a multi-modality 3-D digital atlas system improve signal localization and enhance the interpretation of tomographic data, such as PET images, with low structural contrast?
3) Does spinal LTP have a long-lasting effect on supraspinal neuronal metabolic activity?
4) Can the development of novel PET tracers facilitate preclinical and clinical studies of various subclasses of the endogenous OR system?
5) Does spinal LTP influence supraspinal opioidergic neurotransmission?

# Methods

All animal experiments were performed in conformity with the laws and regulations controlling experiments and procedures on live animals in Norway, Germany and Japan, which is in accordance with the European convention for the protection of vertebrate animals used for experimental and scientific purposes. Details concerning the experimental and analytical procedures are described in the individual papers. This section will first provide an overview of the employed methods; imaging techniques, electrophysiology recordings, multi-modality co-registration, and computerized 3-D reconstruction. Then, more details will be given about the two main methods utilized in the present thesis: PET and digital atlasing.

## Overview of methods

### Induction of spinal LTP

Experimental data show that LTP is induced by various noxious stimuli including electrical conditioning, noxious heat, nerve injury, or tissue damage [46,49]. In the present thesis (papers II and IV), LTP was induced by HFS conditioning (1 ms rectangular 4.5 mA pulses, five trains of 1 s duration, 100 Hz, 10 s intervals between trains). During adequate anesthesia, the left sciatic nerve was dissected free and isolated from the surrounding tissue. An electrode was placed proximal to the main branches of the sciatic nerve for electrical stimulation.

### Electrophysiological recordings

Recordings of spinal field potentials were applied, in papers II and IV, in order to verify that spinal LTP was induced by HFS conditioning of the sciatic nerve. The measurements were based on the C-fibre response to a test pulse, in addition to the lowest stimulus intensity that evokes the first visible C-fibre response, i.e. C-fibre threshold (paper IV).

### Tomographic neuroimaging techniques

Neuroimaging techniques such as PET and magnetic resonance imaging (MRI) provide *in vivo* functional and structural information about the mouse and rat brain. PET reflects function, while MRI reveals both anatomical and functional information depending on the imaging paradigm used. The present thesis focuses on PET imaging, while MRI is utilized as an anatomical refer-

ence (papers I, II, IV, and V), and for exemplifying the use of a digital atlas system in order to localize enhanced MRI signals (paper I).

*Magnetic Resonance Imaging (MRI)*

MRI offers good soft tissue contrast in the rat brain, and is therefore often used as an anatomical reference for the functional signals obtained with PET. An MRI template fitted to Paxinos and Watson atlas space [51] was in papers I, II, and IV used to spatially normalize PET data into a common reference framework.

In paper I, high-resolution *in vivo* $MnCl_2$/MRI pathway tracing was used as an example of how a digital atlas could assign location to tracer injection sites and observed signal enhancements. The $T_1$ weighted data was collected at the Massachusetts General Hospital NMR-Center using a 3 Tesla Trio whole body human scanner (Siemens Medical Solutions, Iselin, NJ) and a custom made loop surface receiver coil.

*Positron Emission Tomography (PET)*

PET is the state of the art imaging technology for studying biological processes *in vivo*. In the present thesis, PET was used for studying nociceptive processing in the brain in papers I, II, and IV, cancerous tissue in paper I, and specific neurotransmitter system in papers I, III, IV, and V. The PET data presented in papers I and II was acquired with the microPET Focus 120 system (Siemens Medical Solutions, Erlangen, Germany) at the Small Animal Imaging Unit at University of Oslo, the PET data in papers III and IV was collected with the Inveon system (Siemens Medical Solutions, Erlangen, Germany) at Technische Universität München, while the PET imaging in paper V was performed with the SHR-770 (Hamamatsu Photonics, Hamamatsu, Japan) at the Medical and Pharmacological Research Center Foundation Hakui-city Ishikawa. Further information about PET imaging is given in a separate subsection.

**Software**

The following software packages were used for image analysis and atlas reconstruction:

- Adobe Illustrator CS2 (Adobe Systems Inc., San Jose, Ca): atlas alignment and segmentation.
- Amira 4.0 (Mercury Computer Systems Inc., Chelmsford, Ma): 3-D atlas surface rendering.
- PMOD (PMOD Technologies Ltd., Zurich, Switzerland): image pre-processing, multi-modality co-

registration, and pharmacokinetic modeling.

- Statistical Parametric Mapping (SPM5, Wellcome Department of Cognitive Neurology, Institute of Neurology, London, Uk) performed in Matlab 7.5.0 and 7.6 on Windows and Mac OS workstations: multi-modality co-registration and normalization, and statistical analysis. The SPM5 software is freely available at http://www.fil.ion.ucl.ac.uk/spm.
- Atlas3D (NeSys, Department of Anatomy & CMBN, University of Oslo, Norway): This multi-platform Java3D based atlas tool was developed in our group to facilitate import and visualization of 3-D digital atlas structures as well as tomographic image data (i.e. PET, CT, and MRI). In addition to co-visualization, a cutting module, i.e. 2-D user-defined slices at any angle and orientation, was developed. The software is freely available at http://www.nesys.uio.no/Atlas3D.

**Multi-modality co-registration and spatial normalization**

To improve interpretation of the functional signals seen in our PET data, MRI, CT, and atlas were utilized as structural references. In order to locate the signal, the various modalities were co-registered and normalized to the same reference space.

*Co-registration of PET, MRI, and CT data*

In papers I, II, and IV, automatic intra-subject co-registration and spatial normalization between various image data were performed in SPM5. The within-subject co-registration was based on a rigid body model involving 3 translations and 3 rotations using a normalized mutual information objective function. Normalization was performed with a linear registration which employs a 12-parameter affine transformation procedure.

*3-D atlas reconstruction*

A 3-D digital atlas system was developed to facilitate assignment of location and comparative analysis of signal location in tomographic images with low structural contrast. The 3-D atlas structures were reconstructed from standard 2-D mouse and rat brain atlases. The reconstruction steps included alignment of atlas diagrams, segmentation, and surface rendering. Further details on the digital atlas system are given else-

where in this section.

*Registration to 3-D atlas space*

Tomographic imaging data (PET, CT, and MRI) were manually co-registered to the 3-D atlas space in Atlas3D based on identifiable landmarks in the various data. The most limited amount of structural information is available in PET data, and therefore additional imaging modalities can improve the quality of the registration. Throughout this project, three particular pipelines have been utilized and validated; 1) co-registration of PET to atlas (paper I), co-registration of PET through MRI to atlas (papers I and II) and 3) co-registration of PET through CT to atlas (papers I and IV). The anatomical landmarks used for registration in the various cases are discussed in the individual papers. Also, in paper I, atlas co-registration was used for locating tracer injection sites and observed signal enhancement in a high-resolution *in vivo* $MnCl_2$/MRI pathway tracing study.

## Positron Emission Tomography

PET is a unique imaging modality for studying functional processes *in vivo.* With high sensitivity and quantitative abilities PET has become an important research tool, as well as a routine diagnostic modality. The first human PET tomograph was developed in 1974 and marks the beginning of the modern PET technology [32]. In the recent years, PET scanners with improved sensitivity and resolution dedicated to imaging small animals have been developed to study animal models of disease. One of the early designs was the UCLA micro-PET [5], which is the prototype for the commercially available small animal PET scanners used in this thesis.

### The basics of PET: positron emission, detection, and image reconstruction

PET imaging involves administration of a radiopharmaceutical, labeled with a positron emitting radionuclide, into a subject and external detection of annihilation photons using detectors in combination with coincidence electronics. During positron ($\beta^+$) decay, a proton is converted into a neutron, and a positron and a neutrino are emitted from the nucleus. The positron loses kinetic energy through interactions with the surrounding tissue until it annihilates with an electron. The total rest masses of the two particles are then converted into electromagnetic radiation, creating two annihilation photons of equal energy ($511 \pm 1$ keV) travelling 180 º to each other (Fig. 2). The positron range

| Nuclide | $^{11}C$ | $^{13}N$ | $^{15}O$ | $^{18}F$ |
|---|---|---|---|---|
| Half life (min) | 20.4 | 9.9 | 2.1 | 109.8 |
| $E_{max}$ (MeV) | 0.959 | 1.197 | 1.738 | 0.633 |
| Mean range in water (mm) | 1.1 | 1.5 | 2.5 | 0.6 |

**Table 1. Properties of the main positron-emitting nuclides.**

(i.e. travelling distance before annihilation) depends on the initial energy of the positron and the density of surrounding tissue. The properties of the most important positron emitters used in PET are listed in Table 1. In this thesis, $^{18}F$ was used in papers I and II, and $^{11}C$ in papers III-V. The long half life of $^{18}F$ facilitates more flexible study protocols and improved statistics.

The standard geometry of a PET scanner is a ring of detectors, employing coincidence electronics, which enables detection of the simultaneously emitted annihilation photons. If both photons are detected within limits of timing- and energy-windows, a line-of-response (LOR) will pass close to the site of annihilation representing the site of positron emission (Fig. 2), and hence the injected probe.

Acquired data is, in certain PET tomographs including the microPET Focus 120 and Inveon, written in a list mode data format, which allows the user to dynamically divide the experimental data into customized time frames. To obtain images, each time frame is histogrammed into sinograms and reconstructed using various image reconstruction algorithms; e.g. analytical methods such as the traditional filtered back-projection (FBP) and 3D reprojection (3DRP), or iterative methods such as ordered subsets expectation maximization (OSEM3D) and OSEM3D - maxi-

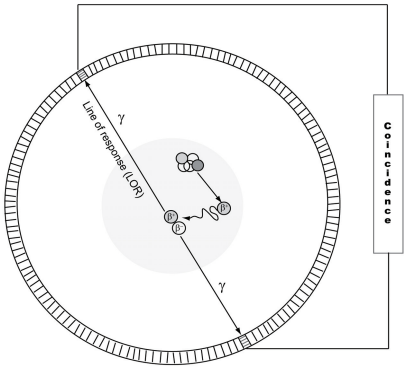


**Figure 2. Positron emission, annihilation, and detection.** The positron is emitted from an unstable nucleus, and annihilates with an electron after interacting with the surrounding tissue. The two particles are converted into two photons (γ-rays) of equal energy (511 keV) traveling 180 º to each other. Simultaneous detection of these photons creates a coincidence event and a line-of-response (LOR).

mum a posteriori (OSEM3D/MAP). The latter algorithms facilitate advantages such as noise modeling, incorporation of image degrading effects, and corrections due to variations in scanner geometry, but are limited by long computational time. In the present work, based on the features offered by the individual software, both analytical and iterative reconstruction algorithms have been used; 2DFBP (paper V), 3DRP (papers III and IV) and OSEM3D/MAP (papers I and II).

To obtain quantitative measurements (i.e. accurate reconstruction of radiotracer concentration (kBq/ml)), several corrections must be applied to the raw image data during reconstruction; e.g. scatter, normalization, and attenuation corrections. The latter corrects for photon attenuation due to scatter or absorption in tissue. In the micro-PET Focus 120 and Inveon system the attenuation correction is performed by acquiring a transmission scan by either a positron emitter source, $^{68}$Ge, or a single photon emitter, $^{57}$Co.

**Applications of PET**

Areas of clinical applications and basic research include neurology, oncology, cardiology, and pharmacology. The main focus of this thesis is imaging of neurochemical processes in the brain, an area which offers a relative large spectrum of available tracers.

*FDG-PET*

The glucose analog 2- [$^{18}$F]fluoro-2-deoxy-glucose ([$^{18}$F]FDG) (used in papers I-II) has been utilized since the late 70s and is the most commonly used molecular probe in PET imaging. The basis for FDG imaging is the coupling between glucose utilization and synaptic activity (neurometabolic coupling) [52]. In paper I, FDG was utilized for illustrating increased metabolic activity in cancerous tissue compared to normal tissue, while, in papers I and II, the use of FDG facilitated comparisons between baseline and noxious conditioning at different time points.

*Ligand-PET*

PET is the state of the art imaging modality for studying receptors systems *in vivo* with the use of highly selective receptor radiotracers. [$^{18}$F]fallypride (paper I, [30]) is a highly selective D2/D3 dopamine receptor antagonist often used to explore changes in the dopaminergic system. During the baseline conditions in paper I, [$^{18}$F]fallypride was used to reveal distributions and concentrations of the dopamine receptors in the

rat brain. The present thesis focuses on the endogenous opioid system, and PET imaging of ORs has provided important insights into the areas of epilepsy, pain processing, neurodegenerative disorders, addiction, and new pharmacological treatments (for reviews see [10,16,43]).

Several PET ligands have been developed with different tracer properties and subclass selectivity; e.g. the μ-selective agonist [$^{11}$C]carfentanil ([$^{11}$C]CAF), non-selective antagonist [$^{11}$C]diprenorphine ([$^{11}$C]DPN), and μ- and κ-selective antagonist [$^{18}$F]fluoro-cyclofoxy ([$^{18}$F]FCyF). The highly potent agonist [$^{11}$C]CAF has been used in human studies of μ-ORs since 1985 [9], but high specific activity is needed to obtain sub-pharmacological doses. Also, it is believed that agonist tracers reflect endogenous binding more specifically than antagonists. Development of structurally matched agonist/antagonist pairs will facilitate testing of such a hypothesis. Therefore, an agonist radiotracer, [$^{11}$C]phenethyl-orvinol ([$^{11}$C]PEO), has been synthesized and characterized in paper III. [$^{11}$C]PEO binds selectively to μ- and κ-ORs, is less potent than the traditional [$^{11}$C]CAF, results from a fairly fast synthesis, and future developments such as [$^{18}$F]labeling and production of an antagonist version are more easily implemented. The present thesis focuses on the role of ORs in pain processing, and the novel opioid PET tracer was, in paper IV, employed to investigate dynamic changes in opioid neurotransmission following noxious stimulus-induced spinal LTP. The agonistic properties along with high affinity for the μ-OR determined the choice of tracer in this study.

Currently, no κ-OR-selective PET-tracer is available for routine clinical applications. [$^{11}$C]GR103545 is a promising κ-OR-selective tracer [45,57] which facilitates high affinity and excellent binding to κ-ORs in the non-human brain. However, the use of [$^{11}$C]GR103545 in clinical studies has so far been limited due to low radiochemical yield. An improved and automated method for radiosynthesis of [$^{11}$C]GR103545 was introduced by Schoultz et al. [50], and paper V evaluates the use of [$^{11}$C]GR103545, synthesized by the new method, in rhesus macaques.

**Quantification**

In order to fully interpret the externally detected PET signal, quantification of the time course of the radiolabeled substance is necessary. This is particularly important in neuroreceptor imag-

ing, where the total detected signal is "contaminated" by free ligand in tissue and non-specifically bound ligand. The standard way of estimating the component-of-interest, the specifically bound ligand, is by pharmacokinetic modeling using compartment models (for reviews see [12,19]). Each compartment represents a certain behavioral state of the tracer, and may exchange material with other compartments (exchange rates are indicated as $K_1$, $k_2$, $k_3$ and $k_4$ in Fig. 3). Compartment modeling requires blood sampling for estimation of tracer concentration in plasma, which also needs to be corrected for metabolites. Ideally, a 3-tissue compartment model (3TCM), containing one compartment for each behavioral state of the tracer, should be used for reversible receptor systems, but the complexity of such a model is difficult to assess experimentally. For practical purposes, free and non-specifically bound tracer is treated as one compartment in a 2-tissue compartment model (2TCM) (Fig. 3). Further simplification into a 1-tissue compartment model (1TCM) is sometimes necessary in order to reduce the number of unknown parameters (i.e. exchange rates). In paper V,

**Figure 3. Pharmacokinetic modeling.** Various models, based on the ratio of concentrations in tissue ($C_T$) and plasma ($C_P$), provide an estimation of the specific binding of tracer. In standard compartment models (1TCM and 2TCM) blood sampling is required to determine $C_P$, while in a reference tissue model this input function is substituted with $C_T$ from a reference tissue avoid of specific binding. 1TCM, 1-tissue compartment; 2TCM, 2-tissue compartment; $K_1$, $k_2$, $k_3$ and $K_4$, exchange rates between compartments.

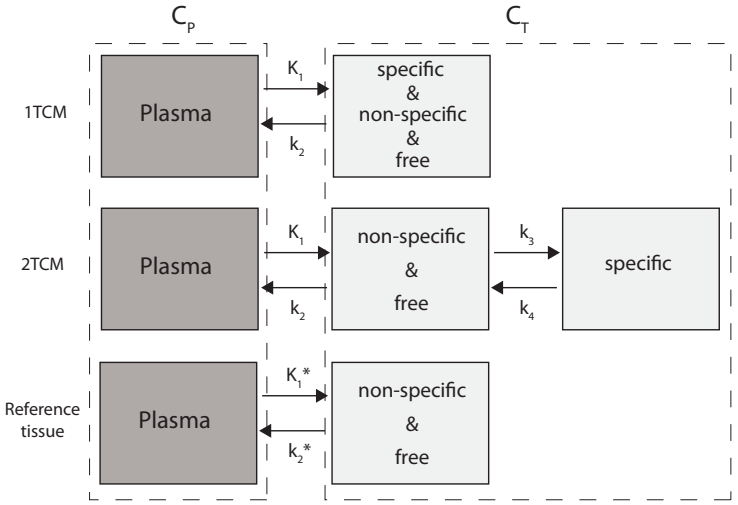

both 1TCM and 2TCM were used in the κ-OR specific binding analysis in the monkey brain study. The estimated parameter of interest, volume-of-distribution ($V_T$), in both models, is equal to the ratio of tissue ($C_T$) and plasma ($C_P$) concentrations at equilibrium.

Compartment modeling requires invasive blood sampling which can, particularly in rodent imaging, be quite a demanding procedure. Therefore, reference tissue models have been developed where the arterial input curve is substituted with the time activity curve of some reference tissue avoid of specific binding. The detected signal from such a reference tissue provides an estimation of the non-specific binding and free tracer in tissue (Fig. 3), which is assumed to be equal in all tissue. Although these models do not provide a full kinetic analysis, they are able to estimate valuable measures of interest. In paper IV, specific OR binding was quantified pixel-by-pixel using the Ichise Multi-linear Reference Tissue Method (MRTM0) [18]. This reference model is based on the Logan Plot [23] and applies for reversible receptor studies. The output parameter of interest is the binding potential ($BP_{ND}$), which provides a measurement of receptor concentration. The cerebellum was chosen as the reference tissue due to the lack of ORs in this region for the rat [26]. $BP_{ND}$ is proportional with the ratio of the concentration of available receptor sites ($B_{max}$) to the *in vivo* equilibrium dissociation constant of the radiotracer ($K_D$).

### 3-D DIGITAL ATLAS SYSTEM

Brain atlases are extensively used in neuroscience for identifying anatomical structures in the brain. Conventional two-dimensional (2-D) book atlases provide series of sections, cut at specified angles and arranged in a standard stereotaxic framework based on reference external and internal landmarks or both. Several of the most commonly known rodent brain atlases [35-37] use a stereotaxic reference system based on the flat-skull positions with the bregma, lambda, and interaural line as landmarks.

Use of such atlases for neuroimaging data is hampered by the 2-D format as well as a lack of an analytical environment for comparison and integration of atlas and image data. Computerized 3-D atlases provide volumetric representation of brain anatomy, in addition to slicing at all angles and orientations, generating customized atlas diagrams which are more compatible with individual image data. Several 3-D representa-

tions of major brain structures have been developed for the mouse [2,4,14,22,24], and are under development for the rat (see e.g. [13,14]). In addition to be used as references and analytical tools, digital atlases might also provide a framework for data sharing [3].

### 3-D atlas reconstruction

In paper I, we presented a method for creating a 3-D computerized stereotaxic brain atlas model from a 2-D stereotaxic book atlas. Our procedure is based on The Rat Brain in Stereotaxic Coordinates, 5th edition, by Paxinos & Watson [37] and the Mouse Brain in Sterotaxic Coordinates, 2nd edition, by Paxinos & Franklin [36], but could be applied to any digitalized stereotaxic atlas. The present versions of the 3-D reconstructed atlases include 30 structures for the mouse brain and 60 structures for the rat brain.

The method for 3-D reconstruction of the atlas structures is explored in detail in paper I. Figure 4 illustrates the applied pipeline. The digital atlas diagrams were organized in separate layers and aligned according to the stereotaxic grid of the atlas using Adobe Illustrator CS2. In each diagram, regions of interest (ROIs) were segmented by colour coding, and then exported as an

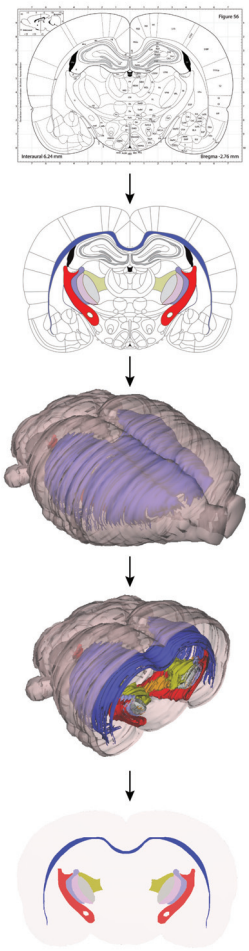

**Figure 4. Workflow for 3-D atlas reconstruction.**
The stepwise procedure is based on a standard 2-D atlas diagram which is segmented according to individual brain regions and then 3-D reconstructed. The 3-D atlas can be sliced at any angles and orientations to create customized atlas diagrams.

image (TIFF) file to Amira 4.0 for 3-D reconstruction. All structures were surface rendered and exported as VRML (Virtual Reality Modeling Language). The reconstructed atlas structures can be visualized in the custom made atlas tool, Atlas3D.

# RESULTS

## SUMMARY OF PAPERS I-V

### Paper I

frontiers
IN NEUROINFORMATICS

**Three-dimensional atlas system for mouse and rat brain imaging data**

Trine Hjornevik[1], Trygve B. Leergaard[1], Dmitri Darine[1], Olve Moldestad[1], Anders M. Dale[2,3], Frode Willoch[1,4] and Jan G. Bjaalie[1,*]

1. Centre for Molecular Biology and Neuroscience & Institute of Basic Medical Sciences, University of Oslo, Norway
2. Departments of Neurosciences and Radiology, University of California, San Diego, USA
3. Martinos Center for Biomedical Imaging, Massachusetts General Hospital, Harvard Medical School, USA
4. Department of Radiology, Aker University Hospital, Norway

Edited by: Maryann Martone, University of California, San Diego, USA

Reviewed by: Richard A. Baldock, Medical Research Council Human Genetics Unit, Edinburgh, United Kingdom
James F. Brinkley, University of Washington, Seattle, United States of America

Interpretation of tomographic neuroimaging data relies on accurate determination of anatomical location, which depends on the structural information available in the images. PET data and some MRI paradigms provide little structural contrast, and the challenge is therefore to assign locations to the data with use of available brain atlases. The comparison is hampered by the standard 2-D format of the atlas as well as a lack of an analytical environment for integration of atlas and 3-D image data.

We have developed a method for reconstructing 3-D atlases from any stereotaxic 2-D atlas. Currently, our atlas system contains 30 mouse brain structures reconstructed from "The Mouse Brain in Stereotaxic Coordinates" by Paxinos & Franklin [34], and 60 rat brain structures from "The Rat Brain in Stereotaxic Coordinates" by Paxinos & Watson [35]. We have, furthermore, developed a multi-platform tool which allows sharing of the reconstructed atlas framework, surface modeling, rotation of selected structures, and slicing at any chosen angle. The tool allows import of PET, CT, and MRI data to facilitate comparison with the atlas and warping of experimental image data into atlas space. The approach taken uses linear registration, with the possibility to scale, rotate, and position

the imported data, either globally, using the whole brain as template, or locally, using smaller parts of the brain as template.

The co-registration is based on recognizable brain or skull landmarks, which depends on the nature of the image data. A PET image volume typically lacks well-defined structural information which may complicate the alignment. As illustrated in the paper, the quality of the co-registration may be enhanced when the researcher has access to other modalities such as MRI or CT or both. The alignment of an MRI volume is based on anatomical landmarks such as the outer boundaries of the brain and white matter. In a CT volume, the definition of bregma and the interaural line simplifies the transformation matrix calculation. The accuracy of the co-registration critically depends on the precision with which anatomical landmarks may be detected, which in turn also depends on voxel size and structural contrast in the data. For the image quality here exemplified, our linear procedures appear to provide sufficient accuracy to resolve most questions related to localization of data and comparisons between animals.

**Paper II**

Pain 140 (2008) 456–464

PAIN

www.elsevier.com/locate/pain

Metabolic plasticity in the supraspinal pain modulating circuitry after noxious stimulus-induced spinal cord LTP

Trine Hjornevik [a], Line M. Jacobsen [b], Hong Qu [a], Jan G. Bjaalie [a], Johannes Gjerstad [b,c], Frode Willoch [a,d,*]

[a] *Centre for Molecular Biology and Neuroscience & Institute of Basic Medical Sciences, University of Oslo, Norway*
[b] *National Institute of Occupational Health, Norway*
[c] *Department of Molecular Biosciences, University of Oslo, Norway*
[d] *Department of Radiology, Aker University Hospital, Norway*

Received 9 April 2008; received in revised form 9 September 2008; accepted 24 September 2008

LTP is defined as a long-lasting increase in neuronal synaptic strength [1,24] and if induced by a noxious stimulus believed to contribute to hypersensitivity, hyperalgesia and/or allodynia [45]. In the present study we have investigated if noxious stimulus-induced spinal LTP might have a long-lasting effect on

supraspinal neuronal activity. First, we verified that spinal LTP was induced by HFS conditioning as a noxious stimulus of the sciatic nerve. Then, to study the brain activation patterns following the same stimulation protocol, we used small animal PET and the glucose analog [$^{18}$F]FDG. We hypothesized that immediately after a noxious stimulation an evoked signal would be observed predominantly in the ascending pathways, and that maintenance of spinal LTP would be followed by adaptations in the supraspinal pain modulating network.

The spinal field potential recordings revealed a twofold increase of the C-fibre response 150 min after HFS. Changes in regional supraspinal neuronal activity were measured at two time points in HFS conditioned and sham animals; acute (immediately after HFS/sham) and late phase (150 min after HFS/sham). Statistical group comparison between HFS and sham revealed acute metabolic changes in S1 and slower metabolic adaptations in brain regions involved in modulation of nociceptive signaling, such as PAG, RVM, and DLPT.

We have here demonstrated that HFS conditioning of the sciatic nerve produced a clear LTP at the spinal level. This study demonstrates that PET is suitable as an *in vivo* method to study changes in regional brain metabolic activity between different conditions, and the observed changes within the CNS reflect a supraspinal maladaptive dysfunction involved in pain hypersensitivity and hyperalgesia.

**Paper III**

Journal of Medicinal Chemistry Letter

# Synthesis and Evaluation of a Full-Agonist Orvinol for PET-Imaging of Opioid Receptors: [$^{11}$C]PEO

János Marton,[†] Bent W. Schoultz,[‡] Trine Hjørnevik,[§] Alexander Drzezga,[∥] Behrooz H. Yousefi,[∥] Hans-Jurgen Wester,[∥] Frode Willoch,[§,⊥] and Gjermund Henriksen*[,∥,‡]

[†] *ABX Advanced Biochemical Compounds, Biomedizinische Forschungsreagenzien GmbH, Radeberg, Germany,* [‡] *Department of Chemistry, University of Oslo, PO Box 1033, Blindern N-0315 Oslo, Norway,* [§] *Centre for Molecular Biology and Neuroscience & Institute of Basic Medical Sciences, University of Oslo, PO Box 1105, Blindern N-0317 Oslo, Norway,* [∥] *Department of Nuclear Medicine, Klinikum Rechts der Isar, Technische Universitat Munchen, Ismaninger Strasse 22, D-81675 Munich, Germany, and* [⊥] *Akershus University Hospital, PO Box 300, N-1471 Lørenskog, Norway*

*Received June 18, 2009*

ORs are known to be involved in pain modulation [50,56] as well as being molecular targets of opioid and stimulant drugs of abuse [10,38]. Non-invasive imaging of the OR system by PET requires highly selective tracers which bind specifically to one or several subclasses (e.g. μ, δ, and κ) of the ORs. Currently, several non-selective OR-antagonists are employed for studies in humans. However, it is believed that antagonistic radioligands target other binding sites than agonists, and their ability to monitor *in vivo* OR occupancy is limited. Hence, high-affinity agonistic radioligands are needed to obtain a detailed comparison of OR agonist/antagonist PET-tracers.

The present paper reports on a fully automated synthesis and characterization of agonist [$^{11}$C]PEO. *In vitro* radioligand binding experiments revealed high-affinity of [$^{11}$C]PEO for μ- and κ-ORs, and low-affinity for δ-ORs. Evaluation of the radiotracer was performed with *ex vivo* biodistribution (with and without pre-treatment of blocking agents) and *in vivo* PET imaging experiments in rats. Both methods showed excellent initial brain uptake, and overtime, highly concentrated binding to brain regions where the μ-OR expression is richest. In

addition, metabolites analysis indicated high metabolic stability.

The agonist radioligand, [$^{11}$C]PEO, presented in this paper was successfully prepared using a fully automated synthesis. The highly selective [$^{11}$C]PEO depicts μ-ORs in the rat brain, and can be used to investigate changes in the OR availability during *in vivo* small animal PET studies.

**Paper IV**

**Spinal long-term potentiation is associated with reduced opioid neurotransmission in the rat brain**

Hjornevik T, Schoultz BW, Marton J, Gjerstad J, Drzezga A, Henriksen G, and Willoch F

OPs are key neurotransmitters involved in nociceptive processing in the brain and in controlling the descending modulatory system to the spinal cord. The ORs are widely distributed in the CNS and play an important role in affective-emotional processing and antinociception. LTP induced by noxious stimulation in the pain pathways may be an underlying cellular mechanism underlying hyperalgesia, and the expression of spinal LTP is more pronounced when the connection between the brain and recording site in the spinal cord is eliminated [11,52]. In the present study we have examined if spinal LTP influences the supraspinal opioidergic system. First, we verified that spinal LTP was induced by electrical HFS conditioning of the left sciatic nerve. Then, to study changes in opioid neurotransmission, we used small animal PET and the novel highly selective μ- and κ-OR ligand, [$^{11}$C]PEO. We hypothesized that changes would occur in brain regions known to be involved in nociceptive responses, e.g. the limbic system, sensory cortex, thalamus, and PAG.

The spinal field recordings showed a clear C-fibre LTP, i.e. increased C-fibre response and reduced C-fibre threshold, 150 min after HFS conditioning. PET scans were acquired at baseline and 150 min after HFS conditioning. A measurement of receptor concentration, the $BP_{ND}$ was calculated for each data set, and statistical group comparison (baseline vs. HFS) revealed a reduction in opioid neurotransmission in brain regions involved in limbic functions and pain modulation.

Our findings indicate that a reduced descending opioid, antinociceptive activity may be related to the observed spinal C-fibre LTP and associated states with abnormal pain sensitivity. Furthermore, the dynamic changes in opioid neurotransmission in the limbic structures may connect the findings with an affective-emotional response to the applied noxious stimulus.

## Paper V

### Evaluation of the Kappa-Opioid Receptor Selective Tracer [$^{11}$C]GR103545 in Awake Rhesus Macaques

Schoultz BW*, Hjornevik T*, Willoch F, Marton J, Noda A, Murakami Y, Miyoshi S, Nishimura S, Årstad E, Drzezga A, Matsunari I, and Henriksen G

*Shared first authorship

Currently, no κ-OR-selective PET-tracer is available for routine clinical applications. A promising κ-OR-selective tracer, [$^{11}$C]GR103545, was introduced by Ravert et al. [41,42], and evaluated in non-human primates by Talbot et al. [54]. They reported high affinity and excellent binding to κ-ORs in the non-human primate brain. However, the low radiochemical yield limited the use of [$^{11}$C] GR103545 in clinical trials. A new and automated method for radiosynthesis of [$^{11}$C]GR103545 was introduced by Schoultz et al. [47]. The improved method provided excellent yields with reduced total synthesis time. The present study evaluates the use of [$^{11}$C]GR103545, synthesized by the new method, in awake rhesus macaques.

*In vivo* PET imaging 0-90 min after injection of [$^{11}$C]GR103545 in awake rhesus macaques showed excellent brain penetration and uptake patterns which correlated with known κ-OR distribution. The regional distribution volumes, $V_T$, which were derived by kinetic analysis of regional time-activity curves (TACs) using 2TCM, was significantly higher than reported by Talbot et al. [53], but with a consistent pattern. In addition, *in vitro* binding studies revealed high affinity and excellent selectivity to κ-ORs.

The improved method for radiosynthesis of [$^{11}$C]GR103545 enables the translation to clinical studies. The presented evaluation supports the role of [$^{11}$C]

GR103545 as a promising tracer for selective depiction and quantification of κ-OR by means of PET in humans.

# Discussion

The main aim of this thesis was to investigate nociceptive signaling mechanisms in the rat brain using PET and digital atlasing. Two different PET tracers were used to study changes in regional neuronal activity and opioid neurotransmission following spinal LTP induced by noxious sciatic nerve conditioning. A digital 3-D atlas system was developed to improve the interpretation of the PET signals. The main methodological considerations and implications of the findings are discussed below.

## Main Findings

Referring to the main aims listed in the Introduction, the present thesis contains the following main findings:

1) The results obtained in papers II and IV demonstrate that small animal PET is suitable for detecting supraspinal changes in regional metabolic activity and opioid neurotransmission after induction of spinal LTP.
2) As demonstrated in paper I, registration of low structural contrast MRI and PET data to a 3-D digital atlas framework facilitates assignment of signal location and comparative analysis of image data. The approach outlined was used in the PET data analysis in papers II and IV.
3) In paper II, FDG-PET was used to identify acute activity changes and slower metabolic adaptations in the brain, resulting from induced spinal LTP. These changes in metabolic activity were found in brain regions involved in modulation of nociceptive signalling.
4) The fully automated radiosynthesis of the agonist [$^{11}$C]PEO introduced in paper III provides a highly selective μ- and κ-OR ligand which can be used to investigate changes to the OR availability during *in vivo* small animal PET studies. In addition, the evaluation, based on imaging studies in non-human primates, reported in paper V indicates that [$^{11}$C]GR103545 is a candidate tracer for selective depiction and quantification of κ-OR in humans.
5) [$^{11}$C]PEO, a highly selective μ- and κ-OR ligand was used in paper IV

to study changes in opioid neurotransmission 2.5 hrs after induction of spinal LTP. Reduced opioid tonic activity was found in brain regions involved in pain modulation, and in processing emotions, learning, and memory.

## Methodological considerations

The present thesis builds on the combined use of a number of methods, ranging from the development of novel opioid PET tracers to PET imaging studies with traditional and novel probes. In addition, a customized digital atlas framework was used for interpretation of the specific PET signals. Limitations and strengths of the methods employed in the present thesis along with the applied interpretation of image data are discussed below.

### PET imaging

**Spatial resolution and interpretation of signal.** The amount of details which can be studied is limited by the spatial resolution provided by the PET modality. For dedicated high-resolution small animal scanners, the spatial resolution is dependent on the size of the crystal and the intrinsic resolution (i.e., positron range and photon non-colinearity). For the small animal PET tomographs employed in this project, voxel sizes in the reconstructed images are ~1 $mm^3$. Clusters of signal smaller in size will not be detected by the system and therefore result in false negative findings.

Further, for FDG-PET, increased signal activity resulting from increased metabolism is considered to be related to an increase in neuronal, synaptic activity. However, the functional nature of the increased activity is not well defined, and can be caused by several functions related to e.g. on and off cells, excitatory, and inhibitory synapses. Consequently, the employed method is unable to decipher the original nature of the increased signal activity.

**Anesthesia.** The choice of anesthetic agent is important for optimizing imaging protocols, and inhalation anesthesia such as isoflurane (utilized in papers I-IV) facilitates greater control over depth and duration of anesthesia. However, the physiological effects of anesthesia can influence the biodistribution of PET tracers (for review see [17]). Toyama and colleagues reported

a decrease in FDG uptake in the brain in mice anesthetized with isoflurane gas [59]. Nevertheless, since the FDG-results presented in the present thesis are obtained from comparisons between two different conditioning states, the effect of isoflurane on FDG uptake can in this case be disregarded. The possible interaction by anesthetics is particularly important in neuroreceptor radioligand studies, where interference with the receptor system in question may alter the interpretation of data. Despite the importance, there are currently few studies which have thoroughly investigated the interference of anesthetics with radioligand binding (for the serotonin and dopamine receptor system see [6]). In the present thesis, isoflurane gas was chosen as an agent because it facilitates greater control over duration (i.e. animals were kept in anesthesia for 3.5 hrs in papers II and IV), and for not interacting severely with the OR system (paper IV) [42,58]. However, negative results obtained in the latter study (e.g. no significant change in OR binding in main pain processing brain regions such as the cingulate cortex) could be caused by such interactions. In addition, in the present study anesthesia is not used only to constrain the animal during scanning, but is also used so that the animals do not consciously experience pain. To achieve this, isoflurane must interact with the supraspinal pain processing network. The significance of these interactions is not fully understood, but can not be avoided due to ethical regulations.

**Radiotracers.** PET is the state of the art imaging modality for qualitative and quantitative assessment of receptor systems *in vivo*, and requires highly selective radiotracers for targeting particular receptors and their subclasses. The development of such specific radiolabeled compounds is an ongoing challenge in the field of radiopharmaceutical chemistry, and while paper III describes the development and evaluation of a novel μ- and κ-OR-selective tracer, [$^{11}$C]PEO, paper IV demonstrates its usefulness by measuring changes in opioid neurotransmission following a noxious stimulus. Despite binding to two subclasses of the ORs, the observed signal mainly reflects μ-binding due to the relative high abundance of μ-ORs (41 %) compared to κ-ORs (9%) in the rat brain [26]. However, in the human brain, κ-sites comprise 37 % of the total number of OR compared to 29 % for the μ-OR. Specific studies of the κ-ORs are also of interest due to their function in analgesia and dysphoria [16]. However, rats are not appropriate as study subjects

because of the low κ-ORs density. With the [$^{11}$C]GR103545 tracer available, it would be natural to study the κ-OR function in human in relation to pain perception and processing. Further, the agonistic/antagonistic properties of a PET tracer are important for data interpretation as agonists bind preferably to receptors in a high-affinity state, while antagonists bind to both high- and low-affinity states. The results obtained in the agonist PEO-PET study will therefore represent changes in binding to μ-ORs in a high-affinity state, which is believed to correlate to the state of endogenous OP binding.

**Quantification.** A PET receptor ligand can exist in various functional compartments in tissue; free ligand in tissue, non-specifically and specifically bound ligand. To estimate the latter compartment, a reference tissue method was used in order to calculate $BP_{ND}$, a measurement of OR receptors concentration. The observed increase in $BP_{ND}$ can be interpreted as reduced endogenous OP release or an increase in the concentration of available OR sites ($B_{max}$) or increased receptor affinity ($1/K_D$) or a combination of all three. Further interpretation can not be obtained with the employed modality, but complementary technologies such as real-time polymerase chain reaction (RT-PCR) and immunohistochemistry should be applied in order to explore this in more detail. The present study only shows that the observed binding of PET tracer represents a state of the supraspinal OR system which is associated with spinal LTP.

### Multi-modality co-registration and spatial normalization

PET imaging reflects function and not primarily structure, and therefore, reveals few landmarks in the brain and skull. Hence, complementary imaging modalities and brain atlases are often used as spatial references. Comparisons of image data require co-registration or spatial normalization or both, either by manual or automatic procedures. The latter method excludes user-dependency, but involves complex algorithms which depend on a degree of mutual information in the different data sets. Throughout this project, automatic intra-subject alignment and spatial normalization were performed in SPM5. Depending on the available imaging modality, our ultimate aim was to register PET data to atlas space on the basis of the landmarks identifiable in the various image data. This registration performed in Atlas3D can currently only be made manually.

Hence, the registration procedure here presented is not fully-automatic. In addition, all registrations are based on linear transformation which might introduce local alignment errors due to inter-subject variations in rodent brain shape and size. Non-linear warping is complex and demanding, and results in deformation of data. For the low structural contrast image data presented in this thesis, linear registration has been sufficient in order to obtain a valid localization.

### LTP AND HYPERALGESIA

In papers II and IV the focus has been on induction of LTP at C-fibre synapses, i.e. C-fibre LTP, applying electrical stimulation at 1.5 x C-fibre threshold. These observations do not include Aδ responses which are activated with lower test stimulus intensity. The measured C-fibre threshold in paper IV is defined as the lowest threshold for firing of the second order spinal neurons in the superficial laminae of the spinal cord. Many of these neurons project to supraspinal sites, and hence, the spinal LTP measured in laminae I-III in the present studies may be important for the activity in the ascending pain pathways.

LTP induced by electrical conditioning is often used to study mechanisms underlying long-lasting pain states. Moreover, Zhang and colleagues [61] have demonstrated that spinal C-fibre LTP is also induced by acute nerve injury, such as cutting and crushing of the sciatic nerve, which is known to produce a long-lasting neuropathic pain. In addition, a link between electrical HFS conditioning of nociceptive afferents and enhanced pain perception has also been demonstrated in humans [20].

Previous studies have shown that the expression of spinal LTP is more pronounced when the connection between the brain and recording site in the spinal cord is eliminated [11,55], i.e. when the synaptic activity is not modulated by the descending network. Therefore, it is tempting to speculate that the increased C-fibre response and the reduced C-fibre threshold observed in our studies, which also may be linked to hyperalgesia and allodynia, may be supported by a reduced descending inhibition. The correlation between hyperalgesia and spinal LTP is further strengthened by behavior animal studies which show a long-lasting reduction of paw withdrawal latency after induction of spinal LTP [62]. These evidences support the use of HFS conditioning as a valid model for studying central sensitization. However, whether

this observed hypersensitivity is caused by a local spinal increase in synaptic efficacy or changed supraspinal processing remains to be investigated.

### The opioid receptor system

The OR-selective radioligands presented in this project facilitate investigations of the functional role of opioid neurotransmission in the CNS. OPs are key neurotransmitters involved in pain modulation, and activated ORs mainly inhibit nociceptive transmission, which might explain the role of ORs as an analgesic. The antinociceptive effect is regulated by changes in the amount of endogenous OP release or OR availability or receptor affinity or a combination of all three. A reduced neurotransmission, as seen in paper IV, indicates a dysfunction in this inhibitory network, and hence a reduced antinociception (i.e. pronociception). Whether this dysfunction supports the maintenance of spinal LTP in the spinal cord remains to be investigated. However, the study reveals a significant correlation between supraspinal opioid neurotransmission and hypersensitivity in the spinal cord. Such knowledge is important for understanding how chronic pain develops and for obtaining an optimal treatment for patients suffering from chronic pain.

### Functional changes in supraspinal nociceptive processing

Amygdala was the sole brain region which showed functional changes following noxious conditioning in both studies (papers II and IV). Increased neuronal activity (hypermetabolism) was observed in the FDG-PET study, while a reduction in opioid neurotransmission was detected in the opioid PET study. Amygdala encompasses 13 nuclei and subnuclei [47], all with different structural and functional signature. In the present thesis, amygdala is referred to as a homogenous structure due to the spatial resolution provided by the PET modality. As part of the limbic system, amygdala plays a key role in memory formation and learning, emotional evaluation of sensory stimuli, and in affective disorders such as anxiety and depression. Recent evidences, including results from *in vivo* imaging studies, indicate amygdala as an important contributor to pain and its emotional component (for review see [31]). Particularly, a reciprocal relationship exists between persistent pain and negative affective states such as fear, anxiety, and depression. Koepp and colleagues [21] have demonstrated a correlation between endogenous opioid release and the regulation of positive emotions in humans. In addition,

amygdala is also critically involved in pain modulation, including both pain enhancement and pain reduction. Antinociception through the descending inhibitory network has been shown to be activated either through stressors (e.g. fear) or by introduction by exogenous opioids [33,34]. Amygdala is known to exploit a high degree of plasticity, which correlates to the functional changes seen in the present work. Our findings support the role of amygdala both in affective-emotional response to noxious stimuli and in pain modulation.

In addition to amygdala, reduced opioid neurotransmission was also observed in other limbic structures such as the hippocampus, Acb, CPu, and hypothalamus. A painful experience is known to contain both sensory and affective dimensions, where the latter encompasses feelings of unpleasantness and emotions associated with future implications (for review see [39]). Motivational, emotional, and affective responses are processed in the limbic network, and particularly the hippocampus plays a key role in the formation of so-called "pain memory" where nociceptive stimuli leaves memory tracks in the CNS in order to prevent, prepare, and protect the organism in the future. Paper IV reveals functional changes in the affective component of pain, which most likely also influence the adaptations seen in the brain regions involved in pain modulation.

As the main aim of this thesis was to investigate possible mechanism underlying the development of persistent pain, the most interesting finding was a possible dysfunction in the pain modulatory network. This hypothesis is based on the observed metabolic changes in amygdala PAG, RVM, and DLTP, regions all involved in descending modulation (see Fig. 1 in Introduction). In addition, reduced opioid neurotransmission was seen in the amygdala. The activity in the supraspinal pain processing network is closely linked to the firing properties of the second order neurons in the dorsal horn of the spinal cord, which transmits the nociceptive information through ascending pathways.

The spinal neurotransmission is modulated by descending pathways, either directly or by interneurons in the dorsal horn. A dysfunction in these modulating mechanisms may affect the sensitivity in the neurotransmission at the spinal level. We suggest that the long-lasting increase in spinal excitability observed in this study may be supported by a dysfunction in the descending pain modulatory network. Hence, this dys-

function might explain mechanisms seen in central sensitization such as hyperalgesia and allodynia.

# Conclusions and future prospects

- Small animal PET is suitable for measuring functional changes in the rat brain. In particular, PET is superior for *in vivo* qualitative and quantitative investigations of receptor systems using highly selective radioligands.

- Digital 3-D atlas systems enhance interpretation of the signals seen in PET and MRI data with low structural contrast.

- Advancements in radiopharmaceutical chemistry might contribute to an enhanced understanding of the functional role of the endogenous opioid receptors, e.g. to study specific κ-OR mechanisms and extending selective tracer studies to a clinical level.

- Induction of spinal LTP by electrical noxious conditioning results in supraspinal functional adaptations. Changes in neuronal activity and opioid neurotransmission occur in brain regions involved in pain modulation. We suggest that these findings indicate an insufficient inhibition in the descending pain modulatory network, which might cause states of abnormal pain sensitivity such as hyperalgesia. The following findings support this theory:

  Induction of spinal LTP by HFS results in:

  1. Increased C-fibre response and reduced C-fibre threshold
  2. Long-lasting metabolic adaptations in brain regions involved in pain modulation
  3. Reduced opioid neurotransmission in regions involved in pain memory and processing

The aim of this thesis was to contribute to a better understanding of how chronic pain develops. The ultimate goal is to expand this knowledge to human use and the clinic, where further knowledge enables us to target an improved treatment of patients with chronic pain.

# REFERENCES

[1] Bliss TV and Collingridge GL. A synaptic model of memory: long-term potentiation in the hippocampus. Nature 1993;361:31-39

[2] Boline JK, MacKenzie-Graham AA, Shattuck DW, Yuan H, Anderson SP, Sforza DM, Wang J, Williams RW, Wong W, Martone ME, Zaslavsky I, and Toga AW. A Digital Atlas and Neuroinformatics Framework for Query and Display of Disparate Data. Society for Neuroscience 2006 Abstract and itinerary viewer Program No 100 12 2006

[3] Boline J, Lee EF, and Toga AW. Digital atlases as a framework for data sharing. Front Neurosci 2008;2:100-106

[4] Chan E, Kovacevic N, Ho SKY, Henkelman RM, and Henderson JT. Development of a high resolution three-dimensional surgical atlas of the murine head for strains 129S1/SvImJ and C57Bl/6J using magnetic resonance imaging and micro-computed tomography. Neuroscience 2007;144:604-615

[5] Cherry SR, Shao Y, Silverman RW, Meadors K, Siegel S, Chatziioannou A, Young JW, Jones W, Moyers JC, Newport D, Boutefnouchet A, Farquhar TH, Andreaco M, Paulus MJ, Binkley DM, Nutt R, and Phelps ME. MicroPET: a high resolution PET scanner for imaging small animals. Nuclear Science, IEEE Transactions on 1997;44:1161-1166

[6] Elfving B, Bjornholm B, and Knudsen GM. Interference of anaesthetics with radioligand binding in neuroreceptor studies. Eur J Nucl Med Mol Imaging 2003;30:912-915

[7] Fang FG, Fields HL, and Lee NM. Action at the mu receptor is sufficient to explain the supraspinal analgesic effect of opiates. J Pharmacol Exp Ther 1986;238:1039-1044

[8] Fields HL, Basbaum A. Central nervous system mechanisms of pain modulation. In: Wall P and Melzak R, editors. Textbook of pain.London: Harcourt Publishers Limited, 1999. pp. 309-329

[9] Frost JJ, Wagner HN, Jr., Dannals RF, Ravert HT, Links JM, Wilson AA, Burns HD, Wong DF, McPherson RW, Rosenbaum AE, and . Imaging opiate receptors in the human brain by positron tomography. J Comput Assist Tomogr 1985;9:231-236

[10] Henriksen G, Willoch F, Talbot PS, and Wester HJ. Recent Development and Potential Use of μ- and ê-Opioid Receptor Ligands in Positron Emission Tomography Studies. Drug development research 2006;67:890-904

[11] Gjerstad J, Tjolsen A, and Hole K. Induction of long-term potentiation of single wide dynamic range neurones in the dorsal horn is inhibited by descending pathways. Pain 2001;91:263-268

[12] Gunn RN, Gunn SR, Turkheimer FE, Aston JAD, and Cunningham VJ. Positron Emission Tomography Compartmental Models: A Basis Pursuit Strategy for Kinetic Modeling. J Cereb Blood Flow Metab 2002;22:1425-1439

[13] Gustafson C, Bug W, and Nissanov J. NeuroTerrain - a client-server system for browsing 3D biomedical image data sets. BMC Bioinformatics 2007;8:40

[14] Gustafson C, Tretiak O, Bertrand L, and Nissanov J. Design and implementation of software for assembly and browsing of 3D brain atlases. Comput Methods Programs Biomed 2004;74:53-61

[15] Henderson G and McKnight AT. The orphan opioid receptor and its endogenous ligand--nociceptin/orphanin FQ. Trends Pharmacol Sci 1997;18:293-300

[16] Henriksen G and Willoch F. Imaging of opioid receptors in the central nervous system. Brain 2008;131:1171-1196

[17] Hildebrandt IJ, Su H, and Weber WA. Anesthesia and other considerations for in vivo imaging of small animals. ILAR J 2008;49:17-26

[18] Ichise M, Ballinger JR, Golan H, Vines D, Luong A, Tsai S, and Kung HF. Noninvasive Quantification of Dopamine D2 Receptors with Iodine-123-IBF SPECT. J Nucl Med 1996;37:513-520

[19] Ichise M, Meyer JH, and Yonekura Y. An Introduction to PET and SPECT Neuroreceptor Quantification Models. J Nucl Med 2001;42:755-763

[20] Klein T, Magerl W, Hopf HC, Sandkuhler J, and Treede RD. Perceptual Correlates of Nociceptive Long-Term Potentiation and Long-Term Depression in Humans. J Neurosci 2004;24:964-971

[21] Koepp MJ, Hammers A, Lawrence AD, Asselin MC, Grasby PM, and Bench CJ. Evidence for endogenous opioid release in the amygdala during positive emotion. Neuroimage 2009;44:252-256

[22] Lein ES, Hawrylycz MJ, Ao N, Ayres M, Bensinger A, Bernard A, Boe AF, Boguski MS, Brockway KS, Byrnes EJ, Chen L, Chen L, Chen TM, Chi Chin M, Chong J, Crook BE, Czaplinska A, Dang CN, Datta S, Dee NR, Desaki AL, Desta T, Diep E, Dolbeare TA, Donelan MJ, Dong HW, Dougherty JG, Duncan BJ, Ebbert AJ, Eichele G, Estin LK, Faber C, Facer BA, Fields R, Fischer SR, Fliss TP, Frensley C, Gates

SN, Glattfelder KJ, Halverson KR, Hart MR, Hohmann JG, Howell MP, Jeung DP, Johnson RA, Karr PT, Kawal R, Kidney JM, Knapik RH, Kuan CL, Lake JH, Laramee AR, Larsen KD, Lau C, Lemon TA, Liang AJ, Liu Y, Luong LT, Michaels J, Morgan JJ, Morgan RJ, Mortrud MT, Mosqueda NF, Ng LL, Ng R, Orta GJ, Overly CC, Pak TH, Parry SE, Pathak SD, Pearson OC, Puchalski RB, Riley ZL, Rockett HR, Rowland SA, Royall JJ, Ruiz MJ, Sarno NR, Schaffnit K, Shapovalova NV, Sivisay T, Slaughterbeck CR, Smith SC, Smith KA, Smith BI, Sodt AJ, Stewart NN, Stumpf KR, Sunkin SM, Sutram M, Tam A, Teemer CD, Thaller C, Thompson CL, Varnam LR, Visel A, Whitlock RM, Wohnoutka PE, Wolkey CK, Wong VY, Wood M, Yaylaoglu MB, Young RC, Youngstrom BL, Feng Yuan X, Zhang B, Zwingman TA, and Jones AR. Genome-wide atlas of gene expression in the adult mouse brain. Nature 2007;445:168-176

[23] Logan J, Fowler JS, Volkow ND, Wang GJ, Ding YS, and Alexoff DL. Distribution Volume Ratios Without Blood Sampling from Graphical Analysis of PET Data. J Cereb Blood Flow Metab 1996;16:834-840

[24] MacKenzie-Graham AA, Jones ES, Shattuck DW, Dinov ID, Bota M, and Toga AW. The Informatics of a C57BL/6J Mouse Brain Atlas. Neuroinformatics 2003;1:397-410

[25] Malenka RC and Bear MF. LTP and LTD: an embarrassment of riches. Neuron 2004;44:5-21

[26] Mansour A, Khachaturian H, Lewis ME, Akil H, and Watson SJ. Anatomy of CNS opioid receptors. Trends Neurosci 1988;11:308-309

[27] Melzack R and Wall PD. Pain mechanisms: a new theory. Science 1965;150:971-979

[28] Merskey H and Bogduk N, Classification of Chronic Pain: descriptions of chronic pain syndromes and definitions of pain terms, IASP Press, Seattle, 1994.

[29] Millan MJ. Descending control of pain. Prog Neurobiol 2002;66:355-474

[30] Mukherjee J, Yang ZY, Das MK, and Brown T. Fluorinated benzamide neuroleptics--III. Development of (S)-N-[(1-allyl-2-pyrrolidinyl) methyl]-5-(3-[18F]fluoropropyl)-2, 3-dimethoxybenzamide as an improved dopamine D-2 receptor tracer. Nucl Med Biol 1995;22:283-296

[31] Neugebauer V, Li W, Bird GC, and Han JS. The Amygdala and Persistent Pain. Neuroscientist 2004;10:221-234

[32] Nutt R. 1999 ICP Distinguished Scientist Award. The history of positron emission tomography. Mol Imaging

Biol 2002;4:11-26

[33] Oliveira MA and Prado WA. Antinociception and behavioral manifestations induced by intracerebroventricular or intra-amygdaloid administration of cholinergic agonists in the rat. Pain 1994;57:383-391

[34] Pavlovic ZW and Bodnar RJ. Opioid supraspinal analgesic synergy between the amygdala and periaqueductal gray in rats. Brain Res 1998;779:158-169

[35] Paxinos G and Watson C. The Rat Brain in Stereotaxic Coordinates, Academic Press, San Diego, 1998

[36] Paxinos,G. and Franklin,KB. The Mouse Brain in Stereotaxic Coordinates, Elsevier Academic Press, San Diego, 2001

[37] Paxinos,G. and Watson,C. The Rat Brain in Stereotaxic Coordinates, Elsevier Academic Press, San Diego, 2005

[38] Peyron R, Laurent B, and Garcia-Larrea L. Functional imaging of brain responses to pain. A review and meta-analysis. Neurophysiol Clin 2000;30:263-288

[39] Price DD. Psychological and Neural Mechanisms of the Affective Dimension of Pain. Science 2000;288:1769-1772

[40] Prisinzano TE. Natural Products as Tools for Neuroscience: Discovery and Development of Novel Agents to Treat Drug Abuse. J Nat Prod 2009;72:581-587

[41] Przewlocki R and Przewlocka B. Opioids in chronic pain. Eur J Pharmacol 2001;429:79-91

[42] Quock RM and Vaughn LK. Do inhalation general anesthetic drugs induce the neuronal release of endogenous opioid peptides? Life Sci 2005;77:2603-2610

[43] Ravert HT, Bencherif B, Madar I, and Frost JJ. PET imaging of opioid receptors in pain: progress and new directions. Curr Pharm Des 2004;10:759-768

[44] Ravert HT, Mathews WB, Musachio JL, Scheffel U, Finley P, and Dannals RF. [11C]-methyl 4-[(3,4-dichlorophenyl)acetyl]-3-[(1-pyrrolidinyl)methyl]-1-piperazinecarboxylate ([11C]GR89696): synthesis and in vivo binding to kappa opiate receptors. Nucl Med Biol 1999;26:737-741

[45] Ravert HT, Scheffel U, Mathews WB, Musachio JL, and Dannals RF. [11C]-GR89696, a potent kappa opiate receptor radioligand; in vivo binding of the R and S enantiomers. Nucl Med Biol 2002;29:47-53

[46] Rygh LJ, Svendsen F, Hole K, and Tjolsen A. Natural noxious stimulation can induce long-term increase of spinal nociceptive responses.

Pain 1999;82:305-310

[47] Sah P, Faber ES, Lopez De AM, and Power J. The amygdaloid complex: anatomy and physiology. Physiol Rev 2003;83:803-834

[48] Sandkuhler J. Understanding LTP in pain pathways. Molecular Pain 2007;3:9

[49] Sandkuhler J and Liu X. Induction of long-term potentiation at spinal synapses by noxious stimulation or nerve injury. Eur J Neurosci 1998;10:2476-2480

[50] Schoultz BW, Arstad E, Marton J, Willoch F, Drzezga A, Wester HJ, and Henriksen G. A New Method for Radiosynthesis of 11C-Labeled Carbamate Groups and its Application for a Highly Efficient Synthesis of the Kappa-Opioid Receptor Tracer [11C]GR103545. The Open Medicinal Chemistry Journal 2008;2:72-74

[51] Schweinhardt P, Fransson P, Olson L, Spenger C, and Andersson JLR. A template for spatial normalisation of MR images of the rat brain. J Neurosci Methods 2003;129:105-113

[52] Sokoloff L, Reivich M, Kennedy C, Rosiers MHD, Patlak CS, Pettigrew KD, Sakurada O, and Shinohara M. The [14C]deoxyglucose method for the measurement of local cerebral glucose utilization: theory, procedure, and normal values in the conscious and anesthetized albino rat. J Neurochem 1977;28:897-916

[53] Sprenger T, Valet M, Boecker H, Henriksen G, Spilker ME, Willoch F, Wagner KJ, Wester HJ, and T÷lle TR. Opioidergic activation in the medial pain system after heat pain. Pain 2006;122:63-67

[54] Svendsen F, Tjolsen A, and Hole K. LTP of spinal A beta and C-fibre evoked responses after electrical sciatic nerve stimulation. Neuroreport 1997;8:3427-3430

[55] Svendsen F, Tjolsen A, Gjerstad J, and Hole K. Long term potentiation of single WDR neurons in spinalized rats. Brain Res 1999;816:487-492

[56] Talbot PS, Narendran R, Butelman ER, Huang Y, Ngo K, Slifstein M, Martinez D, Laruelle M, and Hwang DR. 11C-GR103545, a radiotracer for imaging kappa-opioid receptors in vivo with PET: synthesis and evaluation in baboons. J Nucl Med 2005;46:484-494

[57] Talbot PS, Narendran R, Butelman ER, Huang Y, Ngo K, Slifstein M, Martinez D, Laruelle M, and Hwang DR. 11C-GR103545, a Radiotracer for Imaging {kappa}-Opioid Receptors In Vivo with PET: Synthesis and Evaluation in Baboons. J Nucl Med 2005;46:484-494

[58] Tejwani GA, Rattan AK, Gudehithlu KP, and McDonald JS. Modulation

of mu, kappa and delta opioid receptors in the rat brain by isoflurane and enflurane. Neuropharmacology 1991;30:643-649

[59] Toyama H, Ichise M, Liow JS, Vines DC, Seneca NM, Modell KJ, Seidel J, Green MV, and Innis RB. Evaluation of anesthesia effects on [18F] FDG uptake in mouse brain and heart using small animal PET. Nucl Med Biol 2004;31:251-256

[60] Willoch F, Schindler F, Wester HJ, Empl M, Straube A, Schwaiger M, Conrad B, and Tolle TR. Central poststroke pain and reduced opioid receptor binding within pain processing circuitries: a [11C] diprenorphine PET study. Pain 2004;108:213-220

[61] Zhang HM, Zhou LJ, Hu XD, Hu NW, Zhang T, and Liu XG. Acute nerve injury induces long-term potentiation of C-fiber evoked field potentials in spinal dorsal horn of intact rat. Sheng Li Xue Bao 2004;56:591-596

[62] Zhang XC, Zhang YQ, and Zhao ZQ. Involvement of nitric oxide in long-term potentiation of spinal nociceptive responses in rats. Neuroreport 2005;16:1197-1201

# PAPERS I-V

# I

frontiers
IN NEUROINFORMATICS

# Three-dimensional atlas system for mouse and rat brain imaging data

**Trine Hjornevik[1], Trygve B. Leergaard[1], Dmitri Darine[1], Olve Moldestad[1], Anders M. Dale[2,3], Frode Willoch[1,4] and Jan G. Bjaalie[1,*]**

1. Centre for Molecular Biology and Neuroscience & Institute of Basic Medical Sciences, University of Oslo, Norway
2. Departments of Neurosciences and Radiology, University of California, San Diego, USA
3. Martinos Center for Biomedical Imaging, Massachusetts General Hospital, Harvard Medical School, USA
4. Department of Radiology, Aker University Hospital, Norway

Edited by: Maryann Martone, University of California, San Diego, USA

Reviewed by: Richard A. Baldock, Medical Research Council Human Genetics Unit, Edinburgh, United Kingdom
James F. Brinkley, University of Washington, Seattle, United States of America

**Tomographic neuroimaging techniques allow visualization of functionally and structurally specific signals in the mouse and rat brain. The interpretation of the image data relies on accurate determination of anatomical location, which is frequently obstructed by the lack of structural information in the data sets. Positron emission tomography (PET) generally yields images with low spatial resolution and little structural contrast, and many experimental magnetic resonance imaging (MRI) paradigms give specific signal enhancements but often limited anatomical information. Side-by-side comparison of image data with conventional atlas diagram is hampered by the 2-D format of the atlases, and by the lack of an analytical environment for accumulation of data and integrative analyses. We here present a method for reconstructing 3-D atlases from digital 2-D atlas diagrams, and exemplify 3-D atlas-based analysis of PET and MRI data. The reconstruction procedure is based on two seminal mouse and brain atlases, but is applicable to any stereotaxic atlas. Currently, 30 mouse brain structures and 60 rat brain structures have been reconstructed. To exploit the 3-D atlas models, we have developed a multi-platform atlas tool (available via The Rodent Workbench, http://rbwb.org) which allows combined visualization of experimental image data within the 3-D atlas space together with 3-D viewing and user-defined slicing of selected atlas structures. The tool presented facilitates assignment of location and comparative analysis of signal location in tomographic images with low structural contrast.**

**Keywords: 3-D reconstruction, atlas, brain, imaging, magnetic resonance imaging, positron emission tomography, stereotaxic, visualization**

## INTRODUCTION

Positron emission tomography (PET) and magnetic resonance imaging (MRI) techniques are increasingly used for investigations of the mouse and rat brain, in the context of numerous types of general brain mapping or disease model investigations. PET imaging reflects function and not primarily structure, and therefore, reveals few landmarks in the brain or skull. MRI imaging shows a variable degree of structural detail, depending on the specifications of the instrument and the imaging protocols. A common challenge is therefore to assign locations to the data collected with use of available brain atlases.

PET and MRI techniques produce three-dimensional (3-D) volume (tomographic) data, whereas standard brain atlases have until recently been available only in a two-dimensional (2-D) format. The established and most commonly used atlases of the mouse and rat brain (Paxinos and Franklin, 2001; Paxinos and Watson, 1998, 2005; Swanson, 2004) provide series of sections, cut at specified angles, with external surfaces and internal boundaries of areas and nuclei indicated, and names assigned to the delineated structures. Use of such atlases for neuroimaging studies are hampered by the 2-D format as well as a lack of an analytical environment for comparison and integration of atlas and image data. Recently, atlases with 3-D representations of major brain structures have been developed for the mouse (Boline et al., 2006; Chan et al., 2007; Gustafson et al., 2004; Lein et al., 2007; MacKenzie-Graham et al., 2004). Both the 3-D mouse brain atlas of the Biomedical Informatics Research Network, BIRN (Boline et al., 2006), and the 3-D surgical mouse atlas developed at the University of Toronto (Chan et al., 2007) support import of experimental data (e.g., TIFF and Analyze Image format), which can either be visualized as orthogonal slices in a separate window or in the 3-D viewer. Furthermore, the BIRN atlas facilitates alignment of the experimental data with the atlas, with a set of predefined transformation parameters (i.e., 180 degrees rotation, swapping, and mirroring). As concerns 3-D rat brain atlases, several efforts are under development (see e.g., Gustafson et al., 2004, 2007), and a recently deployed neuroanatomical affiliation visualization-interface system demonstrates parts of the rat brain stem in 3-D (Palombi et al., 2006), but there is to our knowledge currently no comprehensive rat brain atlas available.

To further facilitate the task of establishing a spatial mapping between neuroimaging data and atlas space for the mouse and rat brain, we have established a pipeline for 3-D reconstruction of structures from two of the seminal high-resolution standard atlases (Paxinos and Franklin, 2001; Paxinos and Watson, 2005) including the stereotaxic space provided by the atlases. These particular rodent atlases are widely used and share a common nomenclature for both mouse and rat. The present versions of the 3-D reconstructed atlases include 30 structures for the mouse brain and

* Correspondence: Jan G. Bjaalie, Centre for Molecular Biology and Neuroscience & Institute of Basic Medical Sciences, University of Oslo, Norway. e-mail: j.g.bjaalie@medisin.uio.no

Received: 5 Sep. 2007; paper pending published: 24 Sep. 2007; accepted: 9 Oct. 2007; published online: 02 Nov. 2007

Full citation: Frontiers in Neuroinformatics (2007) **1**:4 doi: 10.3389/neuro.11.004.2007

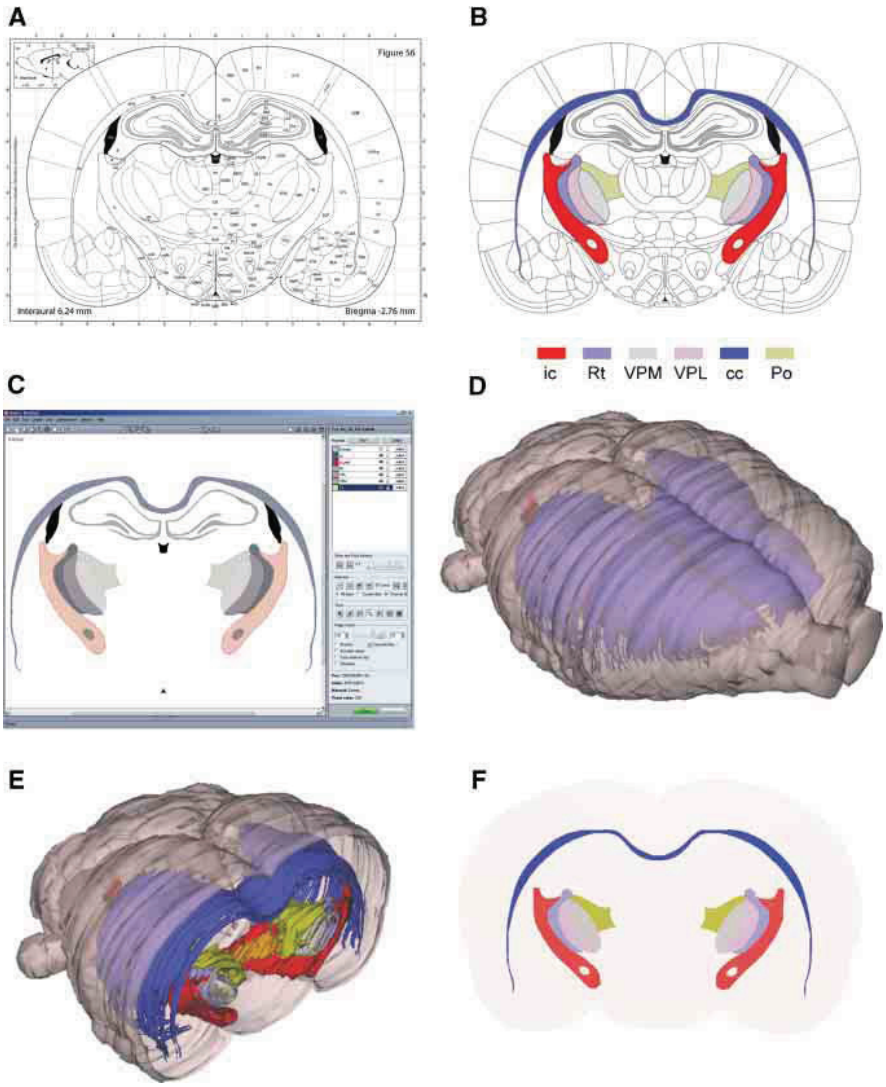


**Figure 1. The stepwise 3-D atlas reconstruction procedure.** *(**A**) A coronal rat brain atlas diagram (reproduced from Paxinos and Watson, 2005, with permission) with the stereotaxic grid, section number, structure labeling and the distance from bregma indicated. (**B**) The same diagram imported to Illustrator, where regions of interest (ROIs) are selected and assigned a color code. (**C**) Image of the Amira GUI showing segmented ROIs. (**D**) Selected 3-D reconstructed structures visualized in the m3d tool. (**E**) The same reconstruction as shown in (**C**) coronally sub-divided using the m3d slicing module. (**F**) Customized atlas diagram, corresponding to (**A**), exported from m3d. A separate module in m3d is used to render the sub-divided surfaces as solid objects. ic, internal capsule; Rt, reticular thalamic nucleus; VPM, ventral posterolateral thalamic nucleus; VPL, ventral posteromedial thalamic nucleus; cc, corpus callosum; Po, posterior thalamic nucleus.*

60 structures for the rat brain. We have, furthermore, developed a multi-platform tool that allows sharing of the reconstructed atlas framework, surface modeling and rotation of selected structures, slicing at any chosen angle, and the possibility to add new structures to the framework according to the requirements of a given study. The tool allows import of PET and MRI data to facilitate comparison with the atlas and warping of experimental image data into atlas space. The approach taken uses linear registration, with the possibility to scale, rotate, and position the imported data, either globally, using the whole brain as template, or locally, using smaller parts of the brain as template. Here we demonstrate the use of this tool as a dynamic and analytical environment for assigning location to image data and discuss advantages of the approach taken as well as some of the remaining challenges.

## MATERIALS AND METHODS

Structures from two atlases, "The Rat Brain in Stereotaxic Coordinates" by Paxinos and Watson (2005) and "The Mouse Brain in Stereotaxic Coor-

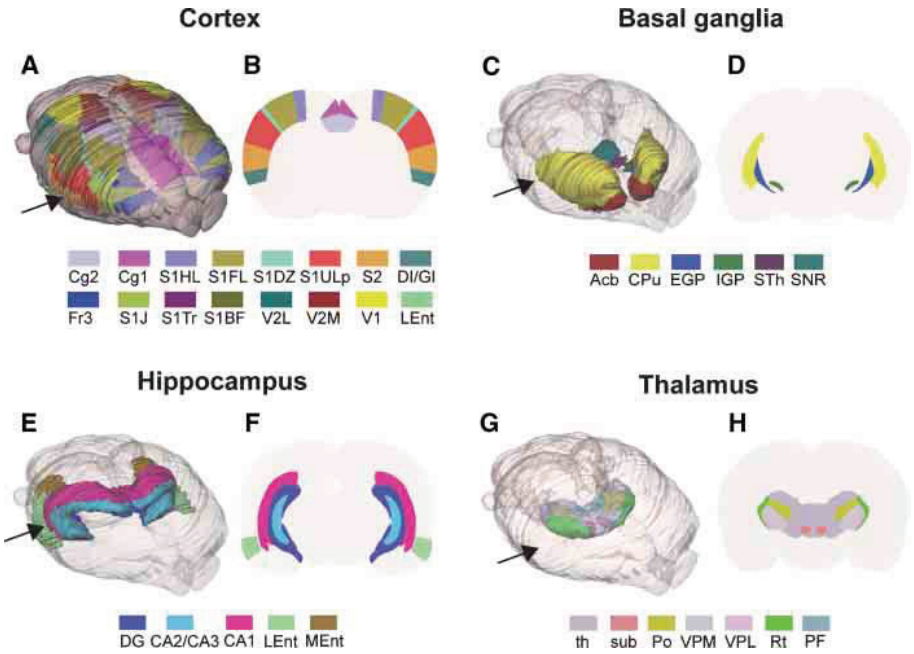


**Figure 2. Examples of rat brain regions included in the 3-D rat brain atlas**. *(**A–H**) Atlas representations of four major brain regions visualized as solid, color coded 3-D surfaces within the transparent outer surface of the brain, and as corresponding 2-D coronal slices, obtained from anteroposterior levels indicated by arrows. (**A, B**) 16 selected cerebrocortical brain regions. (**C, D**) Major regions of the basal ganglia. (**E, F**) Hippocampus and entorhinal cortex. (**G, H**) Selected sub-regions of the thalamus. In (**G**) thalamus (th) is made transparent in order to visualize the underlying sub-regions. Cg2, cingulate cortex area 2; Cg1, cingulate cortex area 1; S1, primary somatosensory cortex; S1HL, hindlimb region; S1FL, forelimb region; S1DZ, dysgranular zone; S1ULp, upper lip region; S2, secondary somatosensory cortex; DI/GI, insular cortex; Fr3, frontal cortex, area 3; S1J, jaw region; S1Tr, trunk region; S1BF, barrel field; V2L, secondary visual cortex, lateral area; V2M, secondary visual cortex, medial area; V1, primary visual cortex; Lent, lateral entorhinal cortex; Acb, accumbens nucleus; CPu, caudate putamen; EGP, external globus pallidus; IGP, internal globus pallidus; STh, subthalamic nucleus; SNR, substantia nigra; DG, dentate gyrus; CA2/CA3, field CA2 and CA3 of the hippocampus; CA1, field CA1 of the hippocampus; LEnt, lateral entorhinal cortex; MEnt, medial entorhinal cortex; th, thalamus, whole region; sub, submedius thalamic nucleus; Po, posterior thalamic nucleus; VPM, ventral posterolateral thalamic nucleus; VPL, ventral posteromedial thalamic nucleus; Rt, reticular thalamic nucleus; PF, parafasicular thalamic nucleus.*

dinates" by Paxinos and Franklin (2001) were 3-D reconstructed. The diagrams in Paxinos and Watson (2005) were derived from coronal sections spaced at intervals of 120 μm, all collected from a single Wistar rat brain. The diagrams in Paxinos and Franklin (2001) were obtained from a sample of 26 adult C57BL/J6 mice. Both atlases use the same stereotaxic coordinate system (Paxinos and Watson, 1982), structure nomenclature and abbreviations. The reconstruction procedure is here exemplified with use of the Paxinos and Watson (2005) atlas, but may be applied to any stereotaxic atlas providing digital drawings. The practical application of the reconstructed 3-D rat brain atlas is exemplified on basis of a set of MRI and PET data.

### 3-D atlas reconstruction and visualization

The coronal atlas of Paxinos and Watson (2005) provides digital diagrams (EPS format; **Figure 1A**) containing separate information layers (i.e., stereotaxic coordinate grid, structure names, and boundary lines). All diagrams were organized in separate layers and aligned to the stereotaxic grid of the atlas using Adobe Illustrator CS2 (Adobe Systems Inc., San Jose, CA). Regions of interest (ROIs, defined by closed boundary lines in the atlas) were segmented in relevant diagrams by assigning a specific color (**Figure 1B**). Occasionally, structures lacked unequivocally defined or closed boundaries, and contour lines were closed arbitrarily after following a set of predefined rules. Each segmented layer was exported separately as an image (TIFF) file to Amira 4.0 (Mercury Computer Systems Inc., Chelmsford, MA) for 3-D reconstruction. Since the export function in Illustrator is based on what is visible in the figure, all other layers and sub-layers were hidden. All exported images were enclosed by a standard invisible (white) rectangular frame, representing the stereotaxic X,Y space for each diagram, to ensure identical dimension and positioning of objects. Anterioposterior positions (Z-values) were defined by the bregma values given in the atlas diagrams. These values were entered upon loading stacks of image files to Amira, resulting in a 3-D atlas reconstruction aligned according to the stereotaxic framework of the atlas. Image colormaps (RGBA-tupels) were converted to intensity values represented as gray scale images, and voxels were assigned to the different structures using the "LabelVoxel" tool in Amira, employing thresholding algorithms (**Figure 1C**). Surfaces were rendered using the Amira SurfaceGen tool and exported as VRML (Virtual Reality Modeling Language) files. A custom Java3D visualization tool (m3d) was developed to import and visualize the VRML atlas structures (Figures **1D**, and **2**) as well as tomographic image data (PET or MRI) in NIfTI (Neuroimaging Informatics Technology Initiative, http://nifti.nimh.nih.gov) file format. The volumetric image data were visualized using texture mapping with transparency and thresholding applied to Texture3D Java3D class, and displayed in m3d together with the 3-D atlas structures. In addition, 2-D user-defined slices, prepared at any angle and orientation, of both the atlas (performed by ModelClip Java3D

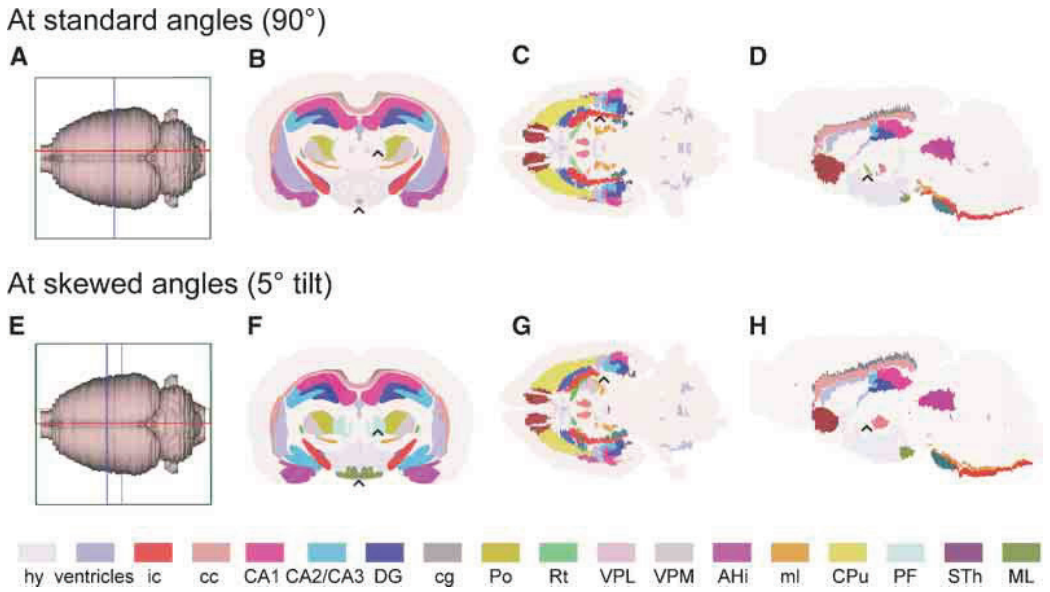


**Figure 3. Customized atlas diagrams**. *Series of customized, color coded coronal (**B, F**), horizontal (**C, G**), and sagittal (**D, H**) atlas diagrams, generated using the slicing and filling module in the atlas tool. Blue, red, and green bounding boxes in (**A, E**) indicate the levels from which the respective slices were obtained. (**A–D**) Standard orientation of atlas slices, oriented perpendicularly to axes of the stereotaxic coordinate system. (**E–H**) Example of atlas slices cut at non-standard angles, tilted 5 degrees from the planes used in (**B–D**). Black arrow heads indicate examples of structural differences between the corresponding diagram pairs, emphasizing the importance of having atlas diagrams with similar orientation as experimental slices. hy, hypothalamus, whole region; ic, internal capsule; cc, corpus callosum; CA1, field CA1 of the hippocampus; CA2/CA3, field CA2 and CA3 of the hippocampus; DG, dentate gyrus; cg, cingulum; Po, posterior thalamic nucleus; Rt, reticular thalamic nucleus; VPL, ventral posteromedial thalamic nucleus; VPM, ventral posterolateral thalamic nucleus; AHi, amygdalohippocampal area; ml, medial lemniscus; CPu, caudate putamen; PF, parafasicular thalamic nucleus; STh, subthalamic nucleus; ML, medial mammillary nucleus.*

class extended by a cutting and contour-filling algorithm; **Figures 2 and 3**) and the image data were generated.

### Image import and co-registration

Co-registration of experimental image data to atlas space can be achieved in several ways. The present version of the m3d program allows affine transformations that are implemented with use of a transformation tool interface for defining scaling, rotation, and translation. As exemplified below, co-registration is based on recognizable brain or skull landmarks, and different strategies may be employed depending on the nature of the image data. The precision of co-registration critically depends on the precision with which anatomical landmarks may be detected, which in turn also depends on voxel size and structural contrast (see also Discussion). Size and shape differences that may occur due to individual variation or by extraction of the brain from its enclosed position in the skull, can be adjusted by non-linear transformation (not included in the present software), or by limiting the co-registration to smaller ROIs.

### Animal experiments

Animal procedures were approved by institutional animal welfare committees at the University of Oslo or Massachusetts General Hospital, and were in compliance with National Institutes of Health guidelines for the use and care of laboratory animals. During all experiments body temperature was kept constant by the means of feedback regulated heating pads. Eye ointment was applied in order to prevent dehydration of the cornea.

***In vivo pathway tracing with $Mn^{2+}$-enhanced MRI.*** MR images were obtained at the Massachusetts General Hospital NMR-Center using a 3 Tesla Trio whole body human scanner (Siemens Medical Solutions, Iselin, NJ). Adult male Sprague–Dawley (SD) rats (Taconic farms, Germantown, NY) were anesthetized with urethane (Abbott, Chicago, IL; 1.2 g/kg i.p., with 10% supplements during surgery as needed). This provided stable anesthesia for the entire imaging session (see also Field et al., 1993). Animals were monitored by pulse oximetry, and body temperature was maintained at 37°C by a water-circulating heating pad (Gaymar T/Pump; Gaymar Industries, Orchard Park, NY). The $T_1$ contrast agent manganese ($Mn^{2+}$) was applied as outlined in Leergaard et al. (2003). Briefly, animal heads were immobilized in a stereotaxic frame, a small opening was made in the skull and dura overlying the SI cortex, and ~10 nl of an aqueous solution of 2.0 M manganese chloride ($MnCl_2$; ICN Biomedicals Inc., Aurora, OH) was slowly injected 1.0 mm below the pial surface through a glass pipette mounted on a 1.0 μl Hamilton syringe placed in a microinjection unit (Kopf 5001, Kopf Instruments, Tujunga, CA). Locations of injection sites were stereotaxically defined according to published topographical maps (Chapin and Lin, 1984). MR images were obtained using the (human) body RF coil for excitation, and a custom made loop surface receiver coil. $T_1$ weighted volumetric images were obtained using a 3-D FLASH sequence with TR/TE/flipangle = 44 ms/13.37 ms/40 degrees. Images were obtained with 195 μm isotropic voxels, field of view = 50 × 50 × 50 $mm^3$, matrix = 256 × 256 × 256, with a scan time of 48 minutes and 4 seconds. The animals were scanned continuously, starting within an hour after the $MnCl_2$ injection, and continuing up to 8–9 hours after injection. At the end of the imaging experiments, animals were euthanized with an overdose of sodium pentobarbital (200 mg/kg).

To optimize visualization of the brain surface, the soft tissue surrounding the brain was stripped away from the raw MR images using PMOD software (PMOD Technologies Ltd., Zurich, Switzerland). The trimmed MR images were imported to the 3-D atlas tool (**Figures 4D and 4G**) and globally fitted to atlas space using affine transformations,

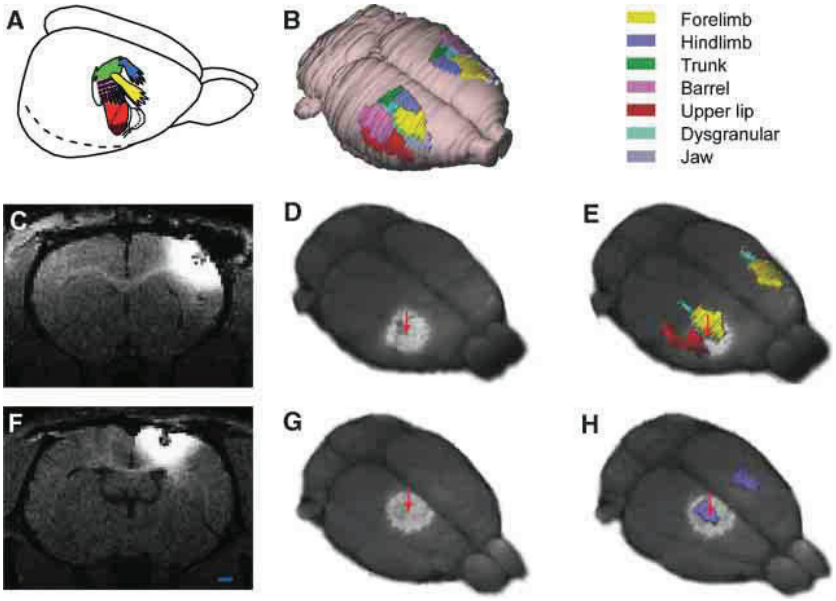


**Figure 4. MRI and 3-D atlas based localization of $MnCl_2$ injection sites in the cerebral cortex**. *(**A**) Color coded drawing of major body representations in the primary somatosensory cortex (SI), modified from Welker (1971), with permission. (**B**) 3-D reconstructed atlas representation of the brain surface with SI regions indicated in corresponding colors. (**C–E**) and (**F–H**) show two different examples, in which $MnCl_2$ was stereotaxically aimed at the forelimb or hindlimb representations of SI, respectively. (**C, F**) Raw $T_1$-weighted MRI images acquired 9 hours after focal application of $MnCl_2$. At the point of injection a central zone of low signal intensity is visible, surrounded by a halo of bright signal enhancement. (**D, G**) 3-D reconstructed MRI volume registered to atlas space, showing $Mn^{2+}$ signal enhancement surrounding the injection sites (arrows). (**E, H**) The same images combined with atlas reconstructions of relevant SI body representations. Comparison of injection site locations with the atlas surface reconstructions revealed that one injection is centered on the dysgranular zone lateral to the SI forelimb representation, while the other injection is centered on the SI hindlimb representation. Bar, 1 mm.*

based on measurements of multiple anatomical landmarks recognizable in the images (brain surface and midline, the genu and splenium of the corpus callosum, the decussation of the anterior commisure, the ventricular system, the boundary between the cortical gray matter and underlying white substance, the external boundaries of the hippocampus, the caudate putamen complex, the optic chiasm, the substantia nigra (intercalated between the cerebral peduncle and the medial lemnisc), and the rostral boundary of the pontine nuclei). Because the *in vivo* position of the cerebellum and of the flaccid brain stem caudal of the pons clearly differed from the atlas, these structures were disregarded in the alignment procedure. For this dataset, the spatial displacement of the different image landmarks with respect to corresponding atlas landmarks, was measured to 164 $\mu$m $\pm$ 23 SEM, (range of 11–446 $\mu$m), which is at the level of the resolution of the image data (voxel size = 195 $\mu$m). The size and location of the $MnCl_2$ injections were analyzed by 3-D combined visualization of the MR based representation of the brain surface and the atlas representations of different cerebrocortical areas (**Figures 4E and 4H**). The position of $Mn^{2+}$ signal enhancement within the thalamus was analyzed by slicing the combined image and atlas volumes in 200 $\mu$m thick slices using the m3d tool (**Figures 5D, 5E, 5I, and 5J**).

***PET experiments.*** PET data were acquired at the Small Animal Imaging Unit of the Center for Molecular Biology and Neuroscience, University of Oslo, Norway, with use of a small animal PET scanner (microPET Focus 120, Siemens Medical Solutions, Erlangen, Germany). Accompanying computer tomography (CT) data were collected with a small animal CT scanner (microCAT, Siemens Medical Solutions, Erlangen, Germany). The microPET scanner provides high sensitivity (6.5%) and high spatial resolution (<1.3 mm; Kim et al., 2007). A multi-modality animal bed was used to collect data with both the PET and CT scanner without re-positioning the animal.

Three different kinds of PET-data were imported to the 3-D atlas tool: individual dopamine D2/D3 receptor binding data acquired using [$^{18}$F]-fallypride, individual brain and glioma tumor glucose metabolism data acquired using [$^{18}$F]-fluorodeoxyglucose (FDG), and statistical parametric mapping (SPM) group data collected from a study of brain activity during nociceptive conditioning using FDG.

***Individual PET receptor binding data.*** SD rats (National Lab Animal Center, Oslo, Norway) weighting 200–250 g, were anesthetized by inhalation of isoflurane 2% (Abbott Laboratories, Illinois, USA). 20 MBq [$^{18}$F]-labeled fallypride (Department of Chemistry, University of Oslo, Norway) was injected intravenously, and the rats were scanned for 180 minutes. Data were collected in list mode and reconstructed using 3-D OSEM-MAP (Jinyi and Leahy, 2000; Jinyi et al., 1998) (2 OSEM iterations, 18 MAP iterations, $\beta = 0.5$, $128 \times 128 \times 95$ matrix size, $0.87 \times 0.87 \times 0.80$ mm$^3$ voxel size). Two image volumes were extracted from the acquired scans: a sum image of the first 5 minutes of the scan reflecting tracer delivery ("perfusion") and a late scan sum image (60–180 minutes) representing the D2/D3 receptor binding of [$^{18}$F]-fallypride. Data were imported and globally aligned to the atlas space in m3d on basis of the "perfusion" image showing the external boundaries of the brain, as well as the receptor binding image, showing a negative image of the brain surface (**Figures 6A–6D**).

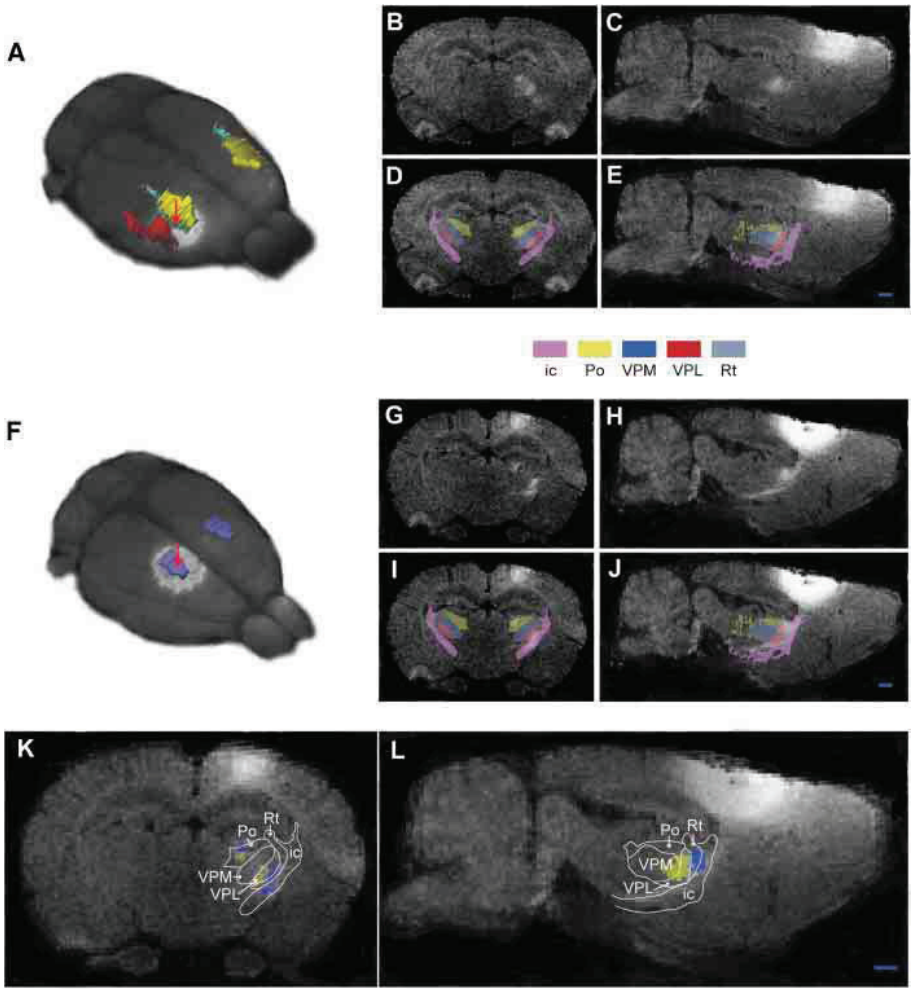


**Figure 5. Corticothalamic topographical organization revealed by $MnCl_2$/MRI tracing and 3-D atlasing**. *Two cases are shown, case 1 (**A–E**), in which $MnCl_2$ was injected in the dysgranular zone adjacent to the SI forelimb representation (**A**), and case 2 (**F–J**), in which $MnCl_2$ was injected in the hindlimb representation of SI. (**B, C** and **G, H**) Raw coronal and sagittal $T_1$-weighted MRI images obtained 9 hours after injection. (**D, E** and **I, J**) Corresponding images with overlay of selected reconstructed atlas structures. (**K, L**) Superimposed, pseudocolored images (case 1, yellow; case 2, blue) with an overlay of atlas derived boundary lines, demonstrating a somatotopical organization of the different signals within the Po and VPM. ic, internal capsule; Po, posterior thalamic nucleus; VPM, ventral posterolateral thalamic nucleus; VPL, ventral posteromedial thalamic nucleus; Rt, reticular thalamic nucleus. Bar, 1 mm.*

***Individual FDG-PET and CT data.*** Inbred BDIX rats (body weight > 220 g; Harlan Olac Ltd. Bicester, UK) were used. The animals were anesthetized by subcutaneous injection (2 ml/kg) of a mixture of equal volumes of Hypnorm (fentanyl citrate 5 mg/mL, Janssen L.P., High Wycombe, UK) and Dormicum (midazolam 5 mg/mL, Hoffmann-La Roche Ltd., Basel, Switzerland). Fifteen days prior to the FDG-PET scan, 50.000 glioma cells ($BT_4$Ce gliomasarcoma cell line) were inoculated. The inoculation was performed with the animal fixed in a stereotaxic frame and injected with a 30G blunt needle through a 1.0 mm burrhole. FDG (GE Healthcare AS, Oslo, Norway) was injected intravenously and the animals were scanned for 60 minutes. Attenuation correction was obtained by a 10 minute transmission scan with a $^{68}$Ge point source prior to injection. Data were collected in list mode and reconstructed using 3-D OSEM-MAP (2 OSEM iterations, 18 MAP iterations, $\beta = 0.5$, 128 × 128 × 95 matrix size, 0.87 × 0.87 × 0.80 mm$^3$ voxel size). The animals were then transferred to the CT scanner utilizing the multi-modality bed ensuring the same position of the head. CT images were acquired using the same settings for all studies (80 kVp, 0.5 mA, 400 ms, 360 degrees rotation). Data were reconstructed using Feldkamp reconstruction (512 × 512 × 512 matrix size, 0.1 × 0.1 × 0.1 mm$^3$ voxel size). The FDG-PET and CT data were co-registered in PMOD, re-slicing the resulting PET image to match the matrix and resolution of the CT volume. The CT data were imported into m3d and linearly fitted to atlas stereotaxic space on basis of the readily identifiable bregma and interaural line (**Figures 6I and 6J**). The same transformation parameters as for the CT data were used to fit the FDG-PET data set into exactly the same atlas space (**Figure 6L**).

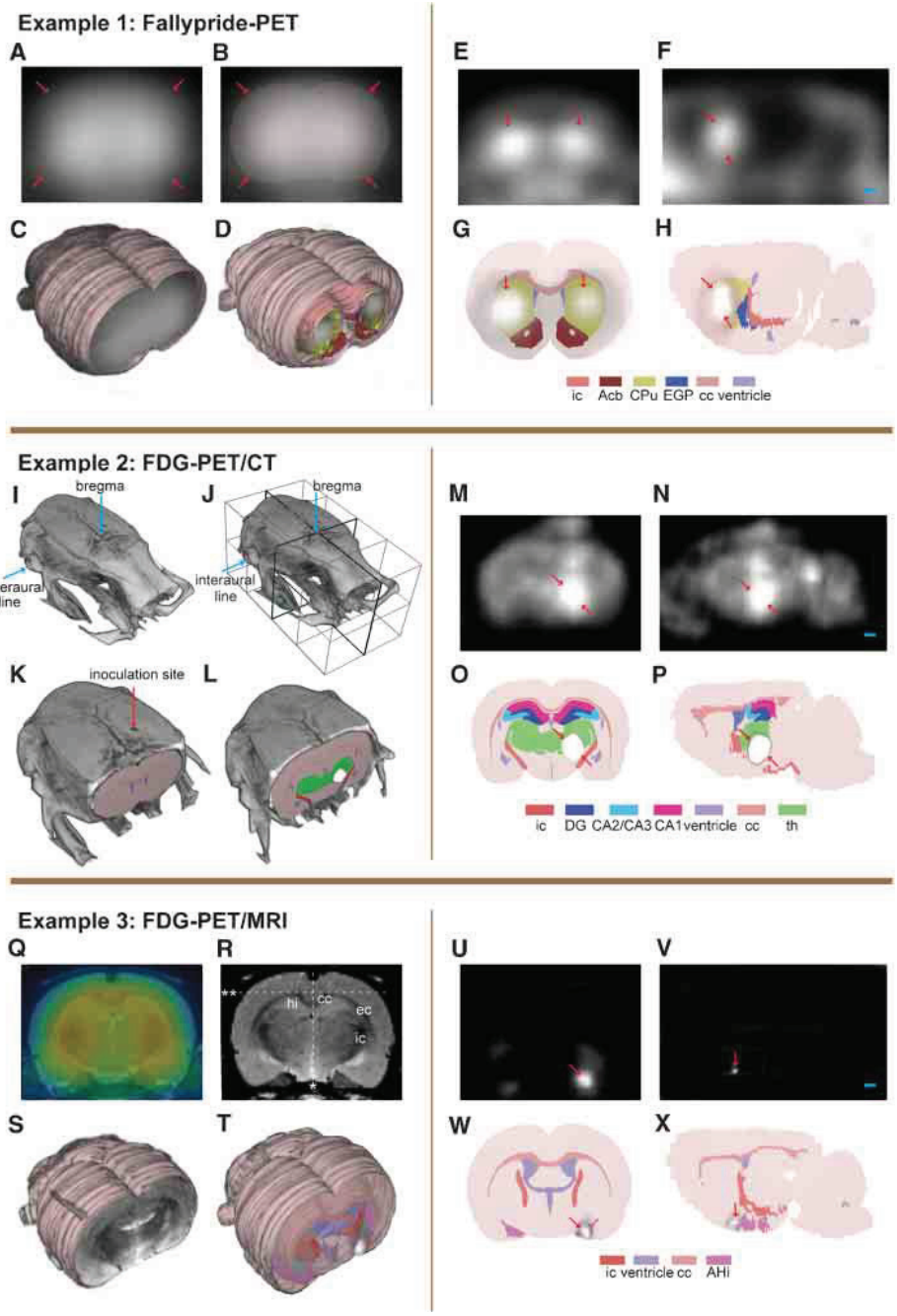


**Figure 6.** (***Continued***).

***SPM group results.*** Twenty female SD (National Lab Animal Center, Oslo, Norway) rats weighing 200–250 g, were adapted for minimum 10 days to the environment and given food and water *ad libitum*. For the experiments, the animals were anesthetized by inhalation of 2% isoflurane (Abbott Laboratories, Illinois, USA) and divided into two groups; nociceptive stimulation condition ($n=10$) and sham ($n=10$). In addition, all animals were scanned at baseline. FDG (20–25 MBq; GE Healthcare AS, Oslo, Norway) was injected through the tail vein and all animals were scanned for 60 minutes. Attenuation correction was obtained by a 10 minutes transmission scan with a $^{68}$Ge point source prior to FDG injection. Data were collected in list mode and dynamically reconstructed using 3-D OSEM-MAP (2 OSEM iterations, 18 MAP iterations, $\beta=0.1$, $128 \times 128 \times 95$ matrix size, $0.87 \times 0.87 \times 0.80$ mm$^3$ voxel size). Statistical comparisons (paired *t*-test stimulation-baseline) between the two groups were performed with SPM5 (Statistical Parametric Mapping, http://fil.ion.ucl.ac.uk/spm) after intra-subject co-registration and spatial normalization to a MRI template fitted to Paxinos and Watson atlas space (Schweinhardt et al., 2003; **Figure 6Q**). Significance was accepted at the 5% level. Localization of statistical significant activity was defined by the use of the 3-D atlas model. The MRI template was aligned with the atlas model in m3d (**Figures 6R and 6S**) by the means of identifiable anatomical landmarks (outer boundaries of the brain surface, gray and white matter contrast, genu and splenium of the corpus callosum, outer boundaries of the hippocampus and caudate putamen, and the ventricle system). Since spatial normalization between the PET data and the MRI template was already performed in SPM5, the same linear transformation obtained from the alignment could be applied to the PET data (**Figure 6T**).

## RESULTS

We have developed a procedure for 3-D reconstruction of a series of 2-D diagrams from conventional brain atlases. The 3-D reconstructed atlases are displayed and utilized in a multi-platform tool (m3d), prepared to include experimental data of different formats (i.e., JPEG, PNG, VRML, and NIfTI). The focus of the present report is to exemplify how a relatively straightforward atlas approach may be useful for the neuroanatomical analysis in the context of import of whole brain MRI and PET data.

The 3-D rat brain atlas currently includes 60 structures, while 30 structures have been incorporated in the 3-D mouse brain atlas. The structures included are the outer boundaries of the brain and areas, zones and nuclei of the cerebral cortex, hippocampus, basal ganglia, thalamus, amygdala, as well as major fiber tracts (**Figures 2A, 2C, 2E, and 2G**). The m3d atlas visualization tool allows interactive inspection of selected 3-D reconstructed structures as well as user-defined slicing to create customized 2-D atlas diagrams at any position and angle of orientation. This feature is particularly suitable for comparison with experimental data cut at angles different from the standard coronal, sagittal, or horizontal orientations used in printed brain atlases (**Figures 3E–3H**).

The current version of the m3d tool allows import of image data and subsequent registration of images to atlas space by interactive scaling, rotation, and translation on basis of recognizable landmarks. Depending on the modality of the experimental data, the alignment can be performed globally for the entire whole brain data set, using the outer boundaries of the brain as a template, and/or locally for parts of the whole brain data set, utilizing smaller readily identifiable landmarks in the brain. In addition, the quality of the registration can be enhanced by a step-by-step alignment of the atlas and image data with use of slicing at different locations and angles. In m3d, co-registered image and atlas representations can be co-visualized as 3-D objects and in 2-D custom defined slices.

In the following, we exemplify the use of the 3-D atlas for assigning location to MRI and PET image volumes.

### MRI example

To illustrate the use of the 3-D atlas to assign location to discrete structural signals observed with MRI, we here describe two experiments in which high-resolution *in vivo* $MnCl_2$/MRI pathway tracing (see e.g., Leergaard et al., 2003; Pautler et al., 1998; Saleem et al., 2002) was used to visualize specific corticothalamic connections, and 3-D atlasing was used to assign location to tracer injection sites and observed signal enhancement. To evaluate the position of injection sites and the corticothalamic signal enhancement, the two MR image volumes were registered to atlas space on basis of multiple recognizable anatomical landmarks and affine transformations.

In the two example experiments, $MnCl_2$ was injected on basis of stereotaxic coordinates, respectively aimed at the forelimb or hindlimb representations of the primary somatosensory cortex (SI). When the animals were scanned ~9 hours after the injection, injection sites were visible in the $T_1$-weighted images as bright regions, surrounding a core with low signal intensity, presumably associated with high concentration of $Mn^{2+}$ (**Figures 4C and 4F**; see also discussion in Leergaard et al., 2003). $Mn^{2+}$ signal enhancement was observed at multiple cortical and sub-cortical locations, as reported in Leergaard et al. (2003). Discrete $Mn^{2+}$ signal enhancement was observed in the internal capsule (ic) and at multiple sites within the thalamus (**Figures 5B, 5C, 5G, and 5H**).

Co-visualization in m3d of the co-registered MR image volumes and atlas reconstructions of SI body representations (**Figures 4D–4H**) demonstrated that the injection site center in one example was located slightly outside the targeted forelimb representation (**Figure 4E**), and in the other example that the injection site center was located centrally in the hindlimb representation (**Figure 4F**). Identical results were obtained with use of manual measurements of the mediolateral and anterioposterior distances from the injection site centers to the midline and the genu and splenium of the corpus callosum in the MR images. The manual measurements were converted to stereotaxic coordinates using the printed atlas of Paxinos and Watson (2005), and compared to known functional maps of SI (Chapin and Lin, 1984).

To evaluate the location of $Mn^{2+}$ signal enhancement within the thalamus, series of contiguous 200 μm thick coronal and sagittal slices were obtained from the combined atlas and MRI volume. Overlay images of

**Figure 6. Alignment and localization of PET data**. *Example 1: (**A–C**) perfusion image of [$^{18}$F]-fallypride image was used for alignment to 3-D atlas space. Arrows indicating surface boundaries. (**D**) Receptor binding image co-registered with the 3-D atlas model. (**E, F**) [$^{18}$F]-fallypride-PET coronal and sagittal images showing high-uptake regions. (**G, H**) Coronal and sagittal atlas sections localizing the high-uptake PET signals to the basal ganglia. Example 2: (**I, J**) Bregma and the interaural line in the CT volume. (**K**) CT volume aligned with the 3-D atlas model. (**L**) FDG-PET signal aligned with the 3-D atlas on the basis of the same transformation matrix as for the CT volume. (**M, N**) Coronal and sagittal PET images showing high-uptake of FDG in the brain tumor. (**O, P**) Coronal and sagittal atlas diagrams locating the brain tumor in the right thalamic region. Example 3: (**Q**) co-registered FDG-PET image (colors) and MRI template. (**R, S**) MRI template aligned to the 3-D atlas space on the basis of defined landmarks. *, midline; **, upper boundary of cc. (**T**) SPM result volume aligned with atlas space using the transformation matrix obtained from the MRI alignment. (**U, V**) Coronal and sagittal SPM result images showing statistical significant voxels ($p < 0.05$). (**W, X**) Coronal and sagittal atlas diagrams locating the significant signal to the rostral part of the amygdala. ic, internal capsule; Acb, accumbens nucleus; CPu, caudate putamen; EGP, external globus pallidus; cc, corpus callosum; DG, dentate gyrus; CA2/CA3, field CA2 and CA3 of the hippocampus; CA1, field CA1 of the hippocampus; th, thalamus, whole region; hi, hippocampal region; ec, external capsule; AHi, amygdalohippocampal area. Arrows indicate boundaries of regions with increased PET signal. Bar, 1 mm.*

relevant atlas structures (thalamic sub-nuclei and the internal capsule) and MR images allowed atlas based anatomical segmentation of the MR images (**Figure 5**). Thus, aided by the atlas overlay, it was possible to distinguish $Mn^{2+}$ signal enhancement located in the internal capsule and within the posterior complex thalamus (Po) and the ventral posterolateral nucleus thalamus (VPL) in both examples. Combined analysis of the two data sets further allowed assessment of topographical organization at a finer scale (**Figures 5K and 5L**). This analysis clearly demonstrated that the discrete clusters of signal enhancement where primarily distributed within the boundaries of Po and VPL (**Figure 5K**), with an inside-out relationship corresponding to the well known internal to external somatotopic distribution of hindlimb and forelimb representations in these thalamic sub-nuclei (Fabri and Burton, 1991). Signal enhancement was also seen in the reticular thalamic nucleus (**Figure 5K**), presumably representing pathways *en route* to the Po and VPL. Furthermore, in our first example (**Figures 5B–5E**) some signal enhancement was also observed in the ventral posteromedial thalamic nucleus (VPM), known to hold representations of the face (Fabri and Burton, 1991). This finding is presumably related to the location of the injection site center in the dysgranular zone between the forelimb and face representations in SI. We conclude that the present 3-D atlas approach provided an anatomical segmentation of the observed signal enhancement sufficiently accurate to resolve finer details of the well-known topographical organization found within sub-nuclei of the thalamus (see e.g., Deschenes et al., 1998; Fabri and Burton, 1991; Price, 1995).

### PET examples

To illustrate the use of the 3-D atlas to assign location to PET data (**Figure 6**), we have used three different sets of experimental data.

***Individual PET receptor binding data.*** The [$^{18}$F]-fallypride data set represents the D2/D3-receptor binding in the brain. The receptor binding image itself contains little anatomical information and could not be aligned to atlas space (**Figures 6E and 6F**). "Perfusion" images of early frames representing the initial hematogeneous tracer distribution were used (**Figures 6A–6C**) to facilitate alignment, since these data show the external contours of the cerebrum and cerebellum, as well to a certain degree the outlining of the basal ganglia using different levels of voxel intensity scaling. The same transformation parameters were then used to fit the receptor binding image into the atlas space in m3d (**Figure 6D**). Visualization of the receptor binding showed the highest density of dopamine D2/D3 receptors to be present in the basal ganglia (**Figures 6G and 6H**). Only a course alignment of the experimental data with the atlas was possible due to limited structural information. A further judgment of details of distribution was not deemed possible with the present approach.

***Individual FDG-PET and CT data.*** FDG is a glucose analog and FDG-PET images represent the rate of glucose metabolism of the cells. Cancer cells mostly utilize more glucose than healthy tissue and tumors can therefore be located as regions with high uptake of FDG in a PET scan (**Figures 6M and 6N**). To be able to decide the size, extent, and location of the brain tumor, the co-registered CT image was imported and aligned to the 3-D atlas space in m3d using the location of bregma and the interaural line which could be readily defined in the CT volume (**Figures 6I and 6J**). The inoculation site for the glioma cells is shown in **Figure 6 K**. The same transformation matrix was applied to the FDG-PET volume in order to fit the data to atlas space (**Figure 6L**). The increased FDG signal defining the brain tumor was located in the right thalamic region. The quality of the alignment procedure was in this case considerably enhanced by utilizing CT as a complementary imaging modality. The readily identifiable bregma and the interaural line provided concrete landmarks which could be aligned in 3-D atlas space. Inaccuracies can occur due to inter-subject variations in brain shape and size, and due to the fusion procedure of the PET and CT data prior to import into m3d.

***SPM group results.*** SPM delivers a result volume (cluster of voxels) at a specified statistical significance value (**Figures 6U and 6V**). This parametric volume was already fitted to the space of a defined anatomic template. The MRI template was imported and aligned to the 3-D atlas space in m3d by the aim of well-defined landmarks, i.e., white matter and the contours of the brain (**Figures 6R and 6S**) The same parameters were applied to the significant parametric volume in order to fit the data to the atlas space (**Figure 6T**). The nociceptive conditioning is an aversive and stressful event, in which amygdala play a crucial role (Sah et al., 2003). After alignment, a significant effect of nociceptive conditioning could be localized to the rostral volume of the amygdala (**Figures 6W and 6X**). The alignment of the MRI template to the 3-D atlas space was performed using a best-fit approach based on large brain regions. Due to variations in the rat brain shape and size, a perfect fit is difficult to obtain. If focusing on specific areas within the brain, the transformation parameters might be altered using smaller local sub-regions as alignment landmarks. However, the resolution of microPET and averaging over several individuals has an inherent inaccuracy limiting the detailed localization and separation of smaller effects to specific, smaller sub-nuclei of any rat or even mouse brain structure. Once the MRI-template has been sufficiently aligned to a 3-D atlas, the same transformation routine and result reading can be established for all data processed with statistical parametric mapping. The 3-D atlas makes the data processing and interpretation less observer dependent. As shown in **Figures 6T–6X**, the 3-D atlas ensures a sufficiently precise allocation of a statistical significant result to a brain area in relation to neighboring structures.

## DISCUSSION

We present a multi-platform tool that provides a new dynamic and analytical environment for comparing experimental image data to a seminal atlas reconstructed in 3-D. Our 3-D reconstruction procedure was applied to two commonly used rodent brain atlases, but could be applied to other atlases as long as they provide diagrams from sections with limited distortions, mapped into a stereotaxic coordinate system. We further demonstrate how the atlas tool can be used to align 3-D data of different origin (PET, PET/CT, and MRI) to the same atlas space, facilitating analysis of localization in the experimental data.

In the example analyses provided, variable amounts of information was available to assist the user with the registration of the experimental data to the 3-D atlas space. The most limited structural information was present in the receptor binding PET data. The global registration performed for these data, based on the outer contours of the brain visible in the early frames recorded, was nevertheless sufficient to identify the caudate-putamen as the region containing the highest [$^{18}$F]-fallypride receptor binding, in agreement with legacy data (Mukherjee et al., 1995). The acquisition of CT images in register with the experimental PET images facilitated the atlas registration considerably, since skull landmarks (readily detected with CT) could be directly mapped to the atlas coordinate space (which is based on the same skull landmarks). Use of MRI in combination with PET is an emerging new approach (Judenhofer et al., 2007). In our analyses, we demonstrate an indirect MRI-based co-registration procedure. With this procedure, the data sets were aligned to a common MRI template, which in turn was registered to the 3-D atlas. In this example, the location of the statistically significant increased activity was found in the expected location in the brain, in our case the amygdala following a nociceptive conditioning (Sah et al., 2003). Finally, direct import of experimental MRI data can be done with a high accuracy since a range of landmarks in the brain are visible in the MRI data. Our high-resolution $MnCl_2$/MRI examples demonstrate the mapping of fine-scale topographical organization within thalamic sub-nuclei (see also Leergaard et al., 2003), corresponding with previous maps of the thalamus (Fabri and Burton, 1991).

The general validity of the linear co-registration approach used in the present study is indirectly demonstrated by the replication of known findings in the shown examples. For example, in the FGD-PET/MRI example,

the majority of the observed PET signal is largely confined to the rostral part of the amygdala, in accordance with Sah et al. (2003). In the $MnCl_2$/MRI example, in which several anatomical landmarks were seen in the MR images, the mean spatial displacement between anatomical landmarks in atlas and image volume was found to be less than the size of one voxel. This correspondence is at a level sufficient to study topographical organization within sub-nuclei. The major displacement between atlas and images in this example, not corrected for in our approach, was found in the hindbrain. This displacement appears to be due to a dislocation of the hindbrain occurring at the time of extraction of the brain from the skull. Further analyses of the hindbrain would therefore require a second step of registration in which the hindbrain is treated in isolation from the remaining part of the brain. Adjustment for size variation alone will clearly facilitate comparison of brain stem data from different rat brains (Brevik et al., 2001; Leergaard et al., 2000). Thus, for tomographic material of the quality here exemplified, our linear procedures appear to provide sufficient accuracy to resolve most questions related to localization of data and comparison between animals. More optimized co-registration of multiple detailed anatomical landmarks derived from histological images (Lein et al., 2007; Toga et al., 1995) or high-resolution structural MRI (Ali et al., 2005; Badea et al., 2007; Benveniste et al., 2000; Ma et al., 2005) would require the use of non-linear methods.

An important feature of the 3-D atlas tool provided is the ability to co-register image data to an atlas framework. The m3d tool supports the import of voxel data in NIfTI file format, which allows import of volume data such as PET, CT, and MRI. Future developments will include other data formats. As discussed above, several approaches can be employed for aligning image data to atlas space. In m3d, image data can be linearly transformed (i.e., transformed with rotation, scaling, and translation) in order to fit the 3-D atlas space. The transformation matrix is calculated based on identifiable landmarks in the image data. A PET image volume typically lacks well-defined structural information which may complicate the alignment. The quality of the co-registration may be enhanced when the researcher has access to other modalities such as MRI and/or CT. The alignment of an MRI volume is based on anatomical landmarks such as the outer boundaries of the brain and white matter. In a CT volume, the definition of bregma and the interaural line provides a rigid aid in calculating the transformation matrix. Since the present approach is based on linear transformations only, local alignment errors may occur due to inter-subject variations in rodent brain shape and size. High-resolution MRI based probabilistic atlasing of the mouse brain indicate that this variation is relatively low (average structure volume variation coefficient in the order of 7%; Badea et al., 2007; Ma et al., 2005). Given that such variations may be partly compensated for by linear transformations, the need to adjust for remaining variability must be viewed in relation to the resolution employed in the tomographic image volumes to be analyzed.

The present approach, with a common analytical environment for experimental data and 3-D atlas reconstructions, not only facilitates direct assignment of anatomical location, but may also be useful in the context of generating probabilistic representations of the brain. Probabilistic maps are typically based on manually segmented cases, but may also incorporate information from reconstructed atlases. Co-registration of manually segmented cases into a common atlas space would thus enable the construction of a probabilistic atlas, containing *a priori* probabilities of various anatomical structures at each location in atlas space. Such a probabilistic atlas, in combination with the image contrast properties of different structures, can in turn be used to automate the process of anatomical segmentation (Ali et al., 2005; Fischl et al., 2002).

A major advantage of reconstructing standard stereotaxic atlases (rather than constructing new customized atlases) is the wide recognition and use, and the high-resolution and comprehensive nomenclature, of these atlases. Similarly, for human brain imaging data, the frequently used reference atlas space (Talairach and Tournoux, 1988) has been made available in many different formats in order to have a common reference space in the scientific community. Digital versions of the human brain atlas exist in three orthogonal planes with a high-speed database server for querying and retrieving data about human brain structures over the internet (ric.uthscsa.edu/projects/talairachdaemon.html). The present application of the 3-D atlases of the rat and the mouse brain makes it simpler and more reliable to use these atlases in combination with 3-D imaging modalities, and to bring data from different modalities into the same environment. A further challenge would be to bring different tomographic data modalities together with primarily 2-D histological or other section-based data, such as optical imaging data and autoradiography. At present, the skull-based stereotaxic coordinate system of Paxinos and Watson (1982) would seem to be a suitable common reference space.

### Tools availability

Information on the availability of tools and atlas data can be found at The Rodent Brain Workbench (http://rbwb.org).

## CONFLICT OF INTEREST STATEMENT

The authors declare that the research was conducted in the absence of any commercial or financial relationships that could be constructed as a potential conflict of interest.

## ACKNOWLEDGEMENTS

Funded by grants from The Research Council of Norway to J. G. B., T. B. L., and F. W., and grants from the NIH (R01-EB00790, U24-RR021382) to A. M. D. We thank Bent Schoultz and Gjermund Henriksen, Department of Chemistry, University of Oslo, for synthesis of [$^{18}$F]-fallypride, Dag R. Sorensen and Hong Qu for expert technical assistance related to PET/CT scanning, Anna Devor and Andre van der Kouwe for expert technical assistance related to MnCl2/MRI tracing, and Johan F. Storm for valuable discussions and facilitation of the present project.

## REFERENCES

Ali, A. A., Dale, A. M., Badea, A., Johnson, G. A. (2005). Automated segmentation of neuroanatomical structures in multispectral MR microscopy of the mouse brain. *Neuroimage* 27, 425–435.

Badea, A., Ii-Sharief, A. A., and Johnson, G. A. (2007). Morphometric analysis of the C57BL/6J mouse brain. *Neuroimage* 37, 683–693.

Benveniste, H., Kim, K., Zhang, L., and Johnson, G. A. (2000). Magnetic resonance microscopy of the C57BL mouse brain. *Neuroimage* 11, 601–611.

Boline, J. K., MacKenzie-Graham, A. A., Shattuck, D. W., Yuan, H., Anderson, S. P., Sforza, D. M., Wang, J., Williams, R. W., Wong, W., Martone, M. E., Zaslavsky, I., and Toga, A. W. (2006). A Digital Atlas and Neuroinformatics Framework for Query and Display of Disparate Data. Society for Neuroscience 2006. Abstract and itinerary viewer. Program No. 100. 12.

Brevik, A., Leergaard, T. B., Svanevik. M., and Bjaalie, J. G. (2001). Three dimensional computerised atlas of the rat brain stem precerebellar system: approaches for mapping, visualization, and comparison of spatial distribution data. *Anat. Embryol. (Berl.)* 204, 319–332.

Chan, E., Kovacevic, N., Ho, S. K. Y., Henkelman, R. M., and Henderson, J. T. (2007). Development of a high resolution three-dimensional surgical atlas of the murine head for strains 129S1/SvImJ and C57Bl/6J using magnetic resonance imaging and micro-computed tomography. *Neuroscience* 144, 604–615.

Chapin, J. K., and Lin, C. S. (1984). Mapping the body representation in the SI cortex of anesthetized and awake rats. *J. Comp. Neurol.* 229, 199–213.

Deschenes, M., Veinante, P., and Zhang, Z. W. (1998). The organization of corticothalamic projections: reciprocity versus parity. *Brain Res. Rev.* 28, 286–308.

Fabri, M., and Burton, H. (1991). Topography of connections between primary somatosensory cortex and posterior complex in rat: a multiple fluorescent tracer study. *Brain Res.* 538, 351–357.

Field, K. J., White, W. J., and Lang, C. M. (1993). Anaesthetic effects of chloral hydrate, pentobarbitone and urethane in adult male rats. *Lab. Anim.* 27, 258–269.

Fischl, B., Salat, D. H., Busa, E., Albert, M., Dieterich, M., Haselgrove, C., van der, K. A., Killiany, R., Kennedy, D., Klaveness, S., Montillo, A., Makris, N., Rosen, B., and Dale, A. M. (2002). Whole brain segmentation: automated labeling of neuroanatomical structures in the human brain. *Neuron* 33, 341–355.

Gustafson, C., Tretiak, O., Bertrand, L., and Nissanov, J. (2004). Design and implementation of software for assembly and browsing of 3D brain atlases. *Comput. Methods Programs Biomed.* 74, 53–61.

Gustafson, C., Bug, W. L., and Nissanov, J. (2007). Neuroterrain—a client-server system for browsing 3D biomedical image data sets. *BMC Bioinformatics* 8, 40.

Jinyi, Q., and Leahy, R. M. (2000). Resolution and noise properties of MAP reconstruction for fully 3-D PET. *Med. Imaging, IEEE Trans.* 19, 493–506.

Jinyi, Q., Leahy, R. M., Chinghan, H., Farquhar, T. H., and Cherry, S. R. (1998). Fully 3D Bayesian image reconstruction for the ECAT EXACT HR+. *Nucl. Sci., IEEE Trans.* 45, 1096–1103.

Judenhofer, M. S., Catana, C., Swann, B. K., Siegel, S. B., Jung, W. I., Nutt, R. E., Cherry, S. R., Claussen, C. D., and Pichler, B. J. (2007). PET/MR images acquired with a compact MR-compatible PET detector in a 7-T Magnet. *Radiology* 244, 807–814.

Kim, J. S., Lee, J. S., Im, K. C., Kim, S. J., Kim, S. Y., Lee, D. S., and Moon, D. H. (2007). Performance measurement of the microPET Focus 120 Scanner. *J. Nucl. Med.*, in press.

Leergaard, T. B., Lyngstad, K. A., Thompson, J. H., Taeymans, S., Vos, B. P., De Schutter, E., Bower, J. M., and Bjaalie, J. G. (2000). Rat somatosensory cerebropontocerebellar pathways: spatial relationships of the somatotopic map of the primary somatosensory cortex are preserved in a three-dimensional clustered pontine map. *J. Comp. Neurol.* 422, 246–266.

Leergaard, T. B., Bjaalie, J. G., Devor, A., Wald, L. L., Dale, A. M. (2003). In vivo tracing of major rat brain pathways using manganese-enhanced magnetic resonance imaging and three-dimensional digital atlasing. *Neuroimage* 20, 1591–1600.

Lein, E. S., Hawrylycz, M. J., Ao, N., Ayres, M., Bensinger, A., Bernard, A., Boe, A. F., Boguski, M. S., Brockway, K. S., Byrnes, E. J., Chen, L., Chen, L., Chen, T. M., Chi Chin, M., Chong, J., Crook, B. E., Czaplinska, A., Dang, C. N., Datta, S., Dee, N. R., Desaki, A. L., Desta, T., Diep, E., Dolbeare, T. A., Donelan, M. J., Dong, H. W., Dougherty, J. G., Duncan, B. J., Ebbert, A. J., Eichele, G., Estin, L. K., Faber, C., Facer, B. A., Fields, R., Fischer, S. R., Fliss, T. P., Frensley, C., Gates, S. N., Glattfelder, K. J., Halverson, K. R., Hart, M. R., Hohmann, J. G., Howell, M. P., Jeung, D. P., Johnson, R. A., Karr, P. T., Kawal, R., Kidney, J. M., Knapik, R. H., Kuan, C. L., Lake, J. H., Laramee, A. R., Larsen, K. D., Lau, C., Lemon, T. A., Liang, A. J., Liu, Y., Luong, L. T., Michaels, J., Morgan, J. J., Morgan, R. J., Mortrud, M. T., Mosqueda, N. F., Ng, L. L., Ng, R., Orta, G. J., Overly, C. C., Pak, T. H., Parry, S. E., Pathak, S. D., Pearson, O. C., Puchalski, R. B., Riley, Z. L., Rockett, H. R., Rowland, S. A., Royall, J. J., Ruiz, M. J., Sarno, N. R., Schaffnit, K., Shapovalova, N. V., Sivisay, T., Slaughterbeck, C. R., Smith, S. C., Smith, K. A., Smith, B. I., Sodt, A. J., Stewart, N. N., Stumpf, K. R., Sunkin, S. M., Sutram, M., Tam, A., Teemer, C. D., Thaller, C., Thompson, C. L., Varnam, L. R., Visel, A., Whitlock, R. M., Wohnoutka, P. E., Wolkey, C. K., Wong, V. Y., Wood, M., Yaylaoglu, M. B., Young, R. C., Youngstrom, B. L., Feng Yuan, X., Zhang, B., Zwingman, T. A., and Jones, A. R. (2007). Genome-wide atlas of gene expression in the adult mouse brain. *Nature* 445, 168–176.

Ma, Y., Hof, P. R., Grant, S. C., Blackband, S. J., Bennett, R., Slatest, L., Mcguigan, S. J., and Benveniste, H. (2005). A three-dimensional digital atlas database of the adult C57BL/6J mouse brain by magnetic resonance microscopy. *Neuroscience* 135, 1203–1215.

MacKenzie-Graham, A., Lee, E. F., Dinov, I. D., Bota, M., Shattuck, D. W., Ruffins, S., Yuan, H., Konstantinidis, F., Pitiot, A., Ding, Y., Hu, G., Jacobs, R. E., and Toga, A. W. (2004). A multimodal, multidimensional atlas of the C57BL/6J mouse brain. *J. Anat.* 204, 93–102.

Mukherjee, J., Yang, Z. Y., Das, M. K., and Brown, T. (1995). Fluorinated benzamide neuroleptics–III. Development of (S)-N-[(1-allyl-2-pyrrolidinyl)methyl]-5-(3-[18F]fluoropropyl)-2, 3-dimethoxybenzamide as an improved dopamine D-2 receptor tracer. *Nucl. Med. Biol.* 22, 283–296.

Palombi, O., Shin, J., Watson, C., and Paxinos, G. (2006). Neuroanatomical affiliation visualization-interface system. *Neuroinformatics* 4, 299–318.

Pautler, R. G., Silva, A. C., and Koretsky, A. P. (1998). In vivo neuronal tract tracing using manganese-enhanced magnetic resonance imaging. *Magn. Reson. Med.* 40, 740–748.

Paxinos, G., and Franklin, K. B. (2001). The mouse brain in stereotaxic coordinates (San Diego, Elsevier Academic Press).

Paxinos, G., and Watson, C. (1982). The rat brain in stereotaxic coordinates (New York, Academic Press).

Paxinos, G., and Watson, C. (1998). The rat brain in stereotaxic coordinates (San Diego, Academic Press).

Paxinos, G., and Watson, C. (2005). The rat brain in stereotaxic coordinates (San Diego, Elsevier Academic Press).

Price, J. L. (1995). Thalamus. In The Rat Nervous System, G. Paxinos, ed. (San Diego, Academic Press), pp. 629–648.

Sah, P., Faber, E. S., De Lopez, A. M., and Power, J. (2003). The amygdaloid complex: anatomy and physiology. *Physiol. Rev.* 83, 803–834.

Saleem, K. S., Pauls, J. M., Augath, M., Trinath, T., Prause, B. A., Hashikawa, T., and Logothetis, N. K. (2002). Magnetic resonance imaging of neuronal connections in the macaque monkey. *Neuron* 34, 685–700.

Schweinhardt, P., Fransson, P., Olson, L., Spenger, C., and Andersson, J. L. R. (2003). A template for spatial normalisation of MR images of the rat brain. *J. Neurosci. Methods* 129, 105–113.

Swanson, L. W. (2004). Brain maps: Structure of the rat brain (San Diego, Elsevier Academic Press).

Talairach, J., and Tournoux, P. (1988). Co-planar stereotaxic atlas of the human brain (New York, Thieme Medical Publishers, Inc.).

Toga, A. W., Santori, E. M., Hazani, R., and Ambach, K. (1995). A 3D digital map of rat brain. *Brain Res. Bull.* 38, 77–85.

Welker, C. (1971). Microelectrode delineation of fine grain somatotopic organization of (Sml) cerebral neocortex in albino rat. *Brain Res.* 26, 259–275.

II

III

# IV

# Spinal long-term potentiation is associated with reduced opioid neurotransmission in the rat brain

Trine Hjornevik*
Centre for Molecular Biology and Neuroscience & Institute of Basic Medical Sciences, University of Oslo,
PO. Box 1105, 0317 Oslo
Norway
Telephone no: +4797087067
trine.hjornevik@medisin.uio.no

Bent W. Schoultz
Department of Chemistry, University of Oslo,
Norway
b.w.schoultz@kjemi.uio.no

János Marton
ABX advanced biochemical compounds
Biochemische Forschungsreagenzien GmbH, Radeberg,
Germany
marton@abx.de

Johannes Gjerstad
National Institute of Occupational Health
Norway
Department of Molecular Bioscience, University of Oslo,
Norway
johannes.gjerstad@stami.no

Alexander Drzezga
Nuklearmedizinische Klinik and Poliklinik, Klinikum rechts der Isar, Technische Universität München,
Germany
a.drzezga@lrz.tu-muenchen.de

Gjermund Henriksen
Nuklearmedizinische Klinik and Poliklinik, Klinikum rechts der Isar, Technische Universität München,
Germany
Department of Chemistry, University of Oslo
Norway
g.henriksen@lrz.tu-muenchen.de

Frode Willoch
Centre for Molecular Biology and Neuroscience & Institute of Basic Medical Sciences, University of Oslo, Norway
Department of Nuclear Medicine, Centre of Diagnostic Imaging, Akershus University Hospital, Norway
frode.willoch@medisin.uio.no

*Corresponding author

**Category of submission:** original article

**Key words:** positron emission tomography, long-term potentiation, noxious stimulation, rat brain, hyperalgesia, opioid receptor, pain modulation

# Abstract

**Background and aims.**

Neuronal events leading to development of long-term potentiation (LTP) in the nociceptive pathways may be a cellular mechanism underlying hyperalgesia. The opioid receptors (ORs) are widely distributed in the central nervous system (CNS) and play a key role in nociceptive processing and in controlling the descending modulatory system to the spinal cord. We use small animal positron emission tomography (PET) to examine how spinal LTP may induce dynamic changes in the supraspinal opioidergic system.

**Methods.**

Spinal LTP was induced by electrical high-frequency stimulation (HFS) applied to the sciatic nerve. To study supraspinal changes in opioid neurotransmission, we used PET and [$^{11}$C]Phenethyl-Orvinol ([$^{11}$C]PEO). All rats were scanned at baseline and 150 min after HFS, and specific binding was calculated with a reference tissue model.

**Results.**

A clear C-fibre LTP, i.e. increased C-fibre response and reduced C-fibre threshold, was observed 150 min after HFS (t-test, $p<0.05$, $n=6$). Statistical comparisons (paired t-test, HFS>baseline, $p<0.05$, $n=8$) revealed increased binding, relative to baseline, ipsilaterally in the amygdala, hippocampus, somatosensory cortex and superior colliculus, and bilaterally in the nucleus accumbens, caudate putamen and hypothalamus. Increased binding was interpreted as increased OR availability due to reduced opioid tonic activity.

**Conclusions.**

In a rat model of spinal LTP PET revealed dynamic changes in supraspinal opioid neurotransmission in structures which constitute a pain modulatory circuitry. Altered opioid activity may be related to the measured spinal LTP and associated abnormal pain states, and the changes in the limbic structures may connect the findings with an affective-emotional response.

# Introduction

Opioid peptides, such as β-endorphin, enkephalin, and dynorphin, exert their action on widely distributed opioid receptors (ORs). There are three major receptor subtypes, μ, δ, and κ, in addition to the opioid-receptor-like NOP (Henderson and McKnight, 1997). The ORs play an important role in nociceptive and antinociceptive processing in the brain, and in controlling the descending modulatory system to the spinal cord. In particular μ-OR activation has been shown to be important for the mechanisms underlying opioid analgesia (Mansour et al., 1988). The OR-mediated neurotransmission is involved in various molecular mechanism altered in humans with chronic pain (for review see Przewlocki and Przewlocka (2001)).

We have, in the present study, employed a long-term potentiation (LTP) model in order to investigate the functional role of the ORs in nociceptive processing. It has been suggested that spinal LTP induced by noxious stimuli contribute to chronic abnormal pain states, such as hypersensitivity, hyperalgesia, and/or allodynia (Rygh et al., 2005). This powerful increase in spinal neuronal excitability observed following noxious conditioning has been shown to last for hours (Svendsen et al., 1997). However, previous findings have revealed that the expression of spinal LTP is more pronounced when the connection between the brain and recording site in the spinal cord is eliminated (Svendsen et al., 1999; Gjerstad et al., 2001).

We have recently shown that spinal LTP of synaptic strength is induced by high-frequency stimulation (HFS) conditioning of the sciatic nerve (Hjornevik et al., 2008). In this animal model of noxious stimulus-induced LTP, we studied the effects on brain activity using small animal positron emission tomography (PET) and the glucose analogue 2- [$^{18}$F]fluoro-2-deoxy-glucose ([$^{18}$F]FDG). The study demonstrated acute effects, due to the noxious HFS, and more interestingly slow (after 150 min) metabolic adaptations as a result of the spinal LTP in the supraspinal pain modulating network.

PET is the state of the art modality for quantitative studies of receptor systems *in vivo*, and the function of specific receptor systems can be investigated using highly selective receptor radiotracers. Hence, in order to investigate the role of the OR system, we have in the present study employed the μ- and κ-OR agonist ligand [$^{11}$C]PEO (Schoultz et al., Submitted to J Med Chem) for monitoring changes in the availability of μ- and κ-ORs after induction of spinal LTP. The observed signal mainly reflects μ-binding due to the relative high abundance of μ-ORs (41%) compared to κ-ORs (9 %) (Mansour et al., 1988). We hypothesised that adaptations would occur in brain regions known to be involved in nociceptive responses, e.g. the limbic system, sensory cortex, thalamus, and periaqueductal grey (PAG).

Using small animal PET we demonstrate dynamic changes in opioid neurotransmission in pain processing regions in the brain caused by the induction of spinal LTP. The findings in this study might illustrate a dysfunction in the OR system involved in pain hypersensitivity and hyperalgesia.

# Methods

The experiments were carried out with the approval of the institutional animal care committee (Regierung von Oberbayern, Munich, Germany) and in accordance with the German Animal Welfare Act (Deutsches Tierschutzgesetz). Animal husbandry followed the regulations of European Union (EU) guideline No. 86/609. All rats were sacrificed immediately after the experiments.

## Animals and surgery

In all experiments, animals were anaesthetized by inhalation of isoflurane 2 % (Abbott Laboratories, Illinois, USA). Absence of foot withdrawal to pinch indicated adequate anaesthesia. Different animals were used in the electrophysiological study (female Sprague-Dawley rats (SD; Scanbur BK, Sollentuna, Sweden; National Lab Animal Center, Norway); 200-350 g) and the PET study (Male Wistar rats (WI; Charles River); 320-370 g). As previously described in Hjornevik et al. (2008), the left sciatic nerve was dissected free at the mid-thigh level and isolated from the surrounding tissue by a plastic film. A bipolar silver hook electrode (1.5 mm distance between the hooks) was placed proximal to the main branches of the sciatic nerve for electrical stimulation. Induction of spinal LTP was obtained by HFS conditioning (1 ms rectangular 4.5 mA pulses, five trains of 1 s duration, 100 Hz, 10 s intervals between trains).

## Recording of spinal field potentials

A laminectomy was performed at vertebrae Th13-L1, corresponding to spinal cord segments L3- S1 where the sciatic nerve roots enter the cord. The vertebral column was rigidly fixed and the meninges were carefully removed with a cannula. Parylene-coated tungsten microelectrodes with impedance 1.0-1.4 MΩ (Friedrick Haer & CO, Bowdoinham, USA) were lowered vertically into the dorsal horn of the spinal cord by an electronically controlled micromanipulator. The signals from the microelectrodes were amplified with an AC pre-amplifier, filtered with band-width 1-300 Hz, digitalized with the interface CED 1401µ and continuously captured on a PC with the software CED Spike 2 (Cambridge Electronic Design, Cambridge, UK). The C-fibre threshold was defined as the lowest stimulus intensity that evoked the first visible C-fibre response. Only recordings with a clear C-fibre response corresponding to the latency of the primary afferent C-fibres at depths of 100–300 µm from the surface of the spinal cord were included in the study. The C-fibre response was calculated as the amplitude of the C-fibre volley. Every 4$^{th}$ minute a rectangular 2 ms test pulse with intensity of 1.2 x C-fibre threshold was delivered to the sciatic nerve. Three stable C-fibre responses served as a baseline for the subsequent experiment. See Hjornevik et al. (2008) for more details.

## Radiochemistry ([$^{11}$C]PEO synthesis)

The radiosynthesis of [20*R*)-4,5-α-Epoxy-17-methyl-3-hydroxy-6-[$^{11}$C]methoxy-α,17-dimethyl-α-(2-phenylethyl)-6,14-ethenomorphinan-7-methanol [$^{11}$C]PEO was preformed by $^{11}$C-methylation of the 3-*O*-trityl-6-*O*-desmethylated precursor employing a fully automated radiosynthesis module as published elsewhere (Schoultz et al., Submitted to J Med Chem). [$^{11}$C]PEO was purified by preparative high-performance liquid chromatography. After dilution, the product fraction was immobilized on a reversed-

phase cartridge, washed, eluted with ethanol, and diluted with phosphate buffered saline, pH 7.4. Quality control was performed with an analytic high-performance liquid chromatography system. The entire synthesis was completed within 40 min after end of bombardment. [$^{11}$C]PEO was obtained in a decay-corrected radiochemical yield of 57 ± 16 % (n=18), based on [$^{11}$C]MeI) and specific activity of 1622 ± 233 mCi/μmol at end-of-synthesis (EOS). The radiochemical purity was > 98%.

## PET data acquisition and image analysis

PET and CT data were acquired by a dedicated small animal microPET scanner (Inveon, Siemens Medical Solutions, Erlangen, Germany). The Inveon multimodality scanner provides high sensitivity (≥10 %) and high spatial resolution (≤ 1.46 mm FWHM, 2D FBP) (Constantinescu and Mukherjee, 2009).

Eight animals were included in this study and each animal underwent two scans; baseline and HFS. The baseline scans were acquired for all animals a few days prior to the intervention scan. For the HFS scans, the animals were stimulated according to the LTP protocol given above; 1 ms rectangular 4.5 mA pulses, five trains of 1 s duration, 100 Hz, 10 s intervals between trains, and scanned according to the late phase stage as reported in Hjornevik et al. (2008) (injection 150 min after HFS conditioning). [$^{11}$C]PEO (32.64 ± 7.12 MBq) was injected intravenously in the tail and all animals were scanned for 60 min. Data were collected in list mode and dynamically reconstructed into 20 timeframes using 3DRP (Kinahan and Rogers, 1989) (128x128x159 matrix size, 0.78x0.78x0.80 mm$^3$ voxel size).

Activity from the lacrimal glands was removed in PMOD (PMOD Technologies Ltd., Zurich, Switzerland) and pixel-wise modelling using the Ichise Multi-linear Reference Tissue Method (MRTM0) (Ichise et al., 1996) was applied to the data. This reference model is based on the Logan Plot (Logan et al., 1996) and applies for reversible receptor studies. A measurement of receptor concentration, the binding potential ($BP_{ND}$), is calculated by

$$BP_{ND} = \frac{V_t - V_{ref}}{V_{ref}} = \frac{k_3}{k_4} \propto \frac{B_{max}}{K_D}$$

where $V_t$ and $V_{ref}$ are the distribution volumes in tissue and in a reference volume which is devoid of the receptors of interest, respectively. $V_{ref}$ provides an estimation of the non-specific binding and free tracer in tissue, which the model assumes to be equal for all tissues. $k_3$ and $k_4$ describe the rates of association (per min) to and dissociation (per min) from the receptors, respectively. $BP_{ND}$ is proportional with the ratio of the concentration of available sites ($B_{max}$) to the *in vivo* equilibrium dissociation constant of the radiotracer ($K_D$). In the present study, the cerebellum was chosen as a reference volume due to the lack of ORs in this region for the rat (Mansour et al., 1988).

Statistical analysis of the parametric $BP_{ND}$-maps was performed with SPM5 (Wellcome Department of Cognitive Neurology, Institute of Neurology, London, UK). Firstly, a PET template was created from an average of summed images (15-60 min) of all animals. Then, intra-subject co-registration and spatial normalization to the customized PET template, employing a twelve-parameter affine transformation procedure, were applied to the summed PET images and hence the parametric $BP_{ND}$-maps of each animal. The parametric maps were then

smoothed with a 2 mm FWHM Gaussian filter, and group analysis (paired t-test, HFS vs. baseline) was performed. All images were normalized using grand mean proportional scaling. Significance was accepted at the 5 % level, and inference was tested for both increased (HFS>baseline) and decreased (HFS<baseline) specific binding. In addition, an average $BP_{ND}$ dataset was created from all baseline scans (n=8).

The statistical significant image ($p<0.05$) obtained from the group analysis was first co-registered, based on the PET template, to a customized CT template made from an average of all CT scans (n=8). Then, based on skull landmarks (i.e. bregma and interaural line) visible in the CT data, the result image was aligned with a 2-D digital version of the Rat Brain atlas by Paxinos & Watson (2005). In addition, a Magnetic Resonance Imaging (MRI) template fitted to Paxinos and Watson atlas space was co-registered to the same atlas space (Schweinhardt et al., 2003). Statistical T-values were extracted from the SPM result image by applying volumes of interest (VOIs) in PMOD. The spherical (1 mm radius) VOIs were placed at predefined regions, and peak and average T- and $BP_{ND}$-values within these VOIs were reported. The areas of interest were regions of significant OR density (Mansour et al., 1988) known to be involved in pain processing; nucleus accumbens (Acb), amygdala, hippocampus, hypothalamus, caudate putamen (CPu), sensory cortex, superior colliculus (SC), and regions where metabolic adaptations were observed in our previous study (Hjornevik et al., 2008); PAG, rostral ventromedial medulla (RVM), and dorsolateral pontomesencephalic tegmentum (DLPT).

For visualization and localization purposes, the parametric T-maps were fitted to a 3-D atlas framework reconstructed from “The Rat Brain in Stereotaxic Coordinates” by Paxinos & Watson (2005) (for details, see Hjornevik et al., 2007). Our group has developed a multi-platform atlas tool (available via The Rodent Workbench, http://rbwb.org) which allows combined visualization of experimental image data and 3-D atlas structures. Co-registration was performed by the use of well-defined skull landmarks attainable from the CT data which is aligned with the PET template. These landmarks (i.e. bregma and interaural line) are the same landmarks that the Paxinos & Watson atlas framework is based upon. The same linear transformation obtained from the alignment was applied to the T-maps.

# Results

## Spinal field potential recordings

The HFS conditioning applied to the sciatic nerve caused a long-lasting increase in neuronal excitability at the spinal level (Fig. 1 a,b). Notably, the data demonstrated an increase in the C-fibre response (Fig. 1 c), but also a decrease in the C-fibre threshold (Fig. 1 d) of nociceptive dorsal horn neurons after HFS conditioning (Students t-test, $p<0.05$, 160-168 min after HFS versus baseline).

## PET measurements

The extracted T-values passing the probability threshold ($p<0.05$) together with baseline $BP_{ND}$ values are listed in Table 1. The statistical significant results are comparisons between rest and stimulation condition within each animal (HFS>baseline; SPM contrasts [1 -1]). No significant results were found for decreased $BP_{ND}$ values (HFS<baseline; SPM contrast [-1 1]). The listed $BP_{ND}$ values represent specific binding of [$^{11}$C]PEO to μ-ORs, and to a lesser degree, κ-ORs in selected tissues relative to a reference region (i.e. cerebellum). No ORs are located in the rat cerebellum (Mansour et al., 1988), which therefore was used to estimate the extent of non-specific binding and free tracer in tissue. The statistical significant result image was superimposed onto the 2-D digital atlas (Fig.2 g-l) and a reference MRI template (Fig.2 a-f) for localization of the predefined VOIs.

An increase in $BP_{ND}$ due to the noxious conditioning stimulation was observed in the ipsilateral amygdala (Fig. 2 d,j) and adjacent cortical areas. No increased $BP_{ND}$ was observed on the contralateral side in these regions. Similarly, increased specific binding was observed at two individual locations in the hippocampus, exclusively on the ipsilateral side (Fig. 2 d,e,j,k). At a more caudal level, an area of significant signal was located in the ipsilateral SC (Fig. 2 f,l). Specific binding was also registered in the somatosensory cortex on the ipsilateral side (Fig. 2 c,i). The relative high T-value (peak= 3.16) witnesses a strong effect in this cortical region. An increased $BP_{ND}$ was also observed through several levels of the CPu (Fig. 2 a-c,g-i). The significant signal was located bilaterally, but with a higher effect on the ipsilateral side (Table 1). Another region with a bilateral signal localization was the Acb (Fig. 2 a,g). This area had the strongest effect (peak T-value= 4.82).

# Discussion and conclusions

In the present study, we show for the first time that in an animal model of spinal LTP, which is likely to represent an increased excitability in the ascending pain pathways from the spinal cord to the brain stem, also results in dynamic changes in OR binding in brain regions involved in pain processing. Below, we discuss the specific findings of the different sites of the CNS and how our findings might influence nociceptive processing.

## Methodological considerations

LTP is a well used model for studying cellular memory of nociception, and the long-lasting increase in synaptic activity has been observed independently of sex and rat strains (Gjerstad et al., 2001; Vikman et al., 2003) .

Previous data show that the operation for isolating the sciatic nerve never causes any increase in neuronal excitability neither at the spinal level nor in the brain (Rygh et al., 1999; Hjornevik et al., 2008). Hence, the spinal LTP and the subsequent supraspinal functional changes in the present study are directly related to the electrical repetitive stimulation, i.e. the HFS conditioning.

The BP was calculated using a reference tissue model, and although these methods do not provide a full kinetic analysis, they are able to estimate valuable measures of interest. In the present study, group comparison between HFS and baseline (HFS>baseline) revealed increased $BP_{ND}$ values in supraspinal regions 150 min after conditioning. Increased binding can be interpreted as reduced endogenous opioid peptide release or an increase in OR availability ($B_{max}$) or both. The existence of a baseline tonic activity in the endogenous opioid system was suggested by Gestreau et al. (2000). Previous studies have demonstrated reductions in the tonic activity resulting in an increase in OR availability following spontaneous epileptic seizures (Hammers et al., 2007), and in negative affective states in human (Zubieta et al., 2003). Thus, the density of ORs available at the cell plasma membrane may not be constant, and the G protein-linked receptors can either be newly synthesized or recycled. A study by Gross-Isseroff et al. (1990) showed significantly increased μ-OR density in brains of suicide victims. In order to fully understand these concepts, further studies involving PCR and immunohistochemistry should be applied in order to determine the regulation/dysregulation of opioidergic signalling mechanisms. In any case, the higher binding of PET tracer observed in the present study represents a state of the OR system which is associated with C-fibre LTP, pain hypersensitivity, and hyperalgesia.

## Regional increase in specific binding

One of the most significant regions with increased $BP_{ND}$ was the ipsilateral amygdala (Table 1). Amygdala is part of the limbic network and therefore involved in the affective-motivational dimensions of pain processing (Davidson, 2002). One main function is to coordinate emotional and autonomic responses to noxious stimuli. In addition, amygdala contributes to memory formation and learning through its reciprocal projections to hypothalamus, thalamus, hippocampus, and the cerebral cortex (Price, 2003). Amygdala also plays an important role in the descending pain modulation circuitry, through direct reciprocal connections to the PAG, and indirect connections to the RVM (Fields and Basbaum, 1999). Antinociception is either activated through physiological factors (e.g. fear) or by introduction of exogenous opioids (Oliveira and Prado, 1994; Pavlovic and Bodnar,

1998). The medial and lateral nuclei of the amygdala contain a high concentration of μ- and δ-ORs (Mansour et al., 1988), while κ-OR are the sole OR located in the central nucleus. The observed ipsilateral effect is in agreement with the findings by Manning (1998), who reported an ipsilateral topography of pain control circuits including the amygdala, hypothalamus, PAG, RVM, and the dorsal horn of the spinal cord after an unilateral inactivation of the central amygdala. The strong effect observed might indicate a dysfunction in the antinociceptive properties of amygdala.

Increased binding was also observed in the hypothalamus (Fig. 2 c,i). As previously mentioned, hypothalamic regions have reciprocal connections to the amygdala and therefore contribute to the coordination of sensory and autonomic information. Hypothalamus is also involved in pain modulation through descending projection to PAG, RVM, and the dorsal horn of the spinal cord (Fields & Basbaum, 1999), and injection of opioids into this regions have been reported to induce behavioural antinociception (Manning and Franklin, 1998).

Two distinct areas of increased $BP_{ND}$ were observed in the hippocampus (Fig. 2 d,e,j,k). Cortical inputs to hippocampus contribute to cognitive functions while subcortical modulatory inputs affect the behavioural state of an organism (Amaral and Lavenex, 2007). As part of the limbic system, hippocampus is involved in emotions, memory formation, and learning. Hippocampus is connected to various brain regions including the thalamus, amygdala, hypothalamus, and cerebral cortex, and contains a dense distribution of ORs, in particular μ-ORs (Mansour et al., 1988). An involvement of hippocampus suggests an affective and emotional response to the applied noxious stimuli, together with a role in memory formation in the nociceptive pathways.

ORs are widely distributed throughout the basal ganglia, in particular in the CPu and Acb (Mansour et al., 1988). Increased binding was observed in these regions and adjacent cortical structures (Fig. 2 a,b,g,h). In contrast to previously discussed structures, the effect was distributed bilaterally (Table 1). The basal ganglia are involved in motor, cognitive, and limbic functions. Acb is part of the ventral striatum, linked with the cortex, hippocampus, amygdala, and hypothalamus (Groenewegen et al., 1991), and known for its role in emotion and behaviour. As part of the dorsal striatum, CPu receives information in particular from the cerebral cortex (Gerfen, 2004). Processed information from the basal ganglia is projected to brain regions such as thalamus and brain stem regions (e.g. superior colliculus (SC)) (Bolam et al., 2000).

In addition to projections from the basal ganglia, SC also receives nociceptive inputs from spinomesencephalic neurons (Willis et al., 2004). This pathway, which also includes PAG, is believed to play an important role in the motivational-affective aspect of pain, and contributes to descending antinociception. The SC has a dense population of μ-OR and a moderate distribution of κ-OR (Mansour et al., 1988). The observed ipsilateral effect (Fig. 2 f,l) correlates with the ipsilateral pain modulating topography previously described. The observed binding located in this region further strengthens the hypothesis regarding a dysfunction in the descending pain inhibitory system.

Increased $BP_{ND}$ was also observed in the ipsilateral somatosensory cortex (Fig. 2 c,i). Even though it is known that the cerebral cortex plays an active role in nociceptive processes (Millan, 2002; Ohara et al., 2005), the role

of the somatosensory cortex is not clearly understood. In Bushnell et al. (1999), strong evidences are listed which support the modulating role of S1 in sensory aspects of pain. Although the OR BP is low in the primary somatosensory cortex (S1) in humans (Baumgartner et al., 2006), S1 has a relevant proportion of OR in rats (see Table 1). In the present study, it is clearly shown that the opioid neurotransmission in the somatosensory cortex is involved in the expression of spinal LTP induced by noxious conditioning.

In our previous study (Hjornevik et al., 2008), metabolic adaptations were observed in major regions involved in the descending pain modulating circuitry (i.e. PAG, RVM, and DLPT). However, no significant changes in $BP_{ND}$ were observed in these regions in the present study. PAG is a relative small brain region in size with low abundance of ORs (Mansour et al., 1988). The low number of ORs and the signal-to-noise ratio due to small volume might explain the negative findings in this region. Moreover, a reduced activation in the brain stem areas which control the descending antinociceptive system may not necessarily involve a brain stem change in the opioid peptide release and/or an increase in OR concentration. Many other transmitters may be important for the descending seretonergic, noradrenergic, and enkephalinergic descending modulatory tone.

Interestingly, increased tracer binding was observed in the amygdala, hypothalamus, hippocampus, and Acb, all so-called limbic structures which are involved in processing emotions, mood, motivation and pain sensations. Together with hippocampus, amygdala is involved in learning and memory of noxious stimuli. In particular, amygdala plays a major role in associating the stimuli with emotions. A recent study demonstrated that positive emotions were related to increased opioid release in amygdala, and OR BP was negatively correlated with positive mood (Koepp et al., 2009). Their findings fit with the present results where a negative emotional state following a noxious stimulus resulting in a spinal LTP is associated with increased OR binding. The involvement of these structures indicates both an affective-emotional response to the applied noxious stimuli and possible functional alterations in the pain modulatory circuitry.

Release of endogenous peptides in the brain predominantly inhibits nociceptive transmission. A reduced activity in this system may therefore reflect an insufficient inhibition in the supraspinal antinociceptive system. Clearly, this may also influence the descending bulbospinal pathways to the dorsal horn. Previous studies have shown that the expression of spinal LTP after 2.5 h is more pronounced when the connection between the brain and the recording site in the dorsal horn is eliminated (Svendsen et al., 1999; Gjerstad et al., 2001). This shows that maintenance of spinal LTP can be reinforced by a reduction in the descending inhibition.

In accordance with these data, we here demonstrate that the noxious conditioning leading to an altered state of the OR system is associated by both an increased C-fibre response as well as a reduced C-fibre threshold. Hence, it is tempting to speculate that spinal LTP may involve a reduced tone in the descending inhibitory pathways. The fact that sensitization at the spinal level induced by noxious stimuli and development of persistent hyperalgesia can be modulated by descending pathways to the spinal cord, has also been demonstrated in humans (Matre et al., 2006).

Behaviour studies have shown that induction of spinal LTP is followed by a long-lasting ipsilateral reduction of paw withdrawal latency, i.e. hyperalgesia (Zhang et al., 2005). Moreover, a perceptual correlate to LTP in nociceptive pathways has also been described in humans (Klein et al., 2004). It is therefore likely that the conditioning used in the present study to induce spinal LTP may contribute to hypersensitivity, hyperalgesia, and/or allodynia, mechanisms seen in central sensitization (Sandkuhler and Liu, 1998; Rygh et al., 2005). However, whether development of persistent hyperalgesia after this form of conditioning may be caused by a local spinal increase in synaptic efficacy or changed supraspinal processing, including a reduced tone in the descending inhibitory pathways, remains to be investigated.

## Concluding statements

The data shows that HFS is associated with a regional increased OR availability that is interpreted as reduced opioid tonic activity. The involved structures, amygdala in particular, constitute a pain modulatory circuitry. Therefore, a reduced descending opioid, antinociceptive activity may be related to states of abnormal pain sensitivity, such as hyperalgesia. Furthermore, the dynamic changes in opioid neurotransmission in the limbic structures may connect the findings with an affective-emotional response to the applied noxious stimulus.

Strong natural noxious stimuli (e.g. skin burns, contusions, inflammation, and acute nerve injury) which may induce spinal LTP (Sandkuhler and Liu, 1998), also trigger injury-induced hyperalgesia. Consequently, spinal LTP is an attractive and relevant animal model of central sensitization and hyperalgesia, which can be studied with small animal PET. The obtained results may contribute to the understanding of how chronic pain develops and potentially enables us to target an improved treatment of patients with chronic pain.

## Acknowledgements

The authors would like to thank Dmitri Darine for excellent technical assistance with the 3-D atlas development, and Line Jacobsen for electrophysiology measurements.

This study was supported by grants from the Research Council of Norway, University of Oslo, and Aker University Hospital.

## Conflict-of-interest Statement

The authors declare that the research was conducted in the absence of any commercial or financial relationships that could be constructed as a potential conflict of interest.

# References

Amaral D & Lavenex P. Hippocampal Neuroanatomy. In: Andersen P, Morris R, Amaral D, Bliss T, & O'Keefe J, Eds.. The Hippocampus Book. Oxford University Press; 2007: 37-114.

Baumgartner, U, Buchholz, HG, Bellosevich, A, Magerl, W, Siessmeier, T, Rolke, R, Hohnemann, S, Piel, M, Rosch, F, & Wester, HJ. High opiate receptor binding potential in the human lateral pain system. Neuroimage 2006; 30(3): 692-699.

Bolam, JP, Hanley, JJ, Booth, PA, & Bevan, MD. Synaptic organisation of the basal ganglia. Journal of Anatomy 2000; 196 ( Pt 4): 527-542.

Bushnell, MC, Duncan, GH, Hofbauer, RK, Ha, B, Chen, JI, & Carrier, B. Pain perception: is there a role for primary somatosensory cortex? Proc.Natl.Acad.Sci.U.S.A 1999; 96(14): 7705-7709.

Constantinescu, CC & Mukherjee, J. Performance evaluation of an Inveon PET preclinical scanner. Physics in Medicine and Biology 2009; 54(9): 2885-2899.

Davidson, RJ. Anxiety and affective style: role of prefrontal cortex and amygdala. Biological Psychiatry 2002; 51(1): 68-80.

Fields, H. L. & Basbaum, A. Central nervous system mechanisms of pain modulation. In P. Wall & R. Melzak (Eds.). Textbook of pain. London: Harcourt Publishers Limited;1999: 309-329.

Gerfen C.R Basal Ganglia. In Paxinos G (Ed.). The Rat Nervous System. London: Elsevier Academic Press;2004: 458-508.

Gestreau, C, Le, GS, & Besson, JM. Is there tonic activity in the endogenous opioid systems? A c-Fos study in the rat central nervous system after intravenous injection of naloxone or naloxone-methiodide. J.Comp Neurol. 2000; 427(2): 285-301.

Gjerstad, J, Tjolsen, A, & Hole, K. Induction of long-term potentiation of single wide dynamic range neurones in the dorsal horn is inhibited by descending pathways. Pain 2001; 91(3): 263-268.

Groenewegen H.J, Berendse H.W, Meredith G.E, Haber S.N, Voorn P, Wolters J.G, & Lohman A.H.M Functional Anatomy of the Ventral, Limbic System-Innervated Striatum. In Willner P & Scheel-Kruger J (Eds.). The Mesolimbic Dopamine System: From Motivation to Action. John Wiley & Sons Ltd;1991: 19-59.

Gross-Isseroff, R, Dillon, KA, Israeli, M, & Biegon, A. Regionally selective increases in [mu] opioid receptor density in the brains of suicide victims. Brain Research 1990; 530(2): 312-316.

Hammers, A, Asselin, MC, Hinz, R, Kitchen, I, Brooks, DJ, Duncan, JS, & Koepp, MJ. Upregulation of opioid receptor binding following spontaneous epileptic seizures. Brain 2007; 130(4): 1009-1016.

Henderson, G & McKnight, AT. The orphan opioid receptor and its endogenous ligand--nociceptin/orphanin FQ. Trends in Pharmacological Sciences 1997; 18(8): 293-300.

Hjornevik, T, Leergaard, TB, Darine, D, Moldestad, O, Dale, AM, Willoch, F, & Bjaalie, JG. Three-dimensional atlas system for mouse and rat brain imaging data. Frontiers in Neuroinformatics 2007; 1(4). DOI: 10.3389/neuro.11/004.2007.

Hjornevik, T, Jacobsen, LM, Qu, H, Bjaalie, JG, Gjerstad, J, & Willoch, F. Metabolic plasticity in the supraspinal pain modulating circuitry after noxious stimulus-induced spinal cord LTP. Pain 2008; 140(3): 456-464.

Ichise, M, Ballinger, JR, Golan, H, Vines, D, Luong, A, Tsai, S, & Kung, HF. Noninvasive Quantification of Dopamine D2 Receptors with Iodine-123-IBF SPECT. The Journal of Nuclear Medicine 1996; 37(3): 513-520.

Kinahan, PE & Rogers, JG. Analytic 3D image reconstruction using all detected events. Nuclear Science, IEEE Transactions on 1989; 36(1): 964-968.

Klein, T, Magerl, W, Hopf, HC, Sandkuhler, J, & Treede, RD. Perceptual Correlates of Nociceptive Long-Term Potentiation and Long-Term Depression in Humans. Journal of Neuroscience 2004; 24(4): 964-971.

Koepp, MJ, Hammers, A, Lawrence, AD, Asselin, MC, Grasby, PM, & Bench, CJ. Evidence for endogenous opioid release in the amygdala during positive emotion. Neuroimage 2009; 44(1): 252-256.

Logan, J, Fowler, JS, Volkow, ND, Wang, GJ, Ding, YS, & Alexoff, DL. Distribution Volume Ratios Without Blood Sampling from Graphical Analysis of PET Data. J Cereb Blood Flow Metab 1996; 16(5): 834-840.

Manning, BH. A Lateralized Deficit in Morphine Antinociception after Unilateral Inactivation of the Central Amygdala. Journal of Neuroscience 1998; 18(22): 9453-9470.

Manning, BH & Franklin, KBJ. Morphine analgesia in the formalin test: reversal by microinjection of quaternary naloxone into the posterior hypothalamic area or periaqueductal gray. Behavioural Brain Research 1998; 92(1): 97-102.

Mansour, A, Khachaturian, H, Lewis, ME, Akil, H, & Watson, SJ. Anatomy of CNS opioid receptors. Trends in Neurosciences 1988; 11(7): 308-309.

Matre, D, Casey, KL, & Knardahl, S. Placebo-Induced Changes in Spinal Cord Pain Processing. Journal of Neuroscience 2006; 26(2): 559-563.

Millan, MJ. Descending control of pain. Progress in Neurobiology 2002; 66(6): 355-474.

Ohara, PT, Vit, JP, & Jasmin, L. Cortical modulation of pain. Cell Mol.Life Sci. 2005; 62(1): 44-52.

Oliveira, MA & Prado, WA. Antinociception and behavioral manifestations induced by intracerebroventricular or intra-amygdaloid administration of cholinergic agonists in the rat. Pain 1994; 57(3): 383-391.

Pavlovic, ZW & Bodnar, RJ. Opioid supraspinal analgesic synergy between the amygdala and periaqueductal gray in rats. Brain Research 1998; 779(1-2): 158-169.

Paxinos, G. & Watson, C. The Rat Brain in Stereotaxic Coordinates. San Diego: Elsevier Academic Press; 2005.

Price, JL. Comparative aspects of amygdala connectivity. Annals of the New York Academy of Sciences 2003; 985: 50-58.

Przewlocki, R & Przewlocka, B. Opioids in chronic pain. European Journal of Pharmacology 2001; 429(1-3): 79-91.

Rygh, LJ, Svendsen, F, Hole, K, & Tjolsen, A. Natural noxious stimulation can induce long-term increase of spinal nociceptive responses. Pain 1999; 82(3): 305-310.

Rygh, LJr, Svendsen, F, Fiskσ, A, Haugan, Fy, Hole, K, & Tj°lsen, A. Long-term potentiation in spinal nociceptive systems--how acute pain may become chronic. Psychoneuroendocrinology 2005; 30(10): 959-964.

Sandkuhler, J & Liu, X. Induction of long-term potentiation at spinal synapses by noxious stimulation or nerve injury. European Journal of Neuroscience 1998; 10(7): 2476-2480.

Schweinhardt, P, Fransson, P, Olson, L, Spenger, C, & Andersson, JLR. A template for spatial normalisation of MR images of the rat brain. Journal of Neuroscience Methods 2003; 129(2): 105-113.

Svendsen, F, Tjolsen, A, & Hole, K. LTP of spinal A beta and C-fibre evoked responses after electrical sciatic nerve stimulation. Neuroreport 1997; 8(16): 3427-3430.

Svendsen, F, Tjolsen, A, Gjerstad, J, & Hole, K. Long term potentiation of single WDR neurons in spinalized rats. Brain Research 1999; 816(2): 487-492.

Vikman, KS, Duggan, AW, & Siddall, PJ. Increased ability to induce long-term potentiation of spinal dorsal horn neurones in monoarthritic rats. Brain Research 2003; 990(1-2): 51-57.

Willis, W. D., Westlund K.N, & Carlton S.M Pain System. In Paxinos G (Ed.). The Rat Nervous System.Elsevier Academic Press;2004: 853-890.

Zhang, XC, Zhang, YQ, & Zhao, ZQ. Involvement of nitric oxide in long-term potentiation of spinal nociceptive responses in rats. Neuroreport 2005; 16(11): 1197-1201.

Zubieta, JK, Ketter, TA, Bueller, JA, Xu, Y, Kilbourn, MR, Young, EA, & Koeppe, RA. Regulation of human affective responses by anterior cingulate and limbic mu-opioid neurotransmission. Archives of General Psychiatry 2003; 60(11): 1145-1153.

# Legends

**Fig. 1 Extracellular field potential recordings, C-fibre responses and threshold**
**(a)** Extracellular field potential recordings at baseline and 168 min after HFS conditioning. C-fibre responses represented as a percentage of baseline, plotted as a function of time (min) relative to HFS conditioning **(b)**, and as bar diagrams at two time points; baseline and 160-168 min after HFS conditioning **(c). (d)** Bar diagrams showing the C-fibre threshold at two timepoints; baseline and 168 min after HFS conditioning. The increased C-fibre responses and reduced C-fibre threshold relative to baseline are statistical significant ($p<0.05$). HFS, high frequency stimulation; *, statistical significant results ($p<0.05$).

**Fig. 2 Regional increase in specific binding**
Brain regions with increased specific binding after comparison between HFS and baseline. The statistical significant PET signals ($p<0.05$; colors) are overlaid on a digital versions of the Paxinos & Watson the rat brain atlas **(a-f)**, and on a MRI template **(g-l)**. Left side in the image represents the left side of the brain. Increased specific binding was observed in the nucleus accumbens **(a,g)**, caudate putamen **(b,h)**, somatosensory cortex **(c,i)**, hypothalamus **(c,i)**, hippocampus **(d,e,j,k)**, amygdala **(d,j)**, and superior colliculus **(f,l)**. Blue: a slight increase (low T-value) in specific binding; red: a high increase (high T-value) in specific binding. Red circles, volumes of interest (VOIs); Bar, 1 mm.

**Fig. 3 Alignment and localization of PET data with a 3-D digital atlas system (Atlas3D)**
**(a)** 3-D atlas structures reconstructed from Paxinos & Watson (Paxinos & Watson, 2005) and visualized in Atlas3D. **(b)** CT template with skull landmarks (i.e. bregma and interaural line) used for alignment with 3-D atlas space. **(c)** CT template and SPM result image coregistered to atlas space based on the transformation matrix obtained from the CT alignment. Area of significant binding is shown in blue. **(d)** Coronal atlas diagram locating the significant signal to the hippocampus, amygdala, hypothalamus, and somatosensory cortex. S1, primary somatosensory cortex; hi, hippocampus; am, amygdala; hy, hypothalamus.

| Region | Baseline $BP_{ND}$ | | T-value | |
|---|---|---|---|---|
| | Peak | Average | Peak | Average |
| S1, left | 1,51 | 1,17 | 3,16 | 2,47 |
| S1, right | 1,55 | 1,19 | - | - |
| Amygdala, left | 1,40 | 1,03 | 4,03 | 3,35 |
| Amygdala, right | 1,52 | 1,15 | - | - |
| Acb, left | 1,89 | 1,53 | 4,82 | 2,93 |
| Acb, right | 1,93 | 1,59 | 3,48 | 1,37 |
| Hypothalamus | 1,81 | 1,26 | 3,31 | 1,56 |
| SC, left | 2,06 | 1,81 | 2,41 | 1,66 |
| SC, right | 2,13 | 1,86 | - | - |
| Hippocampus, left | 1,24 | 0,84 | 3,88 | 1,86 |
| Hippocampus, right | 1,32 | 0,88 | - | - |
| CPu, left | 2,12 | 1,88 | 2,59 | 1,00 |
| CPu, right | 2,07 | 1,87 | 3,35 | 1,51 |
| Cerebellum | 0,36 | 0,36 | - | - |

**Table 1. Baseline $BP_{ND}$ and T-values extracted from predefined volumes of interest.** Group results from studies of [$^{11}$C]PEO binding by means of PET, where average and peak T- values were extracted from volumes of interest (VOIs) passing the predefined probability threshold of $p<0.05$ and regions outside the VOI at $p<0.001$. T-values are obtained from group comparisons between baseline and stimulation condition within each animal (SPM contrasts [-1 1]). $BP_{ND}$ values represent the average binding potential within the VOIs from all baseline scans (n=8). $BP_{ND}$, binding potential; S1, primary somatosensory cortex; Acb, nucleus accumbens; SC, superior colliculus; IC, inferior colliculus; CPu, caudate putamen;

Figure 1

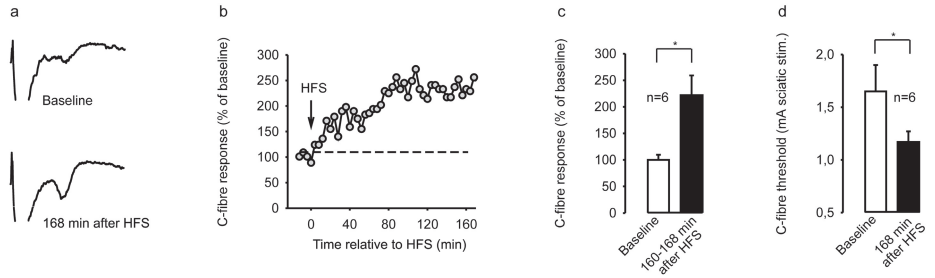


Figure 2

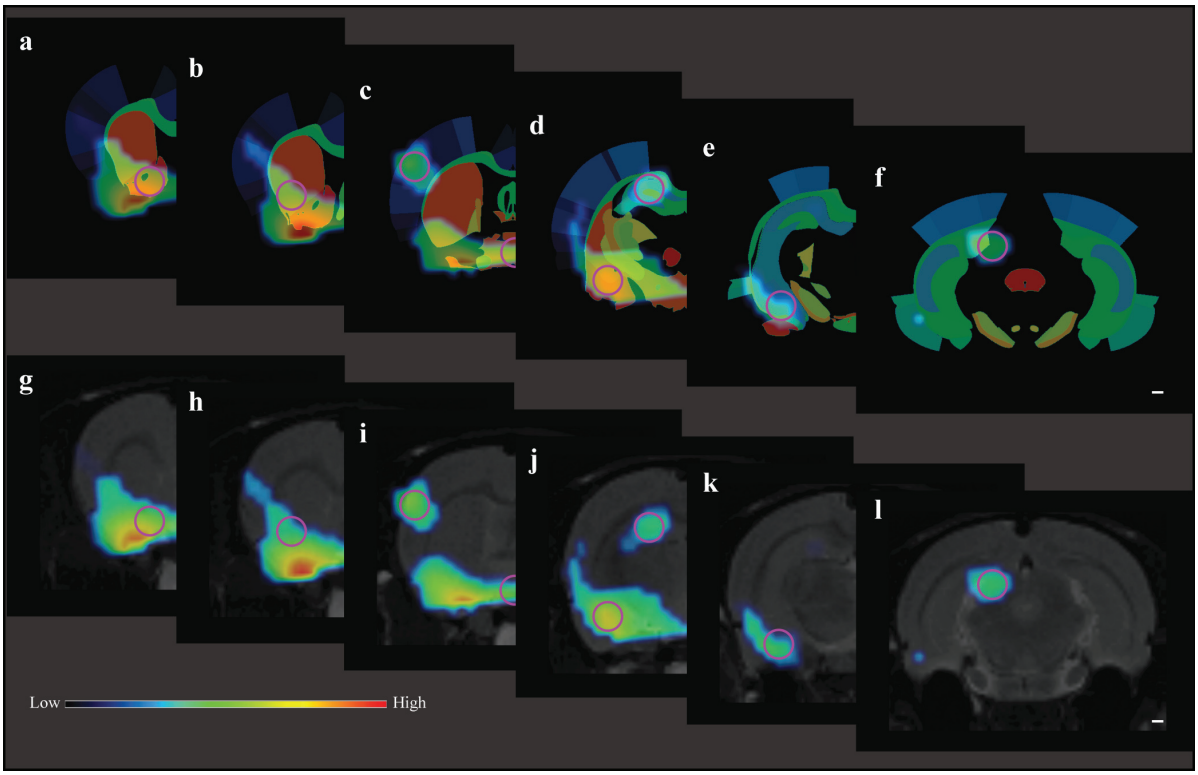

Figure 3

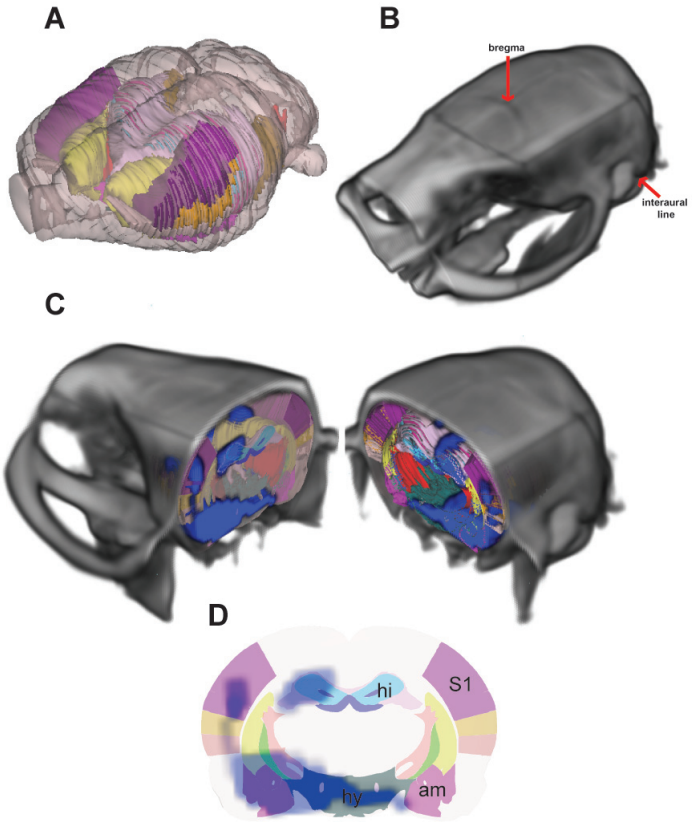

# Evaluation of the Kappa-Opioid Receptor Selective Tracer [$^{11}$C]GR103545 in Awake Rhesus Macaques

Bent W. Schoultz[1,#], Trine Hjornevik[2,3,#], Frode Willoch[2,3], János Marton[4], Akihiro Noda[5], Yoshihiro Murakami[5], Sosuke Miyoshi[5], Shintaro Nishimura[5], Erik Årstad[6], Alexander Drzezga[7], Ichiro Matsunari[8], Gjermund Henriksen[1,7,*]

*[1]Department of Chemistry, University of Oslo, Norway. [2]Centre for Molecular Biology and Neuroscience & Institute of Basic Medical Sciences, University of Oslo, Norway. [3]Department of Nuclear Medicine, Akershus University Hospital, Norway, [4]ABX Advanced Biochemical Compounds GmbH, Radeberg, Germany, [5]Basic Research Department, The Medical and Pharmacological Research Center Foundation Hakui-city Ishikawa, Japan. [6]Institute of Nuclear Medicine, University College of London, United Kingdom. [7]Department of Nuclear Medicine, Klinikum rechts der Isar, Technische Universität München, Germany. [8] Clinical Research Department, The Medical and Pharmacological Research Center Foundation Hakui-city Ishikawa, Japan.*

* Author to whom correspondence should be addressed at:
Department of Nuclear Medicine
Klinikum rechts der Isar
Technische Universität München
Ismaninger Strasse 22
D-81675 Munich
Germany
Phone: + 49 89 4140 2971
Fax: + 49 89 4140 4841
Email: G.Henriksen@lrz.tum.de

# These authors contributed equally

**Total word count of the manuscript (including references):** 3581

**Running foot line:** PET-Tracer for the kappa-opioid receptor

**Abstract**

*Purpose* The recent development in radiosynthesis of the $^{11}$C-carbamate function increases the potential of [$^{11}$C]GR103545, which for last decade has been regarded promising for imaging the kappa-opioid receptor (κ-OR) with PET. In the present study, [$^{11}$C]GR103545 was evaluated in awake rhesus macaques. Separate investigations were performed to clarify the OR-subtype selectivity of this compound.

*Methods* Regional brain uptake kinetics of [$^{11}$C]GR103545 was studied 0-120 min after injection. The binding affinity and opioid subtype selectivity of [$^{11}$C]GR103545 was determined in cells transfected with cloned human opioid receptors.

*Results* In vitro binding assays demonstrated a high affinity of GR103545 for κ-OR ($K_i$=0.02 nM) with excellent selectivity over μ-OR ($6\times10^2$ fold) and) δ-OR ($2\times10^4$ fold). PET-imaging revealed a volume of distribution ($V_T$) distribution pattern consistent to that previously reported from studies with [$^{11}$C]GR103545 in anesthetized primates, with striatum = temporal cortex > cingulated cortex > frontal cortex > parietal cortex > thalamus > cerebellum, but $V_T$ obtained in the present study was significantly higher for all brain regions.

*Conclusions* [$^{11}$C]GR103545 is selective for κ-OR and may allow a selective depiction and quantification of this receptor in humans by means of PET.

**Keywords** Opioid receptor, kappa, PET-imaging, carbon-11, GR103545.

**Introduction**

Among the opioid receptor (OR) subtypes (μ, δ and κ), the κ-OR has the highest concentration (37%) in the human CNS, with particularly dense expression in the forebrain, midbrain, and brainstem structures [1]. The κ-OR is a potential target for therapeutic intervention of several psychiatric and neurological diseases, such as epilepsy, pain and drug addiction [2-7]. An increased understanding of how occupancy of this receptor affects κ-OR mediated neurotransmission will facilitate development of κ-OR-directed drugs and diagnostic tracers. No κ-OR-selective tracer is currently available for routine clinical application.

Radiolabelling and brain uptake studies in mice of racemic [$^{11}$C]GR89696, a highly potent and selective κ-OR agonist [6], was reported in 1999 by Ravert and coworkers [7]. The same group later reported the separate *in vivo* evaluation of the *R*- and *S*-enantiomers of [$^{11}$C]GR89696 in the mouse, and demonstrated that the regional brain uptake of the *R*-isomer, also known as [$^{11}$C]GR103545, correlates with the distribution of κ-OR [8]. More recently, Talbot and co-workers evaluated [$^{11}$C]GR103545 in non-human primates and found the regional binding pattern of [$^{11}$C]GR103545 to be in excellent agreement with the known distribution of κ-OR in the non-human primate brain [9].

Translation of [$^{11}$C]GR103545 to clinical trials has so far been hampered by lack of an efficient radiosynthesis. Previously, [$^{11}$C]GR103545 has been produced by reduction of [$^{11}$C]$CO_2$ to [$^{11}$C]$CH_2OH$, followed by treatment of [$^{11}$C]$CH_2OH$ with phosgene, and finally reaction with des-carbamate-GR103545 [7-9]. We recently reported an improved method for $^{11}$C-labeling of carbamate groups based on the three-component coupling reaction (Fig. 1) of amines, $CO_2$ and [$^{11}$C]methyl-triflate [10]. The method enables labeling of[$^{11}$C]GR103545 in excellent yields under mild conditions, with a total synthesis time of ~25 min after end-of-bombardment [10].

Here we report PET-studies of [$^{11}$C]GR103545 in awake rhesus macaques using the improved radiosynthesis of this tracer, as well as *in vitro* binding studies for investigating the OR-subtype selectivity and binding profile of this compound.

**Materials and methods**

Tracer Preparation

The radiosynthesis of [$^{11}$C]GR103545 was performed as previously described [10].

PET Experimental Procedures

Experiments were performed according to protocols approved by the Institutional Animal Care and Use Committee of The Medical and Pharmacological Research Center Foundation Hakui-city Ishikawa as previously reported [11]. Three male Rhesus Macaques (8.9, 8.1 and 6.5 kg, respectively), fasted for 4 hours prior to the scan were maintained in awake condition for the study and received 550.0 ± 148.0 MBq of [$^{11}$C]GR103545 with a specific activity of 50.7 ± 7.9 GBq/μmol at time of injection. Two animals were scanned a second time, after injection of 210 and 450 MBq of [$^{11}$C]GR103545, respectively, with a specific activity 26.8 ± 5.3 GBq/μmol at time of injection.

For collection of arterial blood samples, a catheter was inserted in a femoral artery under transient anesthesia condition induced by 2% sevoflurane in a $N_2O$ and $O_2$ gas mixture ($N_2O$:$O_2$ 7:3).

PET-scanning was performed with an SHR-7700 (Hamamatsu Photonics, Hamamatsu, Japan) in 2-dimensional mode. A 30-min transmission scan was obtained before radiotracer injection for attenuation correction. [$^{11}$C]GR103545 was administered by intravenous injection over 30 s and emission data were collected 0-120 min post-injection (p.i).

Arterial samples obtained from the animals were collected at 0, 10, 20, 30, 40, 50 sec, 1, 2, 3, 5, 7, 10, 15, 20, 30, 45, 60, and 90 min. Eight samples, collected at 1, 5, 10, 20, 30, 45, 60, and 90 min p.i., were analyzed by thin layer chromatography (TLC) to determine the percentage intact tracer. Here,

0.1 ml of acetonitrile was mixed with plasma samples (0.1 ml), and centrifuged for 3 min at 12.000·*g*. The resulting supernatant was applied to a TLC-plate which in turn was developed in chloroform:methanol: 25 % $NH_4OH$ (91:8:1 ($^{v}/_{v}$)). The TLC-plate was subsequently exposed to an imaging plate (Fuji Film, Tokyo, Japan). Finally, the imaging plate was analyzed by an imaging plate reader (BAS1800, Fuji Film).

A *bi*-exponential function was fitted to the 8 points representing the percentage intact tracer, and was used to interpolate values between and after the measurements. The input function was calculated as the product of total counts and interpolated parent fraction at each time point. The metabolite corrected input function values were fitted to a sum of three exponentials and the resulting fitted values used as input for the kinetic analyses.

The plasma free fraction ($f_1$) was determined by ultrafiltration of triplicate 0.2-ml aliquots of plasma. The amount of radioactivity in the filter unit and in the filtrate was measured. $F_1$ was calculated as the ratio of the concentration of radioactivity in the filtrate relative to the total.

Peripheral clearance (l/h), *i.e.* washout from plasma, was defined as the ratio of injected dose to the area under the curve of the metabolite corrected input function.

## Image Analysis

Fourty-one successive frames of increasing duration (18 × 10 s, 7 × 1 min, 16 × 5 min) were reconstructed using a filtered back-projection (Hanning filter, 4.5 mm FWHM). Reconstructed images were anatomically standardized using a macaque version of NEUROSTAT (University of Washington, Seattle, WA). Regions of interest (ROIs) were set based on anatomically standardized images for cerebellum, cingulate, frontal cortex, parietal cortex, temporal cortex, striatum and thalamus. Right and left regions were averaged for the generation of time-activity-curves (TACs).

Regional total distribution volume ($V_T$; ml/g) were derived by kinetic analysis of the regional TACs, using the metabolite-corrected arterial plasma concentrations as input functions, according to a

1- or 2-tissue-compartment model (PMOD Technologies Ltd., Zurich, Switzerland). $V_T$ was derived from kinetic parameters in the 1-tissue-compartment model (1TCM) as:

$$V_T = \frac{K_1}{k_2}$$

and in the 2-tissue-compartment model (2TCM) as:

$$V_T = \frac{K_1}{k_2}\left(1 + \frac{k_3}{k_4}\right)$$

Best model fit was calculated using the Akaike information criterion (AIC) *(12)* and statistical comparison (paired *t*-test) of the mean value of all the regions in each scan of each animal.

The binding potential, $BP_{ND}$, refers to specific binding of ligand relative to the nondisplaceble (non-specically bound and free ligand) concentration in tissue. This parameter can be derived from:

$$BP_{ND} = \frac{V_T - V_{T(ref)}}{V_{T(ref)}} = \frac{k_3}{k_4}$$

where $V_{T(ref)}$ represents $V_T$ in a reference region devoid of the particular receptor of interest. In order to compare our results with Talbot et al. [9], cerebellum was employed as reference region. In addition to the plasma input modeling, a reference tissue model, Ichise's Multilinear Reference Tissue Model 2 (MRTM2), with cerebellum as a reference region was applied to estimate $BP_{ND}$. ROI based kinetic modeling was applied for the parameter estimations while pixel-wise modeling was used for visualization purposes.

## Determination of inhibition constants of GR103545 for binding to opioid receptors

The OR-binding profile of GR103545 was determined in radioligand binding experiments in vitro using ORs stably expressed on cloned cells: Human recombinant HEK-293 cells expressing κ-OR, CHO-K1 cells expressing μ-OR, and CHO cells expressing δ-OR according to published procedures [13-15].

**Results**

PET-Scanning

For the total of 5 scans conducted, the injected activity of [$^{11}$C]GR103545 was 462.0 ± 180.8 MBq (mean ± SD) and the specific activity 41.8 ± 13.4 GBq/μmol. The amount of substance injected was in the range 1.15-1.71 nmol/kg body weight (0.47-0.71 μg/kg body weight).

All metabolites observed in the analysis of radioactivity in plasma were polar species that are not likely to be taken up in the brain. Plasma metabolite analysis after the injection of [$^{11}$C]GR103545 revealed no lipophilic metabolites. The fraction of total plasma activity corresponding to the parent compound at 1, 5, 10, 20, 30, 45, 60, and 90 min after injection of [$^{11}$C]GR103545) was 92 ± 3, 80 ± 5, 67 ± 7, 54 ± 7, 49 ± 8, 38 ± 12, 35 ± 12, 30 ± 11 %, respectively (n=5).

$f_l$ and peripheral clearance for [$^{11}$C]GR103545 were 22 ± 7 % and 20.4 ± 5.1 L/hrs, respectively (n=5).

TACs of [$^{11}$C]GR103545 in rhesus macaques (n = 4) are displayed in Fig. 2. The lowest level of radioactivity was found in the cerebellum, where the TAC reached a distinct maximum at approx. 1200 s followed by a slow washout. The activity in regions with high κ-OR density, such as cingulated-, parietal and frontal cortex, together with striatum, reached a higher maximum later in time and remained at a constant level until the end of the examination.

Compared to the corresponding data from Talbot *et al.* [9], we observed a slower wash-out in regions with low and intermediate κ-OR binding of [$^{11}$C]GR103545 in the present study. 2TCM was chosen as the method of choice due to the lowest AIC value, and the calculated $V_T$ (Table 1 and Fig. 2) resulted in the following rank of uptake: striatum = temporal cortex > cingulate cortex > frontal cortex > parietal cortex > thalamus > cerebellum. For all brain regions evaluated in this study, $V_T$ is significantly higher compared to those of Talbot *et al.* [9] (Table 1). There was no significant effect of the mass of injected ligand on the calculated $V_T$ neither in the high κ-OR density region cingulate

cortex (R=0.10, $p$ = 0.24), nor in the cerebellum (R = 0.22, $p$=0.27), where there is a low concentration of κ-OR.

The estimated $BP_{ND}$ for the ROIs are listed in Table 2. The first two columns display the $BP_{ND}$ values calculated by two different methods; by 2TCM with plasma input and by MRTM2 with a cerebellum TAC input function. Cerebellum is used as a reference region in order to compare our results with the $BP_{ND}$ values presented by Talbot et al. [9] (column 3). In general, the $BP_{ND}$ obtained in the present study are lower than the results from Talbot *et al.* [9]. The use of cerebellum TAC as an input function (column 2) resulted in lower $BP_{ND}$ values compared to plasma input (column 1).

### Determination of binding affinity to opioid subtype receptors

GR103545 showed a high affinity to κ-OR ($K_i$ = 0.02 nM) and excellent selectivity for κ-OR over μ-OR ($K_i$ = 16 nM) and over δ-OR ($K_i$ = 530 nM).

## Discussion

Several OR tracers are available for use in PET and have been investigated in animal models and clinical studies. Although [$^{18}$F]fluorocyclofoxy [16], [$^{11}$C]diprenorphine [17] and [$^{18}$F]fluoroethyl diprenorphine [18] possess sub-nanomolar to low-nanomolar affinity for κ-OR, their cross-reactivity to μ and μ-δ, respectively, is limiting their usefulness. A κ-OR selective PET-tracer is needed for a high sensitivity detection of changes to the availability of κ-OR *in vivo*.

Previous studies of the opioid subtype selectivity of methyl 4-[(3,4-dichlorophenyl)acetyll-3-[(l-pyrrolidinyl)methyl]-l-piperazinecarboxylate, which were based on *in vitro* investigations of (±) GR89606 in brain tissue of rhesus monkeys, found only a low selectivity for κ-OR over μ-OR [19]. This prompted us to investigate the binding of GR103545 human opioid receptors, stably expressed on transfected cells. In these assays, GR103545 displays an excellent selectivity for κ-OR over μ-OR ($6\times10^2$ fold) and δ-OR ($2\times10^4$ fold). A broad receptor screening binding assay (MDS Pharma Services,

Taiwan) covering more than 30 receptors and subtypes found no cross-reactivity at 100 nM concentration, suggesting that GR103545 is highly selective for the κ-OR. Furthermore, the regional brain uptake of [$^{11}$C]GR103545 in rhesus macaques found in the present study, and in baboons as reported by Talbot *et al.* [9], correlates with the known expression pattern of κ-OR [1]. These results, as well as the receptor binding profile reported herein, provide a strong support of the κ-OR–selective profile of [$^{11}$C]GR103545.

The new method for $^{11}$C-labeling of the carbamate functionality in [$^{11}$C]GR103545 is based on [$^{11}$C]MeOTf [10], a prosthetic labeling reagent which is routinely produced at PET radiochemistry laboratories with an on-site cyclotron. The high-yielding $^{11}$C-methylation of [$^{11}$C]GR103545 was readily automated using a synthesis module, and provides the tracer with a specific activity of 1792 ± 312 mCi/μmol at end-of-synthesis [10]. In this study, the production of [$^{11}$C]GR103545 was obtained with approx. 40 % of the specific activity of the [$^{11}$C]MeOTf employed for the $^{11}$C-methylation. The specific activity of the $^{11}$C-methylation agent is therefore the limiting factor for the specific activity of the tracer, as opposed to the overall synthesis time. Although identical performance for production of [$^{11}$C]GR103545 at the Ci-level needs to be confirmed, we expect the simple radiosynthesis to allow for up-scaling without major difficulties or fundamental restrictions.

The present study confirms the correlation of the specific binding pattern of [$^{11}$C]GR103545 (Table 1.) to the known distribution of κ-OR in primate brain [1] and is correlating to previously published data [9] obtained with a comparable injected amount of compound per kg of body weight. However, compared to the kinetic data in the previous study [9] with similar peripheral clearance (this study: 20.4 ± 5.1 L/hrs; Talbot *et al.*: 23.3 ± 8.6 L/hrs), we observed a slower clearance kinetics, which indicates a higher effective ligand-receptor binding affinity, and, in accordance with this observation, the values of $V_T$ found in our study are significantly higher (Table 1.), even though the values of $f_1$ of [$^{11}$C]GR103545 found in the two studies are comparable (Talbot et al.: 24 ± 9); this study 22 ± 7 %). The higher $V_T$ may be due to species differences (this study: rhesus macaques; Talbot *et al.:* baboons),

but a more likely explanation is the absence of any anesthesia in our PET experiments. Anesthetics are known to inhibit high-affinity states of the OR [20], and may therefore have led to the comparably lower $V_T$ and faster clearance in the previous study [9].

Calculation of binding potentials using cerebellum or occipital cortex as reference regions have been applied in several studies for OR ligands. This approach may simplify modeling in non-invasive scanning protocols, but the reference region should be devoid, or contain only a negligible concentration, of the receptor in question. It has been previously shown that the cerebellum of non-human primates [1], as well as that of humans [21], has a low, but relevant proportion of κ-OR. The TAC for cerebellum (Fig. 2) indicates a low but existing number of k-OR in the cerebellar region. Consequently, the cerebellum is not optimally suited as a reference region for calculation of binding potentials of [$^{11}$C]GR103535 in these species. Also, occipital cortex is often used as a reference region for quantification of OR studies in human. However, while this region has a relative negligible expression of μ-OR, it contains a significant κ-OR density [22] which will result in an overestimation of nondisplacable binding. Consequently, to our knowledge, there is no ideal reference region for quantification of κ-OR binding in human, and translation of [$^{11}$C]GR103535 into clinical studies will require arterial sampling or using the activity in the carotid arteries as input function.

In the present study, cerebellum was used as a reference region in order to compare our results with Talbot *et al.* [9]. However, as stated above, the presence of κ-OR in the cerebellum will result in an underestimation of specific binding of [$^{11}$C]GR103535. As can be seen in Table 2, the calculated $BP_{ND}$ is relative low compared to the kinetics illustrated by the TACs in Fig. 2. A slow washout effect indicates a significant amount of specific binding, particularly in regions with high κ-OR density (e.g. cingulate cortex and striatum), but also in cerebellum which contains a relative small portion of κ-OR. These results, together with the data presented by Mansour et al. [1], show that cerebellum is not the optimal choice as a reference region for quantification of κ-OR in non-human primates and humans. A direct calculation of BPND from the arterial input method and $k_3/k_4$ relationship is sensitive to noise.

Without a reference region it is necessary to perform two studies, with and without displacement of the tracer, in order to achieve a robust estimate of $BP_{ND}$.

Because tracer kinetic in baboons indicates that this tracer is bound pseudo-irreversible, it needs to be clarified whether alterations in the κ-OR state affect the regional retention of the tracer. The clinical application of this tracer for the determination of κ-OR availability under stimulation and assessment of competition with exogenous agents may involve separate determination of binding at baseline and at stimulation.

**Conclusion**

The present study was undertaken to further evaluate the potential of [$^{11}$C]GR103545 as a PET radiotracer for imaging and quantification of the κ-OR. The regional brain uptake of [$^{11}$C]GR103545 in awake rhesus macaques was in excellent agreement with the known expression pattern of κ-OR. The selectivity of [$^{11}$C]GR103545 for the κ-OR was further supported by binding studies in cells transfected with cloned human opioid receptors. We conclude that the potential $^{11}$C]GR103545 as a lead candidate for imaging of κ-OR in humans is strengthened.

**Acknowledgement**

Financial support was received from Klinikum rechts der Isar, Technische Universität München, KKF-grant 8764175, and the Norwegian Research Council.

**References**

1. Mansour A, Khachaturian H, Lewis ME, Akil H, Watson SJ. Anatomy of CNS opioid receptors. Trends Neurosci. 1988;11:308-14.
2. Glick SD, Maisonneuve IM, Raucci J, Archer S. Kappa opioid inhibition of morphine and cocaine self-administration in rats. Brain Res.1995; 681:147-52.
3. Prisinzano TE. Natural Products as Tools for Neuroscience: Discovery and Development of Novel Agents to Treat Drug Abuse. J Nat Prod 2008 Dec 19.
4. Mathieu-Kia AM, Fan LQ, Kreek MJ, Simon EJ, Hiller JM. Mu-, delta- and kappa-opioid receptor populations are differentially altered in distinct areas of postmortem brains of Alzheimer's disease patients. Brain Res 2001;893:121-34.

5. Romualdi P, Bregola G, Donatini A, Capobianco A, Simonato M. Region-specific changes in prodynorphin mRNA and ir-dynorphin A levels after kindled seizures. J Mol Neurosci1999;13:69-75.
6. Naylor A, Judd DB, Lloyd JE, Scopes DI, Hayes AG, Birch PJ. A potent new class of kappa-receptor agonist: 4-substituted 1-(arylacetyl)-2-[(dialkylamino)methyl]piperazines. J Med Chem 1993;36:2075-83.
7. Ravert HT, Mathews WB, Musachio JL, Scheffel U, Finley P, Dannals RF. [$^{11}$C]-methyl 4-[(3,4-dichlorophenyl)acetyl]-3-[(1-pyrrolidinyl)-methyl]-1- piperazinecarboxylate ([$^{11}$C]GR89696): synthesis and in vivo binding to kappa opiate receptors. Nucl Med Biol 1999;26:737-741.
8. Ravert HT, Scheffel U, Mathews WB, Musachio JL, Dannals RF. [$^{11}$C]GR89696, a potent kappa opiate receptor radioligand; in vivo binding of the R and S enantiomers. Nucl Med Biol 2002;29: 47-53.
9. Talbot PS, Narendran R, Butelman ER, Huang Y, Ngo K, Slifstein M, Martinez D, Laruelle M, Hwang DR. $^{11}$C-GR103545, a radiotracer for imaging kappa-opioid receptors in vivo with PET: synthesis and evaluation in baboons. J Nucl Med 2005; 46:484-94.
10. Schoultz BW, Arstad E, Marton J, Wester HJ, Henriksen G. A New Method for Radiosynthesis of $^{11}$C-Carbamate groups and its application for a highly efficient synthesis of the Kappa-Opioid Receptor Tracer [$^{11}$C]GR103545. The Open Med Chem Journal 2008; 2: 72-4.
11. Noda A, Takamatsu H, Minoshima S, Tsukada H, Nishimura S. Determination of Kinetic Rate Constants for 2-[$^{18}$F]fluoro-2-deoxy-D-glucose and Partition Coefficient of Water in Conscious Macaques and Alterations in Aging or Anesthesia Examined on Parametric Images With an Anatomic Standardization Technique. J Cereb Blood Flow Metab 2003;23:1441-47.
12. Akaike, H. A new look at the statistical model identification. IEEE Trans Automat. Contr AC 1974; 9: 716-23.
13. Simonin F, Befort K, Gaveriaux-Ruff C, Matthes H, Nappey V, Lannes B, Micheletti G, Kieffer B. The human δ-opioid receptor: Genomic organization, cDNA cloning, functional expression, and distribution in human brain. Mol Pharmacol 1994; 46: 1015-21.
14. Simonin F, Gaveriaux-Ruff C, Befort K, Matthes H, Lannes B, Micheletti G, Mattei M-G, Charron G, Bloch B, Kieffer B. Kappa-opioid receptor in humans: cDNA and genomic cloning, chromosomal assignment, functional expression, pharmacology and expression pattern in the central nervous system. Proc Natl Acad Sci USA1995; 92: 7006-10.
15. Wang JB, Johnson PS, Persico AM, Hawkins AL, Griffin CA, Uhl GR Human mu opiate receptor: cDNA and genomic clones, pharmacologic characterization and chromosomal assignment. FEBS Lett 1994; 338:217-22.
16. Cohen RM, Andreason PJ, Doudet DJ, Carson RE, Sunderland T. Opiate receptor avidity and cerebral blood flow in Alzheimer's disease. J Neurol Sci 1997;148:171-80.
17. Hume SP, Lingford-Hughes AR, Nataf V, Hirani E, Ahmad R, Davies AN, Nutt DJ.Low sensitivity of the positron emission tomography ligand [$^{11}$C]diprenorphine to agonist opiates. J Pharmacol Exp Ther 2007;322:661-67.
18. Wester HJ, Willoch F, Tölle TR, Munz F, Herz M, Oye I, Schadrack J, Schwaiger M, Bartenstein P. 6-O-(2-[$^{18}$F]fluoroethyl)-6-O-desmethyldiprenorphine ([$^{18}$F]DPN): synthesis, biologic evaluation, and comparison with [$^{11}$C]DPN in humans. J Nucl Med 2000;41:1279-86
19. Butelman ER, Ko MCH, Traynor JR, Vivian JA, Kreek MJ, Woods JH. GR89696: A potent κ-opioid agonist with subtype selectivity in rhesus monkeys. J Pharm Exp Ther 2001;298:1049-59.
20. Seeman P, Kapur S. Anesthetics inhibit high-affinity states of dopamine $D_2$ and other G-linked receptors. Synapse 2003;50:35-40.
21. Schadrack J, Willoch F, Platzer S, Bartenstein P, Mahal B, Dworzak D, Wester HJ, Zieglgänsberger W, Tölle TR. Opioid receptors in the human cerebellum: evidence from

[$^{11}$C]diprenorphine PET, mRNA expression and autoradiography. NeuroReport 1999;10: 619–24.
22. Pfeiffer A, Pasi A, Mehraein P, Herz A. Opiate receptor binding sites in human brain. Brain Res 1982;248:87-96.

**Table 1.** Volume of Distribution Estimates[a] of [$^{11}$C]GR103545 in Awake Rhesus Macaques

| | **Present study** | | **Talbot et al. 2005** | | **Unpaired t-test** | |
|---|---|---|---|---|---|---|
| | Vt, ml/g | | Vt, ml/g | | 2 degrees of freedom | |
| **Region** | mean | SD | mean | SD | t | p < |
| Cerebellum | 8.3 | 1.6 | 3.7 | 1.6 | 5.0 | 0.020 |
| Cingulate | 18.9 | 4.8 | 10.9 | 6.1 | 4.7 | 0.025 |
| Frontal Cortex | 16.2 | 3.9 | 8.5 | 3.7 | 5.4 | 0.020 |
| Parietal Cortex | 14.4 | 3.2 | 7.5 | 3.8 | 5.1 | 0.020 |
| Temporal Cortex | 20.5 | 2.9 | 8.1 | 4.3 | 4.1 | 0.050 |
| Striatum | 20.5 | 8.2 | 10.5 | 5.9 | 5.1 | 0.020 |
| Thalamus | 11.4 | 1.8 | 6.9 | 3.6 | 3.9 | 0.050 |
| *Mean* | 14.8 | 3.8 | 8.0 | 4.1 | 4.7 | 0.025 |

[a]Fitting and calculation of volume of distribution, Vt, using 2-tissue compartment model. The goodness of fit to the data, as indicated by the Akaike information criterion, was significantly better for the 2-tissue compartment model (mean ± SD: 147 ± 25) than for the 1-tissue compartment model (169 ± 17), $p < 0.04$, which is in agreement with the findings of Talbot *et al.* 2005 [9] The values from Talbot *et al.* [9] are taken from their Table 3.

**Table 2.** Binding estimates[a] of [$^{11}$C]GR103545 in Awake Rhesus Macaques.

| | Present study | | | | Talbot et al. 2005 | |
|---|---|---|---|---|---|---|
| | 2TCM with plasma input | | MRTM2 with cerebellum input | | 2TCM with plasma input | |
| | $BP_{ND}$ | | $BP_{ND}$ | | $BP_{ND}$ | |
| **Region** | mean | SD | mean | SD | mean | SD |
| Cerebellum | 0.00 | 0.00 | 0.00 | 0.00 | 0.00 | 0.00 |
| Cingulate | 1.34 | 0.15 | 1.03 | 0.06 | 1.90 | 0.40 |
| Frontal Cortex | 1.02 | 0.17 | 0.74 | 0.07 | 1.30 | 0.20 |
| Parietal Cortex | 0.84 | 0.23 | 0.57 | 0.07 | 1.00 | 0.20 |
| Temporal Cortex | 0.72 | 0.06 | 0.58 | 0.03 | 1.10 | 0.20 |
| Striatum | 1.60 | 0.73 | 0.99 | 0.10 | 1.70 | 0.50 |
| Thalamus | 0.45 | 0.26 | 0.35 | 0.11 | 0.80 | 0.30 |

[a]Estimation of $BP_{ND}$, i.e. specific binding of [$^{11}$C]GR103545 relative to nondisplaceable (free plus nonspecifically bound) uptake in tissue. $BP_{ND}$ was calculated with two different methods; by 2TCM with plasma input and by MRTM2 with cerebellum TAC as input function. The values from Talbot et al. [9] presented in the last column are taken from their Table 3. Cerebellum is used as a reference region in all models.

## Figures Legends

### Fig. 1. Radiosynthesis of [$^{11}$C]GR103545

### Fig. 2. [$^{11}$C]GR103545 uptake in awake rhesus macaques

A. $V_T$-images calculated using pixelwise 2TCM, and co-registered to a MRI template for anatomical reference. The horizontal slices show high $V_T$ in the cingulate and frontal cortex. Red areas, high $V_T$; Blue, low $V_T$. B. Average regional radioactivity concentration, expressed as the standard uptake value (SUV; radioactivity concentration (MBq/mL)/injected dose (MBq)/body mass (g)) plotted against time (n = 4). Regions with low and intermediate activity (i.e. cerebellum and thalamus) reach an early maximum and have a slow washout effect. Regions with high κ-OR density (cingulate and frontal cortex, and striatum) reach a maximum later in time, and show no significant washout effect.

## Figures

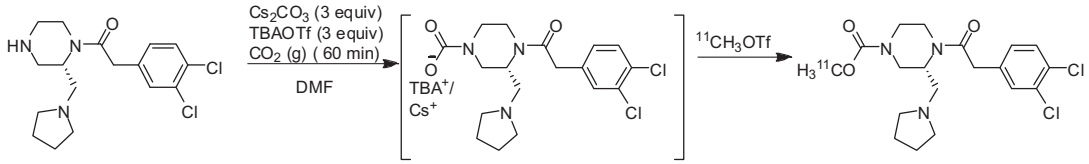


**Fig. 1. Radiosynthesis of [$^{11}$C]GR103545**

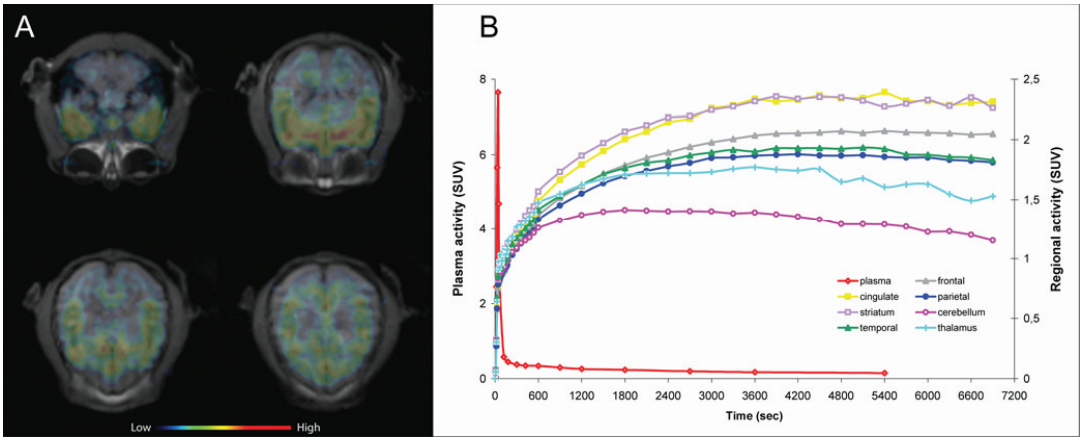


**Fig. 2. [$^{11}$C]GR103545 uptake in awake rhesus macaques**

A. $V_T$-images calculated using pixelwise 2TCM, and co-registered to a MRI template for anatomical reference. The horizontal slices show high $V_T$ in the cingulate and frontal cortex. Red areas, high $V_T$; Blue, low $V_T$. B. Average regional radioactivity concentration, expressed as the standard uptake value (SUV; radioactivity concentration (MBq/mL)/injected dose (MBq)/body mass (g)) plotted against time (n = 4). Regions with low and intermediate activity (i.e. cerebellum and thalamus) reach an early maximum and have a slow washout effect. Regions with high κ-OR density (cingulate and frontal cortex, and striatum) reach a maximum later in time, and show no significant washout effect.